



National Library
of Canada

Acquisitions and
Bibliographic Services Branch

395 Wellington Street
Ottawa, Ontario
K1A 0N4

Bibliothèque nationale
du Canada

Direction des acquisitions et
des services bibliographiques

395, rue Wellington
Ottawa (Ontario)
K1A 0N4

Your file - Votre référence

Our file - Notre référence

NOTICE

The quality of this microform is heavily dependent upon the quality of the original thesis submitted for microfilming. Every effort has been made to ensure the highest quality of reproduction possible.

If pages are missing, contact the university which granted the degree.

Some pages may have indistinct print especially if the original pages were typed with a poor typewriter ribbon or if the university sent us an inferior photocopy.

Reproduction in full or in part of this microform is governed by the Canadian Copyright Act, R.S.C. 1970, c. C-30, and subsequent amendments.

AVIS

La qualité de cette microforme dépend grandement de la qualité de la thèse soumise au microfilmage. Nous avons tout fait pour assurer une qualité supérieure de reproduction.

S'il manque des pages, veuillez communiquer avec l'université qui a conféré le grade.

La qualité d'impression de certaines pages peut laisser à désirer, surtout si les pages originales ont été dactylographiées à l'aide d'un ruban usé ou si l'université nous a fait parvenir une photocopie de qualité inférieure.

La reproduction, même partielle, de cette microforme est soumise à la Loi canadienne sur le droit d'auteur, SRC 1970, c. C-30, et ses amendements subséquents.

Canada

UNIVERSITY OF ALBERTA

**Electrochemical Impedance Studies of
Membrane/Electrode Interfaces**

BY

Alebachew Demoz



A Thesis Submitted
To The Faculty of Graduate Studies and Research
In Partial Fulfillment of The Requirements For The Degree of
Doctor of Philosophy

Department of Chemistry

Edmonton, Alberta

Fall, 1994



National Library
of Canada

Acquisitions and
Bibliographic Services Branch

395 Wellington Street
Ottawa, Ontario
K1A 0N4

Bibliothèque nationale
du Canada

Direction des acquisitions et
des services bibliographiques

395, rue Wellington
Ottawa (Ontario)
K1A 0N4

Your file - Votre référence

Our file - Notre référence

The author has granted an irrevocable non-exclusive licence allowing the National Library of Canada to reproduce, loan, distribute or sell copies of his/her thesis by any means and in any form or format, making this thesis available to interested persons.

L'auteur a accordé une licence irrévocable et non exclusive permettant à la Bibliothèque nationale du Canada de reproduire, prêter, distribuer ou vendre des copies de sa thèse de quelque manière et sous quelque forme que ce soit pour mettre des exemplaires de cette thèse à la disposition des personnes intéressées.

The author retains ownership of the copyright in his/her thesis. Neither the thesis nor substantial extracts from it may be printed or otherwise reproduced without his/her permission.

L'auteur conserve la propriété du droit d'auteur qui protège sa thèse. Ni la thèse ni des extraits substantiels de celle-ci ne doivent être imprimés ou autrement reproduits sans son autorisation.

ISBN 0-315-95173-7

Canada

UNIVERSITY OF ALBERTA
RELEASE FORM

NAME OF AUTHOR: **Alebachew Demoz**

TITLE OF THESIS: **Electrochemical Impedance Studies of
Membrane/Electrode Interfaces.**

DEGREE: **Doctor of Philosophy**

YEAR THIS DEGREE GRANTED: **1994**

Permission is hereby granted to the University of Alberta Library to reproduce single copies of this thesis and to lend or sell such copies for private, scholarly or scientific research purposes only.

The author reserves all other publication and other rights in association with the copyright in the thesis, and except as hereinbefore provided neither the thesis nor any substantial portion thereof may be printed or otherwise reproduced in any material from whatever without the author's written permission.

AUTHOR'S SIGNATURE: *Alebachew Demoz*

PERMANENT ADDRESS: Chemistry Department
Addis Ababa University
P.O. Box 1176
Addis Ababa
Ethiopia

DATE: June 27, 1994

UNIVERSITY OF ALBERTA

FACULTY OF GRADUATE STUDIES AND RESEARCH

The undersigned certify that they have read, and recommend to the Faculty of Graduate Studies and Research for acceptance, a thesis entitled **Electrochemical Impedance Studies of Membrane/Electrode Interfaces** submitted by **Alebachew Demoz** in partial fulfillment of the requirements for the degree of **Doctor of Philosophy**.


SUPERVISOR:


Dr. D. J. Harrison

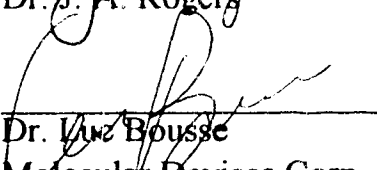

Dr. F. F. Cantwell


Dr. R. G. Cavell


Dr. N. Dovichi


Dr. J. A. Rogers

EXTERNAL EXAMINER:


Dr. Luc Bousse
Molecular Devices Corp.
Menlo Park, CA

Date: June 27, 1994

To my Parents

Abstract

This work focuses on AC impedance investigations of the membrane/insulator/semiconductor (MIS) interface. These interfaces are a big part of many chemical sensors that are envisaged to address the need for remote, selective or continuous chemical analysis.

The MIS represents the widely studied ion selective field effect transistor device. Characterization of the impedance response of the MIS is made possible through an equivalent circuit model of resistors and capacitors that match the elements of the system, namely; the plasticized, poly(vinyl chloride) based K^+ selective membrane and the insulators Si_3N_4 and/or SiO_2 on n-type Si. The impedance characteristics of the MIS are dominated by the membrane above 100 Hz AC signal. Both model calculations and experimental results show that the capacitance-voltage (CV) curves show a complex dependence on the resistance of the membrane and the frequency of the AC signal. The model provided a quantitative description of the experimental observations.

Adsorption of charged surfactants onto a nonionic surface will determine the charge and consequently the surface potential. The adsorption of sodium dodecylsulfate (SDS^-) onto an octadecyldimethylchlorosilane (ODS) silanized SiO_2 causes a shift in the CV curve of the SiO_2/Si electrode in NaCl supporting electrolyte equal to the double layer potential change. A modified Gouy-Chapman-Stern-Grahame theory of the double layer in which the SDS^- is allowed to coordinate with

Na^+ is used in order to determine the adsorption isotherm. The adsorption isotherm of SDS^- onto ODS is found to obey the Langmuir adsorption isotherm. Its free energy of adsorption is -48.2 ± 0.7 kJ/mole, whereas its density at adsorption saturation varies from 7 to 15 nm^2 per molecule depending on the ionic strength. These studies were performed in order to develop an experimental model of the processes occurring during ion-pair chromatography.

Self assembled monolayer films are vital as anchors of redox molecules or are themselves dielectric films that serve as molecularly precise spacers at an interface. They provide a significant barrier towards diffusing redox species in the electrolyte. Hexadecanethiol is demonstrated to form a self assembled monolayer film on Hg surface. Different electrochemical tests reveal the film exhibits a much lower density of molecular or physical defects relative to the films formed on Au. The Hg surface thus provides a method to prepare more ideal films for characterization of fundamental film properties.

Acknowledgments

I received considerable help from many people during my Ph.D. program. Foremost is my supervisor Dr. Jed Harrison. Simple words of thanks can not express my gratitude for his professional guidance, his patience in waiting for me to always come up with something he could work on and his all round commitment to see me through.

I would also like to thank Dr. F. F. Cantwell. Although I had reprints of his interlocking, succinct research papers, he was always available to answer questions. The kindness of the Department Chairman, Dr. B. Kratochvil, deserves special mention. Together with my supervisor, they have shielded me from administrative regulations.

I wish to render my thanks to fellow students in Dr. Harrison's group. Regarding the MIS studies of chapter 2, I trailed behind the able Elisabeth Verpoorte. I have benefitted from her experience and work in our group. Andy Chan was helpful in writing a brief computer program for the acquisition of QCM experiment data and in running low frequency fast Fourier transform impedance studies. I am appreciative of Paul Glavina, Xizhong Li, Dan Raymond, Hugh Fan and Zhong Li for their friendship and support. I also thank Mr. Graham Mckinnon of the Alberta Microelectronic Center for the use of their facilities.

A special word of thanks goes to my friend and colleague Slobodan Petrovic for his concern and encouragement. Fassil Hailu and Tadelech Assfaw have unfailingly been on my side through these many years. It is a pleasure to also acknowledge that I have always felt welcome to the homes of Drs. Fassil and Petrovic. My gratitude also goes to my other friends not named. Their help was equally valuable.

Table of Contents

Chapter	Page
1. Introduction	1
1.1 Blocked and Unblocked Interfaces.....	4
1.1.1 Blocked Electrode-Electrolyte Interfaces	5
1.1.2 Unblocked Membrane-Electrolyte Interfaces	7
1.2 The ISFET.....	9
1.2.1 Carrier concentration of semiconductors	10
1.2.2 The capacitance of the MOS structure	12
1.2.3 The gate is replaced by an ion sensitive layer and reference electrode.....	15
1.2.4 The MIS and ISFET structures	16
1.3 Interfacial potential difference	18
1.4 Ion pair chromatography.....	23
1.5 AC Impedance Analysis.....	26
1.5.1 Modes of representation of impedance	28
1.5.2 Response of single electrical elements to AC signal	32
1.5.3 Impedance of electrochemical cells	33
1.6 References	37
2. An equivalent circuit model of ion selective membrane/insulator/semiconductor interface used for chemical sensors.	 41

2.1	Introduction	41
2.2	Model of Membrane/Insulator/Silicon Electrode Impedance	42
2.3	Experimental Section	51
2.4	Results and Discussion	54
2.4.1	Characterization of Si Electrode Impedance	54
2.4.2	Assignment of MIS Frequency Response Elements	58
2.4.3	Qualitative Analysis of MIS Electrode Capacitance	60
2.4.4	Quantitative Analysis of MIS Electrode Impedance	64
2.5	Conclusions	66
2.6	References	67
3.	Electrochemical impedance study of the adsorption of SDS⁻ onto an ODS silanized surface.	69
3.1	Introduction	69
3.2.1	Introductory theory	71
3.2.2	The Gouy-Chapman-Stern-Graham (GCSG) model	80
3.2.3	Multiple layer blocking interface	86
3.3	SDS ⁻ as the PDI	87
3.4	Experimental Section	90
3.5	Results and Discussion	93
3.5.1	pH of point of zero charge of the ODS surface	94
3.5.2	The resolution of residual charge and SDS ⁻ charge from CV studies	97
3.5.3	Adsorption saturation of SDS ⁻	104

3.5.4	Critical Micelle Concentration of SDS	106
3.5.5	The estimation of K_{Na^+}	110
3.5.6	Adsorption Isotherms of SDS ⁻	113
3.5.7	Adsorption free energy of SDS ⁻	117
3.6	Conclusions	119
3.7	References	122
4.	Characterization of extremely low defect density hexadecanethiol monolayers on Hg surfaces.	126
4.1	Introduction	126
4.2	Experimental Section	128
4.3	Results and Discussion	130
4.3.1	Differential Electrode Capacitance	132
4.3.2	Redox Active Probes	135
4.3.3	Processes at the Hg Surface	143
4.4	Conclusions	148
4.5	References	150
5.	Conclusion	153
5.1	Summary of contributions	154
5.2	Suggestions for future research	156
5.3	References	161

List of Figures

Figure		Page
1.1	The basic MOS capacitor structure	13
1.2	Schematic illustration of a typical MIS (A); and ISFET (B). (C) is the capacitance vs voltage characteristic of the MIS and (D) is the drain current vs gate source voltage characteristic of the ISFET. The dashed lines indicate electrical characteristics with parallel shift along the voltage axis. 1, reference electrode; 2, ion sensitive membrane; 3, gate oxide; 4, substrate Si; S, source; D, drain; V_{gs} , gate-source voltage; V_{ds} , drain-source voltage.....	17
1.3	Schematics showing the variation of the coulombic potential as a function of distance.	20
1.4	A generalized impedance experiment (A), in which AC wave form applied to the system under study and the impedance is obtained from the resultant AC current and their phase relationship (B)....	29
1.5	Representation of the impedance, Z , on a vector diagram. Z_R and Z_I are the real (X-axis) and imaginary (Y-axis) coordinates of the complex impedance Z . $ Z $ is the modulus of Z and θ is the phase shift of Z relative to the input volatge.....	31
1.6	Nyquist (C,D) and Bode plots (E,F) for series and parallel RC circuits.	34

2.1	Model of circuit elements present when an MIS (membrane/insulator/semiconductor) is immersed in aqueous solution. See text for definition of symbols.	43
2.2	Semiconductor band diagram of electron energy and electrode potentials under conditions of a) accumulation induced by a forward bias, b) flat band and c) depletion induced by a reverse bias. The electrochemical sign convention is used, with the potential referenced to a reference electrode in solution, rather than to the semiconductor bulk.	45
2.3	Capacitance-voltage curves for a) moderately doped n-type Si, (m-Si), with no membrane coating at three frequencies; b) the same type of Si after annealing in forming gas (an-Si). Model calculations for the annealed electrode are also shown at 27 Hz with the following parameters: $A = 0.12 \text{ cm}^2$, $C_{in} = 5.8 \text{ nF}$, $N_0 = 10^{15} \text{ cm}^{-3}$, $\gamma = 0.34$	55
2.4	Bode plot of the magnitude of impedance ($ Z $) for an m-Si MIS electrode biased into accumulation in 0.1 M KCl. The electrode was sequentially coated with thicker membranes with resistances, R_g , of (*) 0.69 M Ω , (+) 2.9 M Ω , and (o) 6.7 M Ω . Lines show the expected slope for a pure capacitance, and the limiting value of R_g	57
2.5	Experimental capacitance-voltage curves at several frequencies for an MIS electrode, using an m-Si substrate and a membrane with $R_g = 3.2 \text{ M}\Omega$, $C_g = 20 \text{ pF}$, $A = 0.11 \text{ cm}^2$, $C_{in} = 5.27 \text{ nF}$, $N_0 = 10^{15} \text{ cm}^{-3}$	59

2.6	Calculated capacitance-voltage curves at several frequencies for an MIS electrode using the following parameters: $R_g = 3 \text{ M}\Omega$, $C_g = 20 \text{ pF}$, $A = 0.1 \text{ cm}^2$, $C_{in} = 5 \text{ nF}$, $N_o = 10^{15} \text{ cm}^{-3}$	61
2.7	Capacitance-voltage curves at 27 Hz for a float zone Si (fz-Si) MIS electrode coated with membranes of two different resistances (R_g). Both (—) experimental data and (+) calculated curves are shown. Electrode parameters were: $A = 0.11 \text{ cm}^2$, $C_{in} = 4.4 \text{ nF}$, $N_o = 6 \times 10^{12} \text{ cm}^{-3}$, $\gamma = 0.25$. Membrane parameters were: $R_g = 0.89 \text{ M}\Omega$, $C_g = 40 \text{ pF}$ or $R_g = 5.76 \text{ M}\Omega$, $C_g = 10 \text{ pF}$	63
2.8	Capacitance-voltage curves at several frequencies for an annealed m-Si (an-Si) MIS electrode with a membrane R_g of $9.6 \text{ M}\Omega$, $C_g = 6 \text{ pF}$. Both (—) experimental data and (+) calculated curves are shown, other parameters are as for Figure 3b.	65
3.1	Potential distribution in the electrolyte/SiO ₂ /Silicon system.	74
3.2	Schematic representation of the GCSG model.	82
3.3	Potential shift-pH measurements of 0.03 M NaCl/2mM acetate buffer; at two constant SDS ⁻ activities, where ΔV is measured relative to the 2.87 pH solution.	95
3.4	Plot of the variation of ψ_o as a function of ionic strength at two SDS ⁻ constant activities of 0.1 mM and 0.3 mM and without SDS ⁻ . The pH of the solution is kept at 5 by a 1 mM acetate buffer in all cases.	102

3.5	Plot of the variation of $-\Delta V$ as function of SDS^- at three ionic strengths of 0.01, 0.03 and 0.1 M. The pH of the solution is kept at 5 by a 1 mM acetate buffer in all cases.	105
3.6	Schematic structure of SDS^- molecule.	106
3.7	Plot of literature values of the CMC of SDS vs $[\text{NaCl}]^{-0.5}$. Points generated from the Corrin-Harkins relationship for the identical data are shown by +.	108
3.8	Plot of inverse adsorbed SDS^- concentration vs activity of Na^+ ; at two constant aqueous phase activities of SDS^- equal to 1 and 3×10^{-4} M.	112
3.9	Adsorption isotherms of SDS^- for the data presented in Figure 3.5. $K_{\text{Na}^+} = 7$ lt/mole; $C_{\text{Stern}} = 20 \mu\text{F}/\text{cm}^2$	114
3.10	Linear Langmuir isotherm plots of Figure 3.9.	116
4.1	Differential capacitance as a function of potential at a bare static Hg drop electrode, and a thiol coated electrode. C for the coated electrode is multiplied by 10 for clarity.	131
4.2	Bode plot of $\log Z $ vs $\log \omega$ for a bare SMDE (O) in 0.1 M NaF, and for an HDT coated SMDE (+) at several NaF concentrations.	133
4.3	Cyclic voltammogram at 100 mV/s of 5 mM MV^{2+} and 5 mM $\text{Ru}(\text{NH}_3)_6^{3+}$ in 0.1 M NaF at a bare SMDE (---), and an HDT coated SMDE (—). The latter curve is increased 1000-fold in sensitivity for clarity.	136

4.4	Deposition and stripping waves at 100 mV/s for 5 mM Pb ²⁺ in 0.1 M KNO ₃ at (•••) bare Hg, and at HDT coated on the Hg (---) first cycle, and (—) third cycle. The coated electrode currents are magnified tenfold.....	140
4.5	Current for Hg oxidation <i>vs</i> potential in 0.1 M NaF for both bare (---) and HDT coated (—) SMDE obtained at 100 mV/s. The upper traces show the same data as the lower trace on a 40-times less sensitive scale.	142
4.6	(a) Reduction current at 100 mV/s observed during stripping of an HDT film from an Hg surface in 0.1 M NaF. (b) Reduction current observed at 100 mV/s between 0 and -1.1 V at a virgin HDT coated SMDE during the first and second scans. Note the high current sensitivity.....	144
4.7	Change in differential capacitance as a function of potential for a virgin HDT coated SMDE during cycling from 0 to -0.5 V and then to -1.1 V. The inset shows the ratio of C observed to initial C, C _i , following each potential sweep from 0 to -1.1 V for two typical electrodes.	146

List of symbols

A	area of electrode (cm^2)
a_i	activity of " i " (mol/L)
C	capacitance (F)
C	ionic strength (mol/L)
C^*	redox concentration (mole/l)
C_{dl}	double layer capacitance (F/cm^2)
C_e	equivalent capacitance of the insulator and semiconductor electrode (F/cm^2)
C_f	thiol film capacitance (F/cm^2)
C_{fb}	capacitance at flat band conditions (F/cm^2)
C_g	membrane capacitance (F/cm^2)
C_i	initial film capacitance (F)
C_{IHP}	capacitance of the inner Helmholtz plane (F/cm^2)
C_{in}	capacitance of the insulator layer (F/cm^2)
C_{it}	surface states capacitance (F/cm^2)
C_{min}	minimum capacitance (F/cm^2)
C_{sc}	space charge capacitance (F/cm^2)
C_{Stern}	Stern layer capacitance (F/cm^2)
d	distance (cm)
d	film thickness (cm)
D_{it}	surface state density ($1/\text{cm}^2 \cdot \text{V}$)
E_B	barrier height (eV)
E_g	band gap (eV)
E^o	formal redox potential (V)

E(t)	AC voltage function (V)
F	Faraday constant (96487 C/mol)
f	frequency (Hz)
h	Plank's constant (6.626×10^{-34} J.s)
I	current (A)
I_d	drain current (A)
i_f	Faradaic current (A)
I_o	AC current amplitude (A)
I(t)	AC current function (A)
j	$=\sqrt{-1}$
k	Boltzmann's constant (8.617×10^{-5} eV/K)
K_{ad}	adsorption equilibrium constant (cm)
K_{ad}^x	Langmuir adsorption isotherm mole fraction expression equilibrium constant
k_{ap}	apparent electron transfer rate constant (cm/s)
k^{o'}	standard state rate constant at a naked electrode (cm/s)
K_{Na⁺}	complexation constant of Na⁺ with surface adsorbed SDS⁻ (L/mol)
N_a	acceptor doping concentration (cm⁻³)
N_d	donor doping concentration (cm⁻³)
N_o	doping density (cm⁻³)
n_i	intrinsic electron carrier density (cm⁻³)
p_i	intrinsic hole carrier density (cm⁻³)
Q	charge (C)
Q_{ox}	oxide layer charge (C/cm²)
Q_{sc}	space charge density (C/cm²)

q	magnitude of electron charge (1.602x10⁻¹⁹ C)
R	gas constant (8.314 J/K.mole)
R	resistance (ohms)
R_g	membrane resistance
R_s	electrolyte resistance
r	radius (cm)
SDS_(aq)⁻	aqueous SDS⁻ (mol/L)
SDS_(ODS)⁻	Surface adsorbed SDS⁻ (mol/cm²)
T	absolute temperature (K)
t	time (s)
V	voltage (V)
V_{ds}	drain to source voltage (V)
V_{fb}	flat band potential (V)
V_{gs}	gate to source voltage (V)
V_o	amplitude of AC signal (V)
V_{ox}	oxide voltage (V)
val_(mem)	membrane matrix valinomycin
X_{sc}	space charge width (cm)
W_{Si}	work function of Si (eV)
Y	admittance (siemens)
Y_{im}	imaginary admittance (siemens)
Z	impedance (ohms)
Z_i	charge number of " i "
Z_I, Z_{im}	imaginary component of Z
Z_R	real component of Z (ohms)
α	indication of a specific phase

α	electron transfer coefficient
β	indication of a specific phase
β	$= q/kT$
β	Langmuir adsorption isotherm expression equilibrium constant
β	tunneling parameter (1/cm)
Γ_m	surface density of adsorbent at maximum adsorption coverage (mol/cm ²)
$\Gamma_{(ODS)}$	total amount of adsorbed SDS ⁻ (mol/cm ²)
γ	surface tension (N/m)
ΔG_{ad}^x	Gibbs free energy of adsorption (J/mol)
$\delta\chi_b^j$	change of χ when " j " is in contact with " b " (V)
ϵ_s	relative dielectric constant of Si (11.9)
ϵ_0	permittivity of free space (8.854x10 ⁻¹⁴ F/cm)
ϵ'	relative dielectric constant of the diffuse layer
ζ	zeta potential (V)
η	over potential (V)
μ_i	chemical energy of " i " (J/mol)
$\tilde{\mu}_i$	electrochemical energy of " i " (J/mol)
$\tilde{\mu}_e^j$	electron energy in " j " (V)
σ_d	diffuse layer charge (C/cm ²)
σ_0	total surface charge (C/cm ²)
σ_{SDS^-}	adsorbed charge density of SDS ⁻ (C/cm ²)
σ_{SiOH}	residual silanol charge density (C/cm ²)
σ_β	charge density at IHP (C/cm ²)
Φ^j	inner potential or Galvani potential of phase " j " (V)
Φ_x^j	inner potential or Galvani potential of " j " at x (V)

χ	surface potential (V)
χ^j	surface potential of " j " in contact with vacuum (V)
ψ^α	outer potential of phase " α " (V)
ψ_0	double layer potential (V)
ψ_{OHP}	diffuse layer potential (V)
ψ_β	potential at the inner Helmholtz (V)
ω	angular frequency (s^{-1})
ω_{max}	maximum angular frequency (s^{-1})
\mathfrak{I}_i^α	real potential of " i " in phase " α " (V)

Abbreviations and acronyms

an-Si	annealed Si
CMC	critical micelle concentration
CV	capacitance-voltage
EIS	electrolyte-insulator-semiconductor
EOS	electrolyte-oxide-semiconductor
fz-Si	float zone Si
GCSG	Gouy-Chapman-Stern-Grahame
HDT	hexadecanethiol
HPLC	high performance liquid chromatography
iep	isoelectric point
IHP	inner Helmholtz plane
ISE	ion selective electrode
ISFET	ion sensitive field effect transistor
LAPS	light addressable potentiometric sensor
MIS	membrane/insulator/semiconductor system
MOS	metal-oxide-semiconductor
MV²⁺	methyl viologen
ODS	octadecyldimethylchlorosilane
OHP	outer Helmholtz plane
PDI	potential determining ion
pH_{pzc}	pH of point of zero charge
PVC	poly(vinyl chloride)
SDS	sodium dodecylsulfate

SGC	Stern-Gouy-Chapman
SMDE	static Hg drop electrode
val	valinomycin

Chapter 1

Introduction

At present, sophisticated techniques that perform very complete chemical separations and analyses are available. However, it may be more important to analyze just a few species continuously and at lower cost at the point of interest. For example, an environmental application may involve the mapping of contaminant migration in an effluent gas or liquid. Monitoring one species in a reaction vessel may be adequate for process control. A medical application may require the continuous monitoring of the glucose or oxygen level of the blood for a hospital patient. In these applications, remote, selective, or continuous monitoring become more important than laboratory-based, complete or batch-mode analysis techniques. Chemical sensors address this need.

Chemical sensors comprise a sensing layer interfacing the chemical environment with a physicochemical transducer interfaced to electronic conductors and circuits [1,2]. In electrochemical sensing the most important electrical phenomena involve measurement of interfacial potentials in potentiometry, electrochemical reaction currents in amperometry, and cell impedance in electrical conductivity [1-5]. In general electrochemical sensors involve an exchange of ions or electrons at one, or a series of interfaces. These interfaces are of many different types but can be grouped into metal/solution, insulator/solution and metal/insulator/solution

interfaces. Interfaces across which charge is conducted are termed unblocked, and form the basis for many conventional electrochemical sensors. Blocked interfaces, across which charge does not flow except by capacitive coupling form the basis of a number of newer, less developed sensing schemes.

The interface between an insulator and a solution forms a blocked interface which is sensitive to the adsorption or formation of charged species by physisorption or chemical reaction. This makes these interfaces intriguing as probes of a variety of chemical surface phenomena. Electrochemical studies of such systems may lead to improved understanding of sensors based on such phenomena, other types of chemical processes involving adsorption at surfaces such as ion-pair chromatography, and to the design of new sensors or modified surfaces. Blocked interfaces allow capacitive current flow, but not direct current or Faradaic current due to redox reactions. For this reason they are better studied using AC impedance techniques in which the capacitance of the interface is directly evaluated.

In this thesis AC impedance has been used extensively as a tool to probe both blocked and unblocked interfaces. The interfaces that were studied are quite varied. Chemical sensors based on the semiconductor/insulator/membrane (MIS) interface were examined where the membrane/solution interface was unblocked. The detailed impedance behavior was characterized both experimentally and theoretically, as is outlined in chapter 2 of this thesis.

Experiments with semiconductor/insulator/membrane/solution interfaces establish that the impedance of the semiconductor is highly

sensitive to changes in potential that develop within the membrane. This result indicated that adsorption of charge on a surface could be followed from measurements of the semiconductor impedance. Such measurements could be useful in studying systems where adsorption of charge plays a significant role. Ion-pair chromatography, in which ionic surfactants are adsorbed on an alkyl coating on silica is one such system. The reversed phase of octadecyldimethylchlorosilane (ODS) bonded to silica that is used in ion pair chromatography was modelled by derivatization of ODS on a silicon/silicon dioxide interface. Adsorption of charge at that interface was then followed using the impedance method also used to study the ion-sensitive membranes. This work is discussed in chapter 3.

In attempting to prepare model interfaces for the ion-pair chromatographic study described above many different approaches were examined. One of these involved the formation of self-assembled monolayers of long n-alkyl chain thiols on surfaces such as Au or Hg. Thiol films on Au have been the subject of extensive study over the past decade, both because of their relatively unique ability to form high quality thin films spontaneously and their ability to easily form highly blocked surfaces on metals [6,7]. The presence of defects in the films has led to some difficulty in data interpretation and forced efforts to avoid such defects. In this thesis the use of Hg as a substrate for these films is introduced in chapter 4. The films formed on Hg were found to be more nearly perfect than those on other surfaces, and so warranted a detailed characterization. Because these interfaces are essentially blocked they were again most readily studied using impedance techniques.

In the remainder of this chapter a number of the basic concepts important to the other thesis chapters are introduced, beginning with the nature of various interfaces.

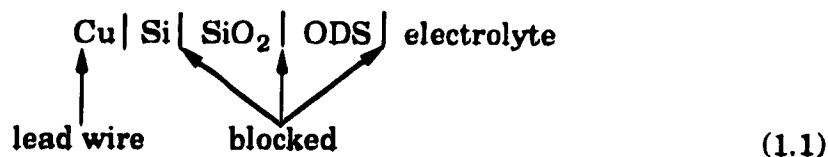
1.1 Blocked and Unblocked Interfaces

At the reversible metal/electrolyte interface, charged species may move across the interface to relax any solution activity change. Likewise, if the interfacial potential is changed, some species will undergo electrochemical reaction and thereby change their activities [8,9]. In the process, electrical current passes between the electronically conducting solid and the ionically conducting electrolyte. An interface that allows the free exchange of ionic charge or electronic current is termed unblocked. Reference electrodes pass electrons or ions at high exchange current density, and as a class are nearly ideally unblocked. Blocked interfaces have the exact opposite characteristics of unblocked interfaces [10-12]. The only type of current flowing at a blocked electrode is due to capacitive charging and discharging current. So, when a direct potential is applied, an unblocked interface develops a steady-state current, while the current through a blocked interface decays to zero.

1.1.1 Blocked Electrode-Electrolyte Interfaces

The SiO₂/electrolyte interface is blocked. Elemental silicon is oxidized in air and forms about 20 Å thick silicon dioxide layer, which is referred to as a native oxide layer. Typically, thick insulating films in the range from 100 Å to 1000 Å are deliberately grown to obtain a well passivated silicon surface. Electronic conductivity across these films is negligible under most circumstances [13]. Moreover, at room temperature ions do not enter the insulators (SiO₂ and Si₃N₄ are the most common insulators) or readily move across them [14,15]. Thus, the insulators do not conduct ionically either. As a dielectric material, the insulators can easily support the few volts of applied potential used in electrochemical experiments [16]. Ionization of the surface silanol groups or surface binding of ions are the kinds of interactions the SiO₂ undergoes with the electrolyte solution at the interface [17-19]. These are all characteristics of a blocked interface.

We have studied two types of "membranes" on Si/SiO₂. Octadecyldimethylchlorosilane (ODS) bonded to silicon dioxide is one of them. ODS bonded to silica is widely used in reverse-phase chromatography. As a monomolecular layer, it may seem not to have two outer surfaces to qualify as a membrane. However, from liquid reverse-phase chromatographic studies, the bonded phase is, in general, known to have significant effect on solute retention. This indicates that ODS can be treated as a layer.



There is neither ion exchange nor Faradaic current passing at the electrolyte/ODS interface. The only process that takes place is adsorption. The ODS/electrolyte interface is therefore blocked.

The potential at the blocked interface should arise because of accumulation of charge and alignment of dipoles [10,11]. In other words, the adsorption of ions can determine the surface potential. The entire analysis of the potential determining ion, based on the rigorous thermodynamic analysis of Gibbs adsorption isotherm, has been extensively tested on the blocked mercury/electrolyte interface. Comparable treatments on interfaces like ODS/electrolyte cannot be made, because on solids, parameters like the surface tension are not directly measurable. This problem is instead normally treated by a combined theory of site coordination and double layer models [14,15,17-19]. Aspects of this theory are presented in chapter 3.

The mercury/thiol film is one of the several interfaces we examined. On exposure to alkane thiols, a self-assembled, compact monolayer forms on the mercury surface. Because of its reversible, unblocked interface, in the past bare mercury was the most used polarographic metal indicating electrode. With a thiol film coating on the Hg, charge transfer to redox couples is prevented by the low permeability of the coating.

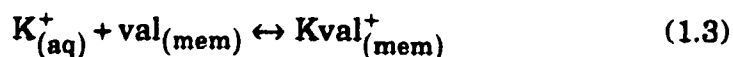


Most of the applied potential drops across the thiol dielectric. It is thus clear that the Hg/thiol and thiol/electrolyte interfaces should behave like blocked interfaces.

1.1.2 Unblocked Membrane-Electrolyte Interfaces

The second type of membrane on the Si/SiO₂ that we studied was a thick, ion selective, polymer membrane. The vast majority of polymer matrix based, ion selective electrodes prepared use poly(vinyl chloride) (PVC) membranes [20-22]. In addition to the ionophore, i.e., the ion selective component such as valinomycin (val), the PVC-based membrane normally incorporates an organic solvent as a plasticizer. The plasticizer offers improved mobility of free and complexed ionophore, establishes the dielectric constant and provides suitable mechanical properties for the membrane. To reduce the interference of lipid soluble ions, a lipophilic ionic salt is also incorporated into the membrane.

The simplest view for interfacial potential generation at a nonblocked interface is that the ionophore, depending on its selectivity towards the ions in solution, is capable of coordinating and transporting ions into the membrane [21,22]. This results in a charge imbalance in the interfacial region that leads to an interfacial potential, known as the Donnan potential.



The coordination reaction between potassium and valinomycin is very strong. As the bathing ion activity changes, the charge imbalance within the membrane also changes. The process stops itself at an interfacial potential commensurate with the electrolyte activities, and this potential is measured to obtain analytical information. The excess of charge within the membrane falls from its highest value closest to the solution to zero somewhere inside the membrane. This creates a space charge in the membrane. The thickness of the space charge (Debye length) is typically in the order of 100 to 1000 Å [23]. This width is negligible in comparison to the thickness of membranes normally used. A thorough description of the potential generation processes which occur at the membrane is outside the scope of this introduction. It is adequate for us to know that the charge exchange at the membrane/electrolyte interface is stable and reversible (i.e., unblocked) towards the potassium ion, and that the membrane space charge width is negligible.

Analogous to its interaction at the electrolyte interface, the interaction of SiO₂ with a membrane interface is limited to protonation or deprotonation of the silanol charge. Unlike a reversible electrode, whose potential is determined by the free exchange of ions and electrons, the membrane-insulator interfacial potential is not thermodynamically well defined. It is, however, poised by adventitious reactions. Therefore, the membrane-insulator interface can be treated as a blocked interface. The typical shorthand form of the SiO₂/membrane half cells we considered, including the nature of the interfaces is given below.

1.2.1 Carrier concentration of semiconductors [24,25]

A pure silicon crystal consists of an orderly three-dimensional array of atoms. The crystal lattice consists of $5 \times 10^{22} \text{ cm}^{-3}$ silicon atoms, each atom covalently bonded to four other equidistant neighbours in a tetrahedral arrangement. The band theory of solids has been successfully used in explaining the electronic structure of semiconductors. The number of valence electrons of the atom determines the occupancy of the resulting solid bands. The highest filled band of the semiconductor is called the valence band and the lowest empty band is called the conduction band. The energy difference between these levels is the band gap. The band gap energy of silicon is 1.12 eV.

In order to control the electronic properties of semiconductor junctions and decrease energy loss due to charge carrier movement, impurities are usually intentionally introduced. This process, which is called doping, serves to decrease the resistance and control the Fermi level of the semiconductor as well. At absolute zero temperature, all the valence electrons are firmly localized in the valence band. At higher temperatures, the thermal motion manages to set some electrons loose and promote them into other bands. This process leaves an electronic vacancy in the valence band. The electronic vacancy is referred to as a hole. Like an electron, a hole can act as a charge carrier. The movement of an electron in one direction in an electric field is equivalent to the movement of holes in the opposite direction.

Both electrons and holes are charge carriers. The equilibrium carrier concentration of an intrinsic semiconductor is given by:

$$n_i p_i = \text{"constant"} \exp\left(-\frac{E_g}{kT}\right) \quad (1.5)$$

where E_g is the band gap energy, n_i and p_i are the concentration of generated electrons and holes respectively.

Dopant atoms can be either donors or acceptors. If it is desired to enhance the free electron concentration, the electron donor atoms are chosen so as to have available for bonding one electron more than the four needed for substitution in the silicon lattice. The dopant is then very easily ionized to produce an electron in the conduction band and a positive charge on the dopant atom. Elements such as phosphorus, arsenic, or antimony will act as donors. It is possible to increase the hole population by introducing atoms which have one valence electron less than the number needed for complete bonding with neighboring silicon atoms. These acceptors become ionized to produce holes in the valence band and negative charges on the dopant site. Elements such as boron and aluminum serve as acceptors in silicon. A material that has been doped with acceptors is called a p-type semiconductor, while one that has been doped with donors is called an n-type semiconductor. The predominant charge carrier is called the majority carrier, so electrons are the majority carrier in an n-type semiconductor and holes are the majority carriers in a p-type semiconductor.

Equation 1.5, often called the mass action law, is valid for doped semiconductors as well. For doping densities of either donor, N_d , or acceptor, N_a , in the range of 10^{14} to 10^{17} cm^{-3} , the carrier concentration of the dopant is so much larger than the thermally generated similarly

charged carrier concentration that $N_d \gg n_i$, or $N_p \gg p_i$ respectively.

1.2.2 The capacitance of the MOS structure [24,26]

The underlying principle behind the function of field effect devices is that the number of charges at the surface of a semiconductor device based on an insulator/semiconductor interface can be changed by an electric field. The conventional metal-oxide-semiconductor (MOS) system, whose cross sectional view is illustrated in figure 1.1, can best be used to explain this effect. The MOS structure is a two terminal device composed of an SiO_2 layer sandwiched between silicon substrate and a metallic field plate. A second metallic layer present along the back or bottom side of the semiconductor provides a contact between the silicon and the outside world. The terminal connected to the field plate and the field plate itself are referred to as the gate; the silicon contact, shown grounded, is simply called the back contact.

Under dc conditions, no current can flow from the gate to substrate because of the presence of the silicon dioxide insulator and, as a result, the capacitor is in thermal equilibrium and can be treated accordingly. There are three regions of interest when the capacitance of the MOS capacitor is plotted as a function of voltage. The case of a MOS capacitor fabricated on an n-type substrate is treated here.

Accumulation: If a positive potential is applied to the gate, the majority carrier electrons will be attracted toward the oxide-semiconductor interface. This particular situation, where the majority carrier

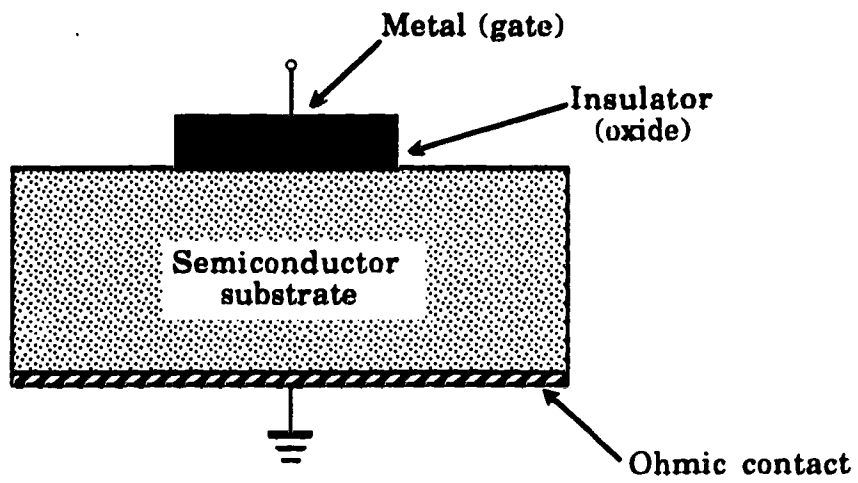


Figure 1.1 The basic MOS capacitor structure.

concentration is greater near the oxide-semiconductor interface than in the bulk of the semiconductor is known as accumulation. In accumulation the metal side has an excess of holes, while an equal excess of electrons exists at the semiconductor interface. Both charge sheets are very thin because of the large number of available states in the two materials. The capacitance is well represented by two thin charge sheets separated by the SiO₂ layer.

Depletion: A negative gate potential applied to the metal tends to drive away electrons in the semiconductor. The electrons are removed from the dopant atoms leaving behind positively charged donors. The number of charges that need to be removed is generally far larger than the dopant atoms that are present in just one atomic layer of the substrate. Thus, it is required that more carriers be removed from atoms further into the bulk of the semiconductor so that charge balance is achieved. This situation, where the electron and hole concentration at the oxide-semiconductor interface are less than the background doping concentration (N_a or N_d), is known as depletion. Now the potential drops across both the insulator and the depletion layer. The MOS capacitance becomes a series combination of the SiO₂ and depletion layer.

Inversion: Suppose the applied potential is taken increasingly negative, the depletion region will continue to widen uncovering more donor dopants. The silicon surface becomes sufficiently positive to attract a significant number of holes. These holes come from the relatively slow process of electron-hole generation in the depletion region. Eventually, with a sufficiently high negative voltage the density of the holes will exceed that of the electrons at the surface. This is a situation opposite from that normally expected in an n-type material and is referred to as inversion.

1.2.3 The gate is replaced by an ion sensitive layer and reference electrode

From the above discussion, it is clear that the density of the mobile carriers in the semiconductor is influenced by an electric field effect. Electric fields are transmitted across vacuum or matter. It is not necessary that a metal electrode on the insulator be used to make the gate contact. Bergveld was the first to take advantage of this fact for the purpose of ion sensing [27]. He replaced the gate (plate and terminal) by a reference electrode and a conducting solution; and isolated the reference gate from the insulator (SiO_2). The electrolyte in addition to being the test solution served as the electrical contact, while the gate oxide was used as the chemical (in particular pH) sensitive element. This opened the area of ISFETs.

The first developed, most frequently described, and commercially available ISFETs are of the pH sensitive type. There is a need to determine ions other than pH. Three different approaches have been explored; chemical grafting, ion implantation, and sensitive membrane deposition are being examined to modify the gate [28]. In the case of chemical grafting the original chemical surface groups that provide the pH sensitivity are chemically coupled to a compound whose terminal group is sensitive to other ions. Cyanosilane, phosphonate, trimethylamine and phosphonatobetaine groups chemically bonded to the silanol of the insulator have been used for the determinations of Ag^+ , Ca^{+2} , UO_2^{+2} , and NO_3^- respectively [29,30]. There are a small number of reports in which the gate insulator is modified by ion implantation. The ion sensitive layer is

supposedly buried in the insulator and is believed to act in a similar way to that of glass electrodes. Li^+ , B^+ , Al^+ , Ga^+ , In^+ , Tl^+ , and Si^+ implanted Al_2O_3 , SiO_2 and Si_3N_4 layers have shown some response to H^+ , Na^+ and K^+ [31-33]. The method has so far been limited to these three cations and even then the responses obtained are not satisfactory.

The third and most widely reported method of sensitization is the physical deposition of thick films of ion sensing substance on to the gate. Insoluble silver halide salts held together by silicone rubber have been shown to be sensitive to F^- , Cl^- , and Br^- [34]. A layer of the sensing substance can be vapor deposited on top of the passivating insulator. LaF_3 , AgCl , AgBr have been deposited in this mode for the determination of the halide ions of the deposited salts [35-38]. Organic based polymeric membranes incorporating an ionophore have more often been used than the above methods. The deposition can be done by a one step casting of the plasticized polymeric ion sensing membrane or the copolymerization of the ionophore on to the gate. Membrane covered ISFETs sensitive to calcium, sodium, ammonium, and nitrate have been reported [30,39]. The membrane deposition (inorganic or polymeric) method provides a multitude of options in getting diverse types of ISFETs.

1.2.4 The MIS and ISFET structures [1-5]

The influence of electrical field on the charge distribution at the insulator-semiconductor interface has been described in section 1.2.2. A MOS whose gate side has been replaced by an ion sensitive layer is referred

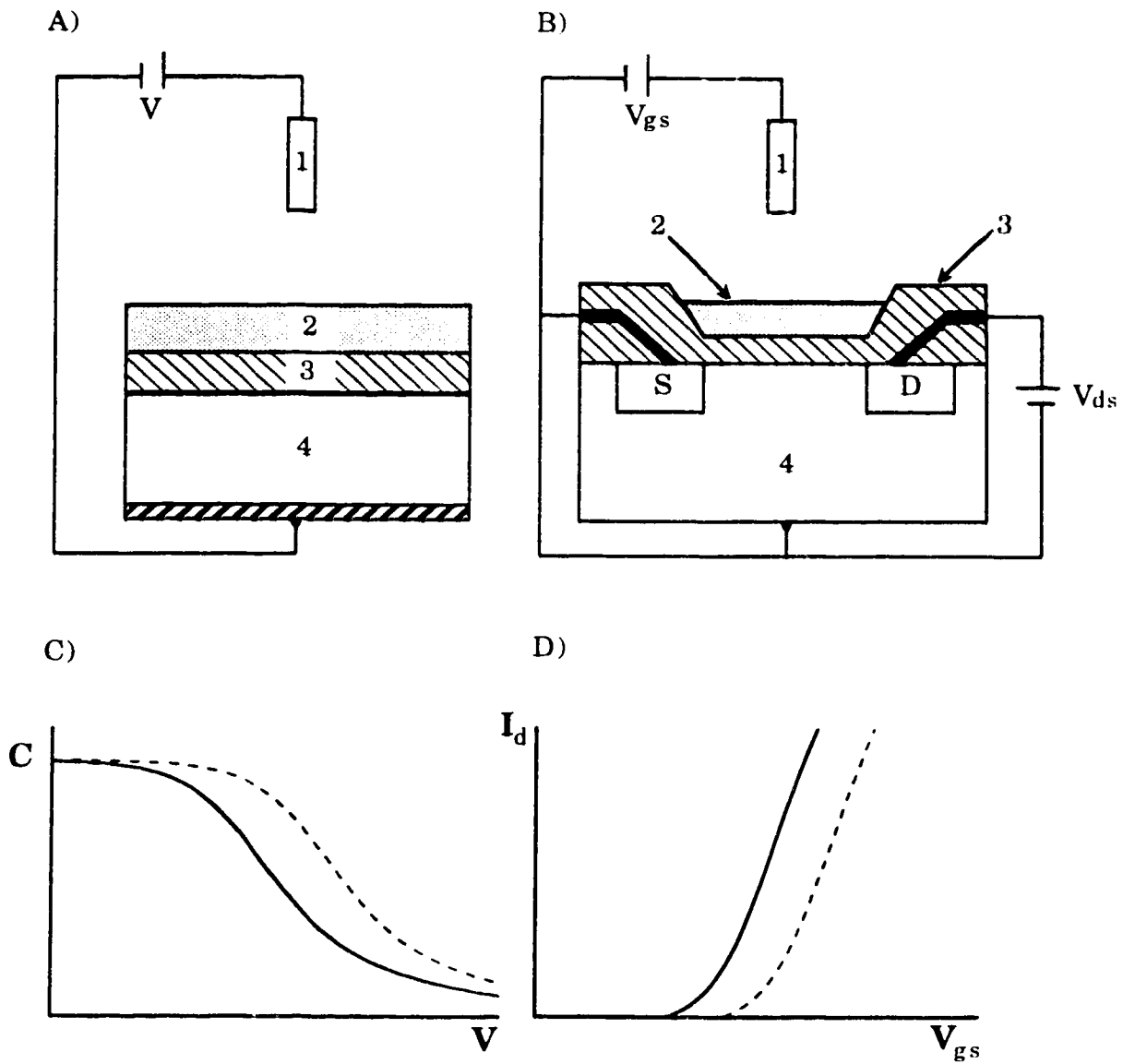


Figure 1.2 Schematic illustration of a typical MIS, A; and ISFET, B. C is the capacitance versus voltage characteristic of the MIS and D is the drain current versus gate voltage characteristic of the ISFET. The dashed lines indicate electrical characteristics with parallel shift along the voltage axis. 1, reference electrode; 2, ion sensitive membrane; 3, gate oxide; 4, substrate Si; S, source; D, drain; V_{gs} , gate-source voltage; V_{ds} , drain-source voltage.

to as a membrane-insulator-semiconductor system, abbreviated as MIS; while a transistor with a similar layer is called an ISFET (figure 1.2).

The operation of the ISFET involves a flow of current between the source and drain, which are separated by several micrometers of semiconductor region called the channel. The current between the source and drain, I_d , depends on the channel conductivity. This conductivity is in turn controlled by the electric field at the semiconductor surface under the gate, which reflects the gate-source voltage, V_{gs} . The potential determining processes at the solution-membrane interface are similar to those in conventional ion sensitive electrodes. Thus, the gate-source voltage will be modulated by the solution-membrane interfacial potential which depends on the ionic concentration of the solution. As a result, I_d vs V_g measurements will show ion concentration dependence as shown in figure 1.2d. In the case of the MIS, at a given value of the reference potential, the capacitance of the device will shift by an amount determined by changes in the membrane-solution interfacial potential (figure 1.2c). A more detailed explanation of the CV analysis used to obtain interfacial potential changes is outlined in chapters 2 and 3. The method involves AC impedance measurements to obtain the capacitance-voltage curves.

1.3 Interfacial potential difference

The plane of contact between two immiscible bulk phases defines the interface. When two phases are in contact there is a tendency for any charged constituents, either electrons or ions, to be attracted to different

degrees into the two phases and for molecules with a permanent dipole at the surface to be oriented selectively with respect to the two phases. The resulting electric field may also cause polarization effects in neighboring molecules. All of these effects tend to produce a difference in the electrical potential between the interior of the two phases. Below we define the various types of potential differences, following the discussion of Hunter (40), that make up the total interfacial potential difference.

Let us first consider purely electrostatic effects by using a homogeneous spherical mass of material (phase α), radius r , net charge Q , situated beside a vacuum. The difference in potential is measured by the work required to move a test charge from one point to the other. At a large distance, d , from the sphere, ($d \gg r$) the coulomb potential as probed by the test charge, varies with $1/d$. When the test charge gets close enough that $r \gg d$, then the coulombic potential remains constant. However, in this and closer distance ranges, the test charge induces an equal and opposite charge in phase α , known as the image charge. Thus, at very short distances from the surface the potential due to the image force is predominant. At very long distances (from 10^{-3} cm to ∞), the coulombic force determines the potential. In the intermediate region, the image force is negligible, yet $d \ll r$, so that the potential is constant. Figure 1.3 depicts the discussed variation of potential as a function of distance.

The outer potential or Volta potential Ψ is defined as the work necessary to bring the test charge from ∞ to the neighbourhood of the surface where the image force begins to have an effect. Since Ψ is a potential difference between two points of the same dielectric fluid (namely, a vacuum) it can easily be measured.

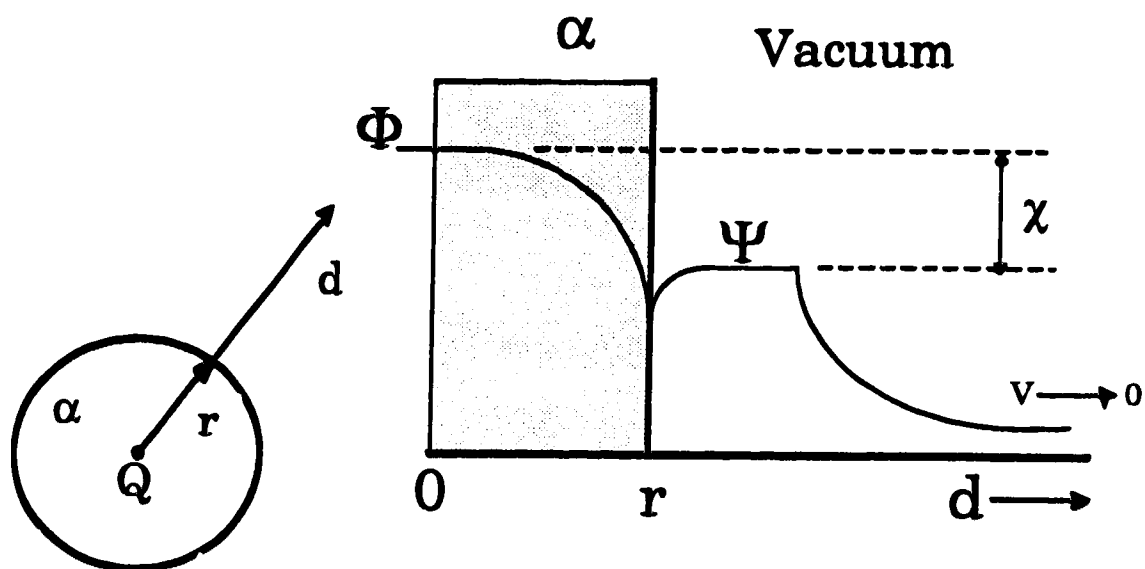


Figure 1.3 Schematics showing the variation of the coulombic potential as a function of distance.

In general, at the interface not only is there charge separation, but there is also preferential orientation of molecular dipoles. Since work has to be done to traverse the surface dipole layer, the corresponding potential is termed surface potential and is represented by χ . The term used for the total or absolute potential across the electrified interface is inner potential or the Galvani potential and the symbol used is Φ .

$$\Phi = \Psi + \chi \quad (1.6)$$

Neither Φ nor χ is experimentally measurable. The difficulty is that the test charge in reality has to be some physical entity such as an electron or ion. Therefore an actual test charge in being transported across the interface in to α , not only encounters the net interfacial charge and the surface charge already discussed, but once inside α it also undergoes different kinds of interactions with the bulk phase. This interaction is equated to the chemical potential of the particle "i" in α , μ_i^α . The sum of the total work done in transferring a species "i" of charge Z , from vacuum into the interior of α is defined as the electrochemical potential $\tilde{\mu}_i^\alpha$.

$$\tilde{\mu}_i^\alpha = \mu_i^\alpha + Z_i F \Phi^\alpha \quad (1.7)$$

$\tilde{\mu}_i^\alpha$ is only conceptually separated into a chemical term μ_i^α and $Z_i F \Phi^\alpha$. It includes all types of work and is therefore a measurable quantity.

For the equilibrium distribution of species "i" between two phases α and β , the following equation holds:

$$\bar{\mu}_i^\beta = \bar{\mu}_i^\alpha \quad (1.8)$$

Because μ depends on the chemical composition and not on the electrical state it is the same in two phases of the same chemical composition. The surface potentials of two phases of the same composition must be identical. Hence, the difference in inner potentials of phases of the same composition becomes:

$$\Phi^\beta - \Phi^\alpha = \Psi^\beta - \Psi^\alpha \quad (1.9)$$

Like the individual outer potentials, this difference is a measurable quantity. A voltmeter is used to measure the electrochemical potential difference obtained by two metal probes. This process introduces additional interfaces and associated potentials. However, using the reasoning used to get equation 1.9, it can be shown that the measured potential obtained using two pieces of the same metal is equal to the Volta potential difference across arbitrary phases α and β [41].

In summary, the electrochemical potential is conceptually understood to have three contributing terms; χ , Ψ , and μ . At equilibrium, there is no electrochemical potential gradient for any species across an interface and the measurement of a voltage difference between two pieces of the same metal is a measure of the difference in the electron electrochemical potential between the pieces. This potential difference is equal to the outer potential difference of the phases containing the metal probes.

1.4 Ion pair chromatography

High-performance liquid chromatography (HPLC) has proved phenomenally successful for the separation and analysis of multicomponent mixtures of nonpolar and polar substances. In particular, reversed phase HPLC with chemically bonded alkylsilica is now characterized by its great operational simplicity and flexibility; its ability to simultaneously separate a wide variety of compounds, both closely related and widely different in structure; and most importantly by its high resolution. The term reverse phase as it is commonly used implies the use of a polar eluent with a non-polar stationary phase. Covalently bound octadecyldecane on silica powders has been extensively used as a stationary phase [42-44]. In fact at present, it is estimated that nearly 80% of all separations performed by HPLC are carried out in reverse phase mode with chemically bonded phase packings [42].

The limitations of ion exchange columns and the high performance of the alkylsilane bonded phases has prompted workers to investigate the usefulness of reversed phase HPLC using organic eluents for the separation of ionized solutes. However, samples in their ionic form are eluted in a time close to the dead time in conventional reversed phase HPLC, i.e., they are not strongly retained by the alkane phase. Another major constraint of the silica bonded phases is the limited pH range between 2.5 and 7.5 over which they are stable. This is troublesome in the separation of poorly retained strong acids and bases whose dissociation constants are either outside or close to the boundaries of this range. The addition of an ion-pairing, moderately hydrophobic surfactant (modifier), below its critical micelle

concentration, into the eluent improves the selectivity for ionic species and increases their retention times markedly [43]. This method is widely known as ion pair chromatography.

Depending on the polarities of the functional groups attached to the silica, two different types of ion pair chromatography are distinguished: normal phase and reversed phase. In normal phase ion pair chromatography, which was the first one to be used, generally, an aqueous solution containing the desired ion pair reagent is applied as a coating onto silica powder to serve as the stationary phase, while the eluent is a weakly polar phase. In reversed phase ion pair chromatography however, the role of the chemically bonded stationary phase is considered to be of lesser importance. In this mode a salt composed of a large hydrophobic ion (modifier) and a small hydrophilic, oppositely-charged ion is added to the aqueous/organic mobile phase. In the presence of the modifier, analyte ions whose charge is opposite to that of the modifier ion experience a marked increase in retention.

Different theories have been presented to explain the observed phenomena of ion pair chromatography. One model directly extrapolated from liquid-liquid ion pair chromatography is the solvophobic theory [42-44]. The model states that the ionized sample forms a stoichiometric complex in the mobile phase with an ion of opposite charge supplied by the counter ion reagent. The neutral ion pair then partitions into the organic stationary bonded phase. However, there is experimental evidence that the amphiphilic modifier reagent can get adsorbed on to the stationary phase on its own too. This would imply that ion pairing would occur on the surface of the stationary phase. The model which postulates this is commonly referred

to as the dynamic ion exchange model [43]. It is called dynamic ion exchange because according to the model the stationary phase becomes a dynamically formed ion exchanger due to binding of the modifier from the mobile phase. Another variation of the dynamic ion exchange model is the dynamic complex exchange model. The most important assumptions of this model is that the modifier in the mobile phase forms ion pairs with the solute which migrate to the surface. There, these solutes are exchanged between the solution phase ion pair and the modifier ions covering the solid stationary phase.

All the models mentioned so far assume that stoichiometric complexes are formed between the solute and the modifier molecules. A non-stoichiometric type of treatment of ion retention is the double layer model developed by Cantwell et.al. [44-47]. In this model the modifier is adsorbed on to the stationary phase. The resulting charged surface establishes an electrical potential distribution, and the sample ion responds to the electrical potential according to the expectations of Stern-Gouy-Chapman double layer theory, with the adsorbed modifier acting as a potential determining ion.

Whatever the mechanism, the amount adsorbed has to be quantitatively determined if a mechanistic study is performed. For example, if a UV-visible spectrophotometer is to be used as a detector, the solute should have the proper chromophoric group. In any analysis scheme that can be devised, several steps would be required which include initial equilibration, followed by the elution of the adsorbed substance and finally its quantification using a detector. The amount of adsorbed material is then assumed to be directly involved in the chromatographic equilibria leading to

separation, either as a potential determining ion, or an ion-pairing reagent.

In our studies we use a silanized silicon dioxide electrode that is based on silicon. Net charge that is adsorbed on the silane surface alters the space charge potential in the semiconductor by a field effect. It is possible to measure this change directly and in situ using the impedance technique. The surface of the electrode, and the substrate onto which it is chemically bonded is the same reversed phase packing material as in reversed phase chromatography. This technique provides an alternate means to study the adsorption phenomena based on measuring potential changes rather than mass changes. It takes advantage of the behaviour of blocked interfaces in order to measure the potentials.

1.5 AC Impedance Analysis

The rapid and accurate measurement of electrochemical phenomena is of considerable importance in a range of fields, including semiconductors, batteries, electrodeposition, corrosion and the characterization of organic polymers [48-50]. It is possible to measure phenomena such as corrosion rate or battery life by direct analytical methods, for example, weight loss measurements or solution analysis by spectroscopy; because the processes are slow these methods are time consuming and inefficient. Several processes can take place concurrently at the Si/SiO₂/membrane/electrolyte or metal/electrolyte interface including charged species exchange, solvation, adsorption, diffusion, space charge and surface states relaxation, etc. Because most of the processes are electrochemical, it is possible to analyze

them using electrochemical techniques. Direct current or voltage methods such as cyclic voltammetry can be used. However, these techniques require relatively large perturbation (or polarization) signals which inevitably changes the properties of the system. In AC impedance analysis small excitation signals from 5 mV to 10 mV peak to peak are used with the system at a state close to equilibrium. By using AC excitation, only those processes which have sufficient time to occur during the alternation of the electric field are observed, so that ultimately each process can be delineated by applying an input signal over a range of frequencies. AC impedance analysis is a suitable method to the study of blocked interfaces as they involve charging and discharging current whose responses are directly affected by frequency changes. Electrochemical interfaces can be viewed as a combination of passive electrical circuit elements, i.e., resistance, capacitance and conductance, that collectively have an impedance behaviour which is mathematically derivable. In instances where the electrical elements, their magnitudes, their circuit arrangement or all are unknown, AC impedance analysis gives the experimentalist a means of obtaining this information. In this section the basic concepts of the method and simple graphical methods of interpreting the AC impedance spectrum that we used are outlined.

1.5.1 Modes of representation of impedance

In an AC experiment a sinusoidal voltage is applied to a cell and the current passing through the cell as a result of this perturbation is determined (Figure 1.4) [51]. In dc measurements the current flowing, I , is related to the potential, V , by just one parameter, the resistance R . The resistance is defined by Ohm's Law:

$$I = \frac{V}{R} \quad (1.10)$$

In an AC measurement two parameters are required to relate the current flowing to the applied potential. One represents the opposition to the flow of charge and is equal to the ratio of the maximum voltage and maximum current, and is analogous to the resistance in dc measurements. The other parameter θ , is the phase difference between the voltage and current (figure 1.4b). The combination of these parameters represents the impedance, Z , of the cell.

Having a magnitude and phase difference, Z is clearly a vector quantity. There are three common ways of presenting impedance. One is by its polar coordinate (sometimes called phasor diagram). The distance of the point from the origin of the axes corresponds to the magnitude of the impedance and the angle formed with the x-axis corresponds to the phase difference between the voltage and current (figure 1.5). The impedance may also be represented by its X and Y components in the cartesian coordinate. The third representation is a complex impedance plane plot. This concept is derived from the complex number plane. The impedance in this case is

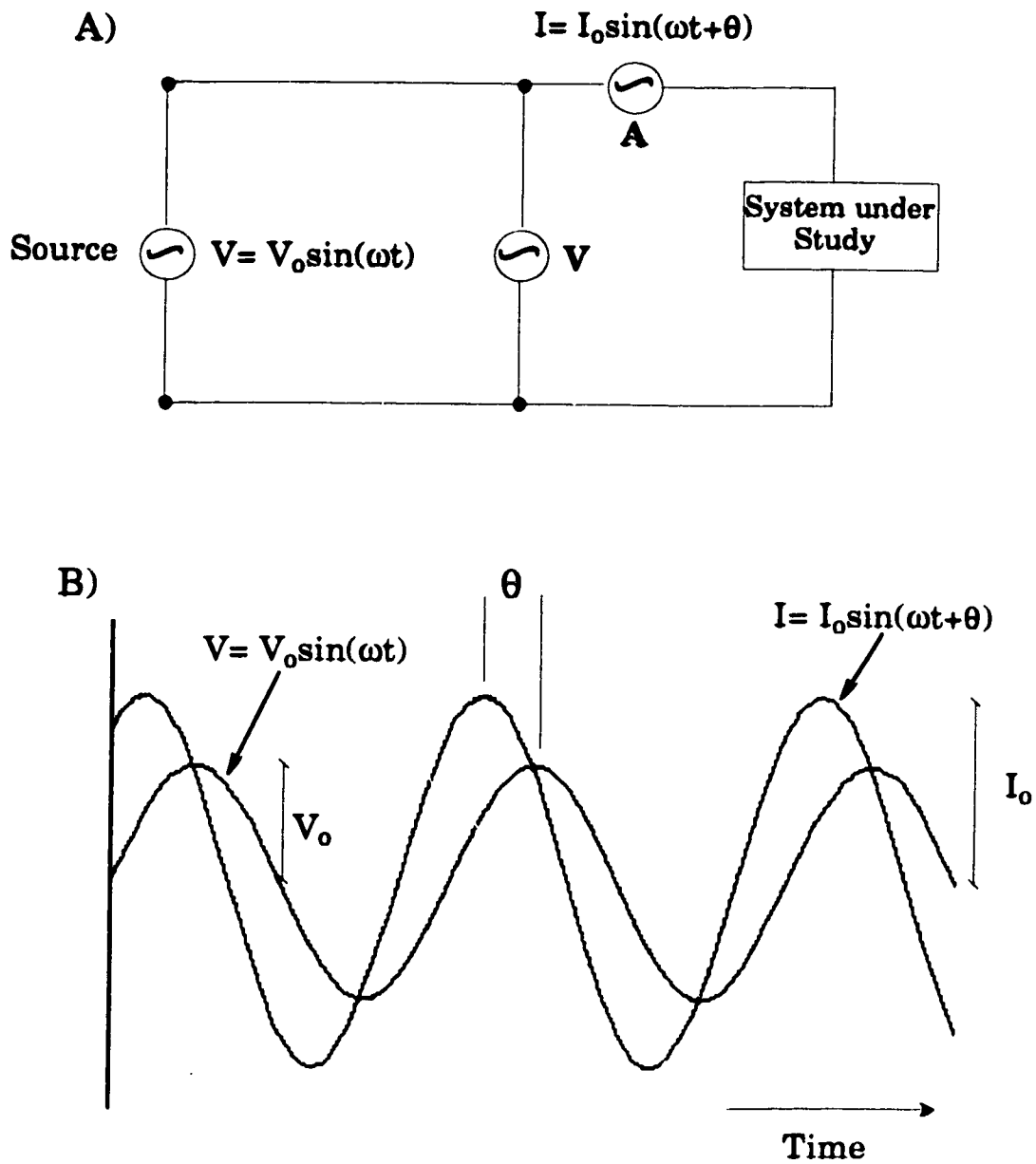


Figure 1.4 A generalized impedance experiment, A; in which AC wave form applied to the system under study and the impedance is obtained from the resultant AC current and their phase relationship, B.

given as a complex number;

$$\mathbf{Z} = Z_R - jZ_I \quad (1.11)$$

Z_R is the magnitude of the real component and the Z_I is the imaginary component of \mathbf{Z} . The mathematical convention for expressing quantities in this coordinate system is to multiply the Z_I coordinate value by $\sqrt{-1}$, symbolized by "j". The complex number representation is valuable since the rules of complex algebra may be used to calculate the impedance of circuits knowing the impedance of the individual components. $|\mathbf{Z}|$ is known as the modulus (magnitude) of the impedance and θ the argument. From simple trigonometric considerations:

$$|\mathbf{Z}| = \sqrt{Z_R^2 + Z_I^2} \quad (1.12)$$

and the phase angle is:

$$\tan(\theta) = \frac{Z_I}{Z_R} \quad (1.13)$$

Note that there is nothing "imaginary" about the imaginary component of impedance. The imaginary component is a measurable quantity and represents that portion of the output signal which is out of phase with the input.

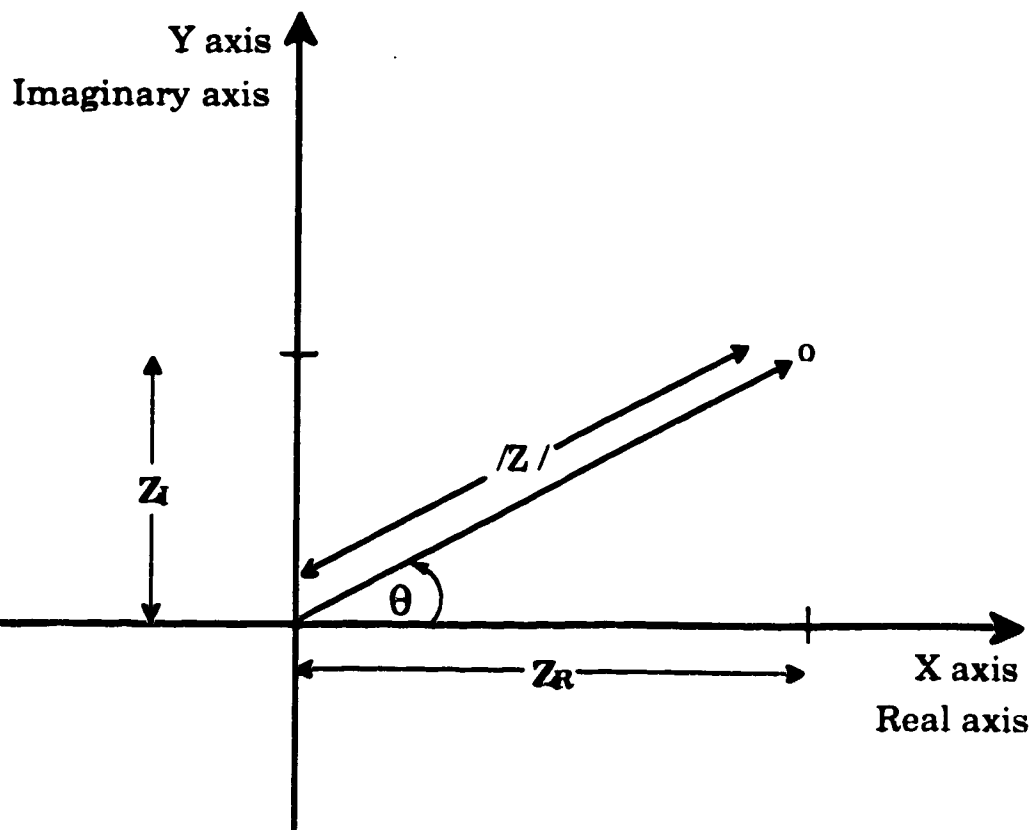


Figure 1.5 Representation of the impedance, Z , on a vector diagram. Z_R and Z_I are the real (X-axis) and imaginary (Y-axis) coordinates of the complex impedance Z . $|Z|$ is the modulus of Z and θ is its phase shift relative to the input voltage.

1.5.2 Response of single electrical elements to AC signal

Before turning to electrochemical cells that have more than one circuit element, let us develop the sinusoidal current-voltage relations of a resistor and a capacitor. Let the sinusoidal input signal, $E(t)$, be of the form

$$E(t) = V_o \sin(\omega t) \quad (1.14)$$

where V_o is the AC signal amplitude, ω is the angular frequency in radians/sec⁻¹ ($\omega = 2\pi f$, where f is the frequency in Hz), and t is the time. If $E(t)$ is applied across a pure resistor of magnitude, R , the resultant time varying current, $I(t)$, can be determined using Ohm's law:

$$I(t) = \frac{V_o}{R} \sin(\omega t) \quad (1.15)$$

Clearly, the magnitude of the impedance $Z=R$, and the phase angle is zero for all frequencies. Across a capacitor, C ;

$$I(t) = C \frac{dE(t)}{dt} \quad (1.16)$$

In expanded form

$$I(t) = \omega C V_o \cos(\omega t) = \omega C V_o \sin(\omega t - \pi/2) \quad (1.17)$$

Thus the current response of the capacitor will lead the input voltage signal by 90° (one quadrant). For this reason, the impedance consists only of an

imaginary component. The impedance is the ratio of voltage to current,

$$Z = \frac{V_o \sin(\omega t)}{\omega C V_o \sin(\omega t - \pi/2)} \quad (1.18)$$

Equation 1.18 shows that the impedance is now dependent on the frequency, according to the relationship $Z = 1/\omega C$. As the frequency increases the magnitude of the impedance decreases.

1.5.3 Impedance of electrochemical cells

The most common components required in modelling of electrochemical cells are resistors and capacitors. Having learned what the impedance of each of these individual elements are we turn now to the impedances of these combined elements. When components are connected together in series the individual impedances are additive.

$$Z_{\text{Total}} = Z_1 + Z_2 + Z_3 + \dots \quad (1.19)$$

For a resistor and capacitor in series:

$$Z_{\text{Total}} = R - \frac{j}{\omega C} \quad (1.20)$$

Z_{Total} has a real and an imaginary component and changes with frequency. This information can be represented by one of several graphical methods. The Nyquist plot (Cole-Cole or Argand plot) uses real (X-axis) and

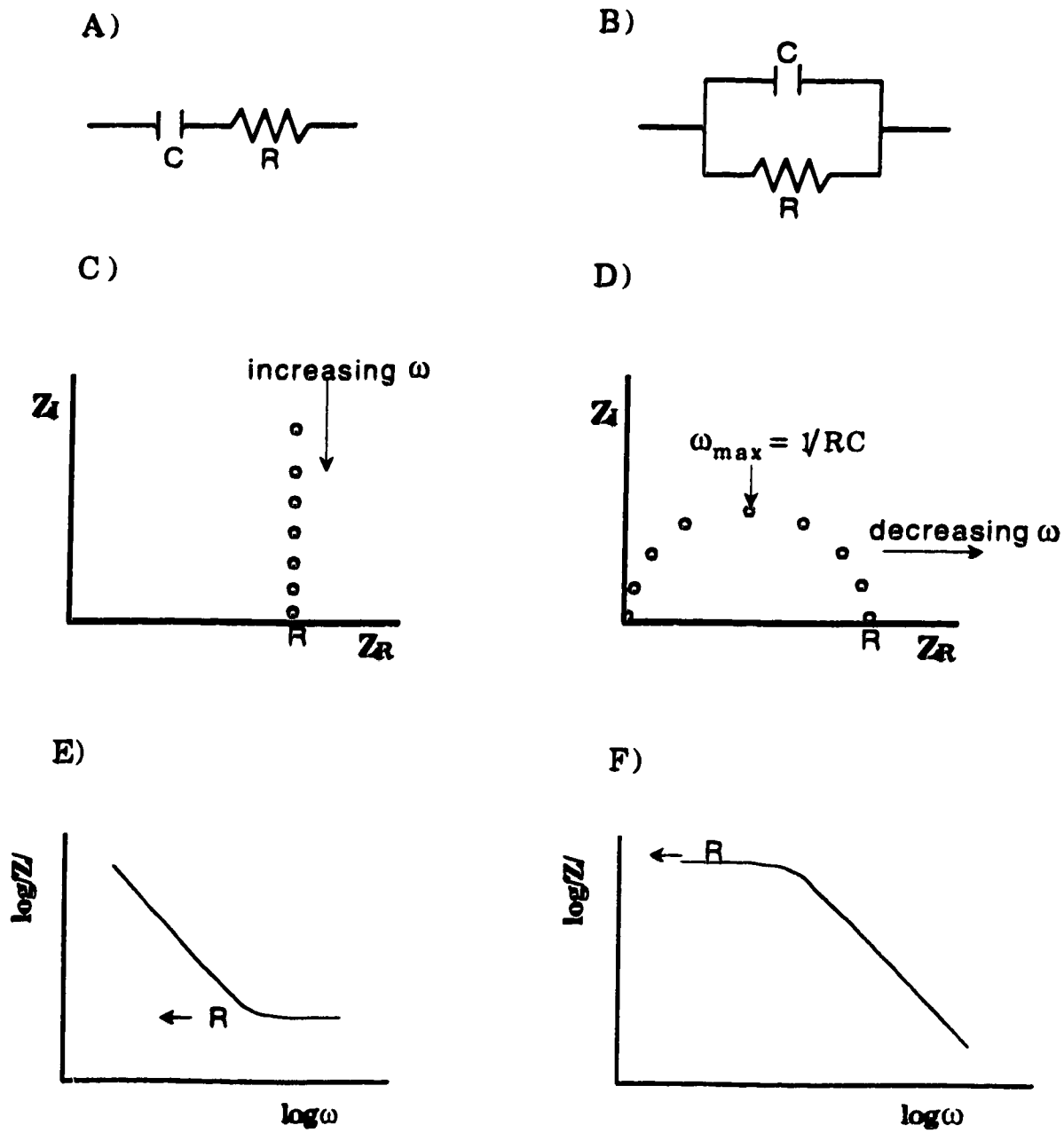


Figure 1.6 Nyquist (C, D) and Bode plots (E, F) for a series and parallel RC circuits.

imaginary (Y-axis) coordinates and displays each frequency impedance measurements as a single point. The other frequently used plot is known as the Bode plot. It is a graph of $\log|Z|$ vs $\log\omega$ or θ vs $\log\omega$. There are other formats but we only use these two and they are demonstrated in figure 1.6.

When components are connected in parallel the impedance are not directly additive, but their complex admittance, \mathbf{Y} , which is the reciprocal of impedance is. Thus

$$\mathbf{Y}_{\text{Total}} = \mathbf{Y}_1 + \mathbf{Y}_2 + \mathbf{Y}_3 + \dots \quad (1.21)$$

The admittance of a resistor and capacitor respectively are $1/R$ and $j\omega C$. So for a parallel combination, the total admittance is given by:

$$\mathbf{Z}_{\text{Total}} = \frac{R}{1 + (\omega CR)^2} - \frac{j\omega CR^2}{1 + (\omega CR)^2} \quad (1.22)$$

It can be shown that equation 1.22 on a Nyquist plot gives a semicircle that is centered at $Z_R = R/2$ and a radius of $R/2$ (figure 1.6). Note that $-Z_1$ is plotted on the ordinate to give plots in the first quadrant, as is conventionally done. At the apex of the semicircle, ω_{max} , the magnitude of the impedance of the resistor and capacitor are equal.

$$R = \frac{1}{\omega_{\text{max}} C} \quad (1.23)$$

Thus

$$\omega_{\text{max}} = \frac{1}{RC} \quad (1.24)$$

The time constant τ for this network is simply the reciprocal of ω_{max} . It is therefore possible, to obtain the values for R and C from a complex impedance plot as shown in figures 1.6d. Equation 1.20 shows that for high frequencies $Z_i \rightarrow 0$ and $Z \rightarrow Z_R$ (figure 1.6) and equation 1.22 shows that as $\omega \rightarrow 0$, $Z \rightarrow Z_R$. This information is more evident when presented in the Bode plot as shown in figures 1.6.

In analogous fashion, equivalent circuit parameters for more complex circuits can be determined from the corresponding impedance spectrum. For real systems, effects such as time constant dispersion, adsorption, diffusion of charged species and the presence of inductive loops can complicate impedance analysis. Under these circumstances an ability to recognize the impedance spectra of networks is necessary.

1.6 References

1. Bergveld, P.; Sibbald, A. *Analytical and Biomedical Applications of Ion-Selective Field-Effect transistors*; Elsevier, Amsterdam, 1988.
2. Sibbald, A. *J. Mol. Electron.* 1986, 2, 51.
3. Gopel, W.; Jones, T.A.; Kleitz, M.; Lundstrom, J.; Seiyama, T. (Eds.), *Sensors, A Comprehensive Survey*, Vol. 2; VCH publishers: New York, 1991
4. Madou, M. J.; Morrison, S.R. *Chemical Sensing with Solid State Devices*; Academic Press: New York, 1989.
5. Janata, J. *Principles of Chemical Sensors*; Plenum Press: New York, 1989.
6. Ulman, A. *An Introduction to Ultrathin Organic Films: From Langmuir-Blodgett to Self-assembly*; Academic Press: Boston 1991.
7. Colvin, V.L.; Goldstein A.N.; Alivisatos, A.P. *J. Am. Chem. Soc.* 1992, 114, 5221.
8. Wiemhofer H. D.; Cammann, K. in *Sensors, A Comprehensive Survey*, Gopel, W.; Jones, T.A.; Kleitz, M.; Lundstrom, J.; Seiyama, T. (Eds.) Vol. 2; VCH publishers: New York, 1991, Chap. 5.
9. Bard, A.J.; Faulkner, L.R. *Electrochemical Methods: Fundamentals and Applications*; Wiley: New York, 1980.
10. Buck, R.P. *J. Chem. Soc. Faraday Trans.* 1986, 82, 1169.
11. Buck R.P. *Ion-Selective Electrodes Rev.* 1982, 4, 3.
12. Fjeldly, T.A.; Nagy, K. *J. Electrochem. Soc.* 1980, 127, 1299.
13. Nicollian, E.H.; Brews, J.R. *MOS (Metal Oxide Semiconductor) Physics and Technology*, Wiley, New York, 1982.

14. Siu, W.M.; Cobbold, R.S.C. *IEEE Trans. Electron. Devices* **1979**, *ED-26*, 1805.
15. Bousse, L.J.; De Rooij, N.F. ; Bergveld, P. *IEEE Trans. Electron. Devices* **1983**, *ED-30*, 1263.
16. Harrison, D.J.; Glavina, P.G.; Manz, A. *Sensors and Actuators* **1993**, *B10*, 107.
17. Bousse, L.J.; De Rooij, N.F.; Bergveld, P. *Surf. Sci.*, **1983**, *135*, 479.
18. Harame, D.L.; Bousse, L.J.; Shott, J.D.; Meindl, J.D. *IEEE Trans. Electron. Devices* **1987**, *ED-34*, 1700.
19. Fung, D.C.; Cheung, P.W.; Ko, W.H. *IEEE Trans. Electron. Devices* **1986**, *ED-33*, 8.
20. Widmer, H.M. *Anal. Meth. Inst.* **1993**, *1*, 60.
21. Buck, P.R.; Nahir, T. M. *Electrochim. Acta.* **1993**, *38*, 2691.
22. Armstrong, R.D.; Horvai, G. *Electrochim. Acta.* **1990**, *35*, 1.
23. Janata, J. *Principles of Chemical Sensors*; Plenum Press: New York, **1989**. pp 116.
24. Sze S. M. *Physics of Semiconductor Devices*; 2nd ed., Wiley: New York, **1981**
25. Pierret, R.F. *Semiconductor Fundamentals*, from *Modular Series on Solid State Devices*, Vols 1, Neudeck G.W.; Pierret, R.F. (Eds.), 2nd ed., Addison-Wesley: Reading, MA, **1988**.
26. Pierret, R.F. *Semiconductor Fundamentals*, from *Modular Series on Solid State Devices*, Vols 4, Neudeck G.W.; Pierret, R.F. (Eds.), 2nd ed., Addison-Wesley: Reading, MA, **1988**.
27. Bergveld, P. *IEEE Trans. Biomed. Engng.* **1972**, *BME-19*, 342.
28. Clechet, P. *Sensors and Actuators* , **1992**, *B4*, 227.
29. Bataillard, P.; Clechet, P.; Jaffrezic-Renault, N; Martelet, C.; Morel, D.; Serpinet, J. *J. Electrochem. Soc.* **1986**, *133*, 1759.

30. Rocher, V.; Jaffrezic-Renault, N.; Perrot, H. *Anal. Chim. Acta.* **1992**, *256*, 251.
31. Sanada, Y.; Akiyama, T.; Ujihira, Y.; Niki, E. *Fresenius Z. Anal. Chem.* **1982**, *312*, 526.
32. Pham, M.T.; Hoffman, W. *Sensors and Actuators* , **1984**, *5*, 217.
33. Wong, H.S.; Hu, Y.; White, M.H. *J. Electrochem. Soc.* **1989**, *136*, 2968.
34. Shiramizu, B.; Janata, J.; Moss, S.D. *Anal. Chim. Acta.* **1979**, *108*, 161.
35. Moritz, W.; Szeponik, J.; Lisdat, F.; Friebe, A.; Krause, S. *Sensors and Actuators* **1992**, *B7*, 497.
36. Moritz, W.; Meierhofer and Muller, L. *Sensors and Actuators* **1988**, *15*, 211.
37. Van Der Spiegel, J.; Lauks, I.; Chan, P.; Babic, D. *Sensors and Actuators* **1983**, *4*, 291.
38. Buck, R.P.; Hackleman, E. *Anal. Chem.* **1977**, *49*, 2315.
39. Sibbald, A.; Whalley, P.D.; Covington, A.K. *Anal. Chim. Acta.* **1984**, *159*, 47.
40. Hunter, R. *J. Zeta Potential in Colloid and Surface Chemistry*: Academic Press, New York, **1981**, Chapter 1.
41. Parsons, R. in *Modern Aspects of Electrochemistry*, Bockris, J. O. M. (Ed.): Butterworth Scientific Publications, London, **1954**, chapter. 3.
42. Szepesi, G. *Reverse-phase HPLC*: VCH Publishers, New York, **1992**, Chapter 1.
43. Hearn, M.T.W *Ion-Pair Chromatography: Theory and Biological and Pharmaceutical Applications*, Marcel Dekker, New York, **1985**, Vol. 31.
44. Liu, H. Ph.D. *Desertation*, Univ. of Alberta, **1988**.
45. Cantwell, F.F.; Puon, S. *Anal. Chem.* **1979**, *51*, 623
46. Cantwell, F.F. *J. Pharmaceutical & Biomedical Analysis* **1984**, *2*, 153.

47. Chen, J.G.; Weber, S.G.; Glavina, L.L.; Cantwell, F F. *J. Chromatog. A*, **1993**, *656*, 549.
48. Macdonald, R.J. (Ed.), *Impedance Spectroscopy: Emphasizing Solid Materials and Systems*, Wiley, New York, **1987**.
49. Basics of AC Impedance Measurements, *Application Note AC-1*, E.G. and G. Princeton Applied Research Company.
50. Sluyters-Rehbach, M.; Sluyters, J.H.; in *Electroanalytical Chemistry*, Vol. 4; Bar, A.J. (Ed.); Marcel Dekker, New York, **1969**, Chapter 1.
51. Kell, D.B.; Davey, C.L. in *Biosensors: A Practical Approach*, Cass, A.E.G. (Ed.), Oxford University Press, New York, **1990**, Chapter 5.

Chapter 2

An Equivalent Circuit Model of Ion Selective Membrane/Insulator/Semiconductor Interface Used for Chemical Sensors

2.1 Introduction

The use of polymer based, ion-selective membrane coatings on semiconductor devices is one of the principal means of inducing chemical selectivity to solid-state surfaces used for chemical sensing [1,2]. The coated wire electrode [3], field effect coupled diode [4,5], the light addressable photo-diode (LAPS) [6,7], and the ion-sensitive field effect transistor (ISFET) [1,2] are examples of such devices. There has been extensive study of the impedance of the electrolyte/insulator/semiconductor interface (EIS), where the insulator is an inorganic oxide [8-11] or when the insulator is coated with a silver halide [12,13]. However, the impedance behaviour of commonly used poly(vinyl chloride) (PVC) based ion-selective membranes on silicon electrodes has received limited study [14,15], despite the potential importance of polymer based membrane/insulator/semiconductor (MIS) structures [1,2,16]. In contrast, the impedance of the membrane component alone has been well

studied [17-26], and provides a strong foundation from which to evaluate MIS device impedance.

In a previous report a simple model for the impedance of MIS devices was presented [14]. However, it was not explored quantitatively. It was noted that the equivalent capacitance of MIS interfaces showed a strong dependence on the membrane impedance, and could result in unusual capacitance-voltage (CV) relationships, but no data was presented. In this chapter the model is developed further to allow calculation of the impedance curves, and is compared to the full range of responses observed as a function of frequency, applied voltage, and electrical parameters of both the semiconductor and membrane. The results show that it is possible to quantitatively describe MIS impedance, although at frequencies below 100 Hz the behavior of surface states may prevent this. The equivalent capacitance is a strong function of the membrane impedance, which has implications for AC measurement schemes, such as those used with ion-selective diodes and LAPS devices [4-7].

2.2 Model of Membrane/Insulator/Silicon Electrode Impedance

The equivalent circuit model we have employed for the MIS structure is composed of several discrete elements and is shown in Figure 2.1. This model includes the bulk impedance and surface impedance of the membrane [17-26] in series with three capacitive elements arising from the electrode [27-31]. A similar circuit has been given by Smith and Janata [15]. However, experimental results show that the time constant of

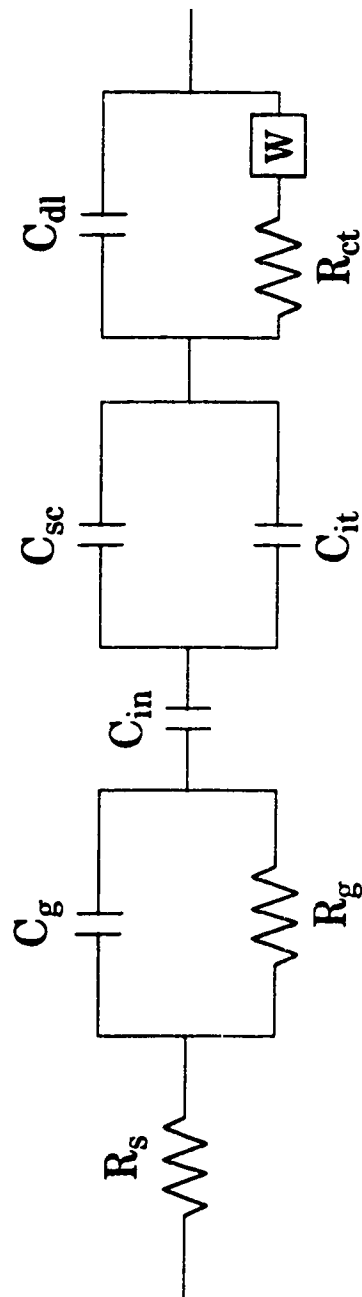


Figure 2.1 Model of circuit elements present when an MIS (membrane/insulator/semiconductor) is immersed in aqueous solution. See text for definition of symbols.

the membrane/insulator interface is large and so this interface can be neglected. The impedance of the MIS in the frequency regime of 5 to 40000 Hz is dominated by the membrane bulk impedance and the insulator/semiconductor contributions. We have in addition included the omnipresent surface states of the insulator/semiconductor interface. The influence of surface states at the semiconductor/insulator interface is represented by a potential dependent capacitance, an approximation discussed by Goetzberger et al [27] for surface states that applies at low frequencies. The membrane contribution to the impedance has been discussed previously and a set of equations was presented [14]. However, the silicon/insulator electrode impedance was expressed as a lumped term, C_e , and not treated in detail. The uncoated electrode impedance is given by equation 2.1,

$$C_e = \frac{C_{in}(C_{sc} + C_{it})}{(C_{in} + C_{sc} + C_{it})} \quad (2.1)$$

where C_{in} , C_{sc} , and C_{it} are the capacitances due to the insulator, the space charge in the silicon, and the surface states, respectively. In model calculations the capacitance of the insulator was determined using the standard equation for a parallel plate capacitor, dielectric values of 3.9 or 7.5 for oxide and nitride insulators, respectively, and the appropriate insulator thickness.

In order to calculate the MIS impedance a functional expression for C_{sc} is required. In this analysis we have used the expression of Garret and Brattain [28,29] for n-type Si,

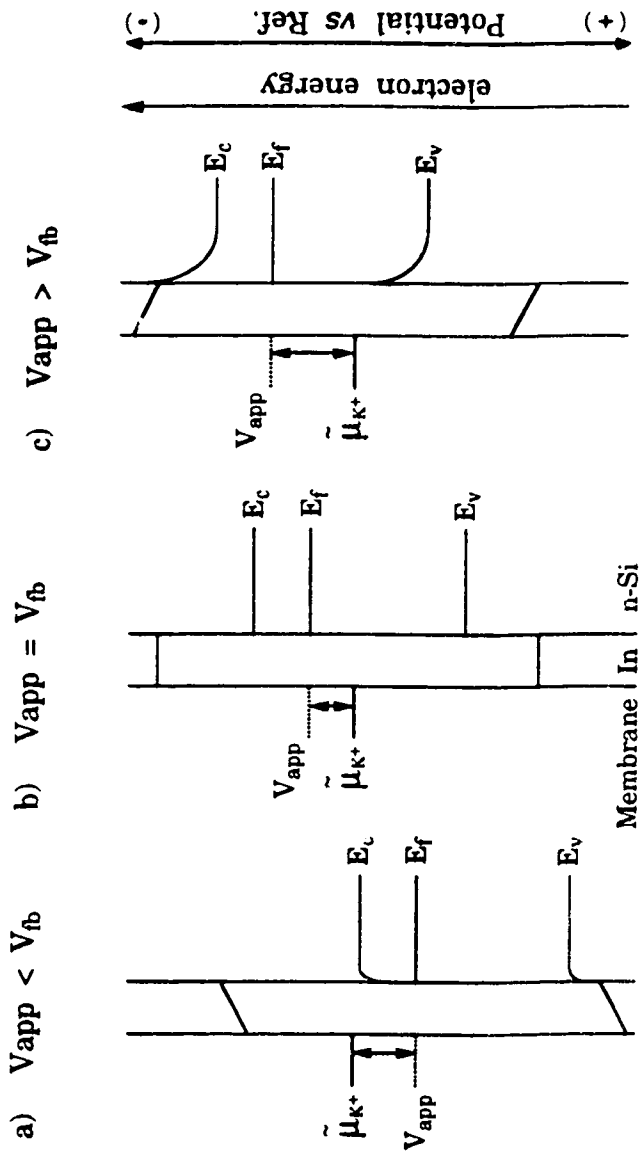


Figure 2.2 Semiconductor band diagram of electron energy and electrode potentials under conditions of a) accumulation induced by a forward bias, b) flat band and c) depletion induced by a reverse bias. The electrochemical sign convention is used, with the potential referenced to a reference electrode in solution, rather than to the semiconductor bulk.

$$C_{sc} = \sqrt{\frac{q\epsilon_s\epsilon_0 N_0 \beta}{2}} \frac{\exp(\beta\psi_{sc}) - 1}{[\exp(\beta\psi_{sc}) - (\beta\psi_{sc}) - 1]^{1/2}} \quad (2.2)$$

$$\psi_{sc} = \psi_b - \psi_s \quad (2.3)$$

where q is the electronic charge, ϵ_s is the silicon dielectric constant of 11.9 [30], ϵ_0 is the permittivity of free space, 8.854×10^{-14} F/cm, N_0 is the carrier density per cm^3 , β is q/kT where k and T have their usual meanings. ψ_{sc} is the potential drop across the space charge layer in the Si. We have used the sign convention of electrochemistry and referred potentials to a reference electrode in solution, rather than to the Si bulk, so that ψ_{sc} is the potential difference between the silicon bulk, ψ_b , and the silicon surface, ψ_s , where the surface is taken as the reference point.

Equation 2.2 describes C_{sc} when the electrode is in accumulation or depletion, but does not consider the case at low frequency when inversion in the space charge region occurs [31]. When $\psi_{sc} = 0$ the energy bands within the semiconductor are not bent (flat band condition) and the capacitance at flatband, C_{fb} , is given by equation 2.4 rather than equation 2.2 [29].

$$C_{fb} = \sqrt{q\epsilon_s\epsilon_0 N_0 \beta} \quad (2.4)$$

Note that equations 2.1-2.4 are expressed per unit area. More exact relationships between C_{sc} and ψ_{sc} exist [31], but the differences are minor from the point of view of this discussion.

Figure 2.2 illustrates the different states of band bending within the MIS structure as a function of applied potential, showing the conditions of accumulation, flat band and depletion. The applied potential, V_{ap} , at which ψ_{sc} is zero is referred to as the flat band potential, V_{fb} . For the diagram the flat band potential was arbitrarily chosen, so that the silicon space charge would be in depletion at open circuit potential. The electrochemical potential of K^+ ion within the membrane coating, $\bar{\mu}_{K^+}$, represents the Fermi level of the potential determining ion for a K^+ -selective membrane coated on the electrode, and was taken as a constant for this diagram (constant K^+ activity in solution).

The potential range between the onset of strong accumulation and the onset of inversion in a surface state free (ideal) capacitance-voltage (CV) relationship must be less than the Si band gap energy of 1.12 V. However, experimental CVs frequently extend across a larger applied potential range, which can be attributed to a fraction of the applied voltage being expended to charge or discharge surface states. The density and distribution of surface states is a complex function of both frequency and potential [27,30,31] and a full treatment of the effects is beyond the scope of this report. However, to model the experimental CV of MIS electrodes the effect of surface states must be considered in some form.

We used a modified version of Terman's high frequency, differential CV method as described below to determine the effect of surface states experimentally, and then develop a simplified model of those states for subsequent calculations [27,29]. First, V_{fb} was determined by matching the calculated ratio of C_{fb}/C_{in} at $\psi_{sc} = 0$ with the experimentally determined capacitance ratio for a given electrode. The capacitance ratio

C_e/C_{in} for the ideal CV without surface states is then calculated as a function of the space charge potential ψ_{sc} . A plot of ψ_{sc} at given calculated values of C_e/C_{in} is then made versus the value of $(V_{ap} - V_{fb})$ required to obtain the same capacitance ratios experimentally. The tangential slope of this plot, γ , gives the fraction of the applied voltage that charges the space charge region of the semiconductor. Making the approximation that ψ_{sc} and $(V_{ap} - V_{fb})$ are linearly related is equivalent to assuming a uniform, linear distribution of surface states. It is also equivalent to modelling the surface states as a capacitive element as in Figure 2.1. This proved to be a reasonable approximation for certain types of electrodes we studied. The experimental CV could then be modelled using equations 2.2 and 2.4, with ψ_{sc} replaced by $\gamma \times (V - V_{fb})$ and C_{it} neglected in equation 2.1.

The bulk membrane and membrane/solution interfacial impedances can be modelled as two lumped impedance networks [14,17-22]. The bulk membrane properties lead to a geometric resistance, R_g , and capacitance, C_g , in parallel. The solution/membrane interface leads to a network consisting of the double layer capacitance, C_{dl} , the charge-transfer resistance at the interface, R_{ct} , and the diffusional, or Warburg, impedance, W [16,17,22]. On the basis of the model in Figure 2.1, but neglecting the Warburg impedance, the impedance for a MIS electrode may be written as:

$$Z_r = R_s + \frac{R_g}{1 + (\omega R_g C_g)^2} + \frac{R_{ct}}{1 + (\omega R_{ct} C_{dl})^2} \quad (2.5)$$

$$Z_{im} = \frac{1}{\omega C_e} + \frac{\omega C_g R_g^2}{1 + (\omega R_g C_g)^2} + \frac{\omega C_{dl} R_{ct}^2}{1 + (\omega C_{dl} R_{ct})^2} \quad (2.6)$$

where Z_r is the real or resistive component of the impedance, Z_{im} is the imaginary or capacitive component, and ω is the radial frequency ($\omega = 2\pi f$, where f is the applied frequency).

Series resistance of the solution and the Si electrode, R_s , is small, typically less than 100 Ω , and is neglected. The elements arising from the membrane/solution interface are not usually observed for valinomycin containing K^+ -selective electrodes [17-20,24]. However, even when such circuit elements are seen, they appear at frequencies below 5 Hz [17-24], indicating a long time constant. This circuit element will show high frequency limiting behaviour over the 3 Hz to 40 kHz range used in this study, so was not observed in our data. This is also true for the contributions of diffusion that lead to the Warburg impedance. Consequently, these elements were not considered in further development of the model.

These equations predict a semicircle at higher frequencies when Z_{im} is plotted versus Z_r in an impedance plane or Nyquist plot (see section 1.5), since bulk membrane properties will dominate the impedance response. When ω becomes sufficiently low the impedance response will be determined by the electrode capacitance, C_e , in the absence of membrane surface impedance effects. Accordingly, a rapidly rising tail will be observed at these lower frequencies in the Nyquist plot because the term $(\omega C_e)^{-1}$ will dominate; this usually occurs at frequencies below 100 Hz.

For a semiconductor/insulator structure the capacitance is directly proportional to the imaginary component of the admittance, Y_{im} . This fact has provided a convenient means to measure the capacitance of such structures. However, with a membrane coated on the electrode the relationship between Y_{im} and C_e becomes much more complex. Using equations 2.5 and 2.6, Y_{im} may be calculated from equation 2.7 to give equation 2.8, when the membrane/electrolyte surface impedance is negligible.

$$Y_{im} = \frac{Z_{im}}{Z_r^2 + Z_{im}^2} \quad (2.7)$$

$$Y_{im} = \frac{\left[\left(1 + (\omega C_g R_g)^2 \right) + (\omega C_e R_g)(\omega C_g R_g) \right] \left[\omega C_e \left(1 + (\omega C_g R_g)^2 \right) \right]}{(\omega C_e R_g)^2 + \left[\left(1 + (\omega C_g R_g)^2 \right) + (\omega C_e R_g)(\omega C_g R_g) \right]^2} \quad (2.8)$$

This expression was used in the model calculations presented below. However, since $C_g R_g$ is approximately $6 \times 10^{-5} \Omega \cdot F$ the assumption $(\omega C_g R_g)^2 \ll 1$ may be made for frequencies below 1000 Hz. Then in the frequency range where $(\omega C_g R_g)(\omega C_e R_g) \leq 1$ and $(\omega C_e R_g) > 10$, equation 2.8 further simplifies to:

$$Y_{im} = \frac{1}{\omega C_e R_g^2} + \omega C_g \quad (2.9)$$

This condition will apply at frequencies in a range from 50 to 500 Hz for typical membrane coatings, when the semiconductor capacitance, C_e is

on the order of 10 nF. Under these conditions Y_{im} is inversely related to both C_e and R_g^2 and linearly dependent on C_g . Y_{im} represents neither a pure electrode capacitance nor a pure membrane capacitance, so that measurement of this quantity at higher frequencies yields an equivalent capacitance. Equation 2.9 shows that at sufficiently high frequencies, bulk membrane properties will dominate, and the equivalent capacitance, Y_{im}/ω , will be independent of applied voltage, provided that C_g is voltage independent. At very low frequencies C_e should become dominant, but in between these extremes the equivalent capacitance will be a strong function of the membrane bulk resistance. This leads to rather unusual equivalent capacitance-voltage curves, as presented below.

2.3 Experimental Section

Semiconductor electrodes were prepared from n-Si wafers having a resistivity of 3 to 4 $\Omega\text{-cm}$ ((100) face, phosphorus doped, Monsanto, 4 in. diam.) or 400-800 $\Omega\text{-cm}$ ((100), float zone, International Wafer Services, 3 in. diam.). These correspond to nominal dopant concentrations of about 10^{15} cm^{-3} for the P-doped wafer, and $7 \times 10^{12} \text{ cm}^{-3}$ for the n-type float zone wafer [30]. Gate quality thermal oxide 500 Å thick, with 450 Å of silicon nitride over top was deposited on the P-doped wafers using chemical vapour deposition by Process Technology, Ltd. (Oromocto, New Brunswick, Canada). Thermal oxide alone was grown on the float zone Si, to 850 Å thickness at the Alberta Microelectronic Centre (Edmonton, Canada). Some wafers were annealed in a fused silica tube under flowing

forming gas (10% H₂ in N₂) at 800 °C for about 30 minutes using a Mini Brute furnace (Thermco Products Corp.). A Gaertner L125B two wavelength ellipsometer equipped with a rotating analyzer was used to measure insulator thicknesses. Software provided by Gaertner for an IBM PS-2 was used for data acquisition and analysis.

The insulating film on the back face was etched with either 5 min. exposure to 10 % in HF (Si/SiO₂ wafers) or 5 min. of concentrated HF (Si/SiO₂/Si₃N₄ wafers). Electrodes were prepared from ~7mm x 7 mm pieces and abraded on the back side using a diamond pen in the presence of gallium-indium eutectic to form a very highly doped, degenerate spot for ohmic contact. It was then contacted to a coiled end of about 15 cm long lead copper wire using silver epoxy to cure. The copper lead was isolated from solution by a 4 mm internal diameter glass tube and the SiO₂/Si-copper contact including some part of the front edge covered with Chem-grip® (Norton performance plastics) leaving an exposed area of ~4 mm x 4 mm. The electrode was recleaned with H₂O, CH₃OH, trichloroethylene, CH₃OH, and H₂O after sealing.

Under a tetrahydrofuran-saturated atmosphere, membranes were cast onto the silicon electrodes by evaporation of 1 to 4 drops of the following solution [14]: 3 mL of tetrahydrofuran (BDH, distilled from K); 0.15 g of dioctyl adipate (Fluka); 0.075 g of poly(vinylchloride) (PVC) (Polysciences, chromatographic grade); 0.0015 g of valinomycin (Sigma); and 25 µg of potassium tetrphenylborate (KBPh₄).

Impedance measurements and capacitance-voltage curves of MIS electrodes were obtained using the apparatus described previously [14,25,26]. A 10 mV peak-to-peak excitation sine wave was used between 3

Hz and 40 kHz, and the dc potential was swept at 5 mV/s. CVs were obtained by sweeping the dc potential from depletion to accumulation conditions. The instrument phase shift was corrected by measurement of the response to a series of standard capacitors. These capacitors were also used to calibrate the quadrature signal and determine the equivalent capacitance. The experiments were performed within a Faraday cage, in the dark in 0.1 M KCl as electrolyte. A standard three-electrode electrochemical cell configuration was used, with a saturated calomel reference electrode (SCE) contained in a double junction filled with 0.1 M KCl, and a large area Pt gauze as a counter electrode. The measured impedance was independent of the choice of reference electrode, even when a bare Ag/AgCl electrode in the test solution was used as the reference.

Several methods exist to evaluate the doping density, including Mott-Schottky analysis of the CV curves. We used that method and a technique adapted from Berman and Kerr [32]. The latter is based on measurement of the minimum capacitance under reverse bias of an uncoated Si/insulator/electrolyte electrode. The doping density N_d is then calculated from equation 2.10 [30],

$$C_{\min} = A \left(\frac{0.5 \epsilon_s \epsilon_0 q \beta N_0}{2u_b - 1 + \ln[1.15(u_b - 1)]} \right)^{1/2} \quad (2.10)$$

where A is the electrode area and u_b is $\ln(N_0/n_i)$, n_i being the intrinsic carrier density. Both methods were usually in agreement, so long as the

Mott-Schottky analysis was performed on data obtained in the depletion region of the CV, near the minimum value of C_e .

2.4 Results and Discussion

2.4.1 Characterization of Si Electrode Impedance

The impedance of the membrane/insulator/semiconductor (MIS) electrode is a function of both the membrane and the semiconductor, and will depend on both frequency and potential. The potential dependence of the semiconductor impedance can be complex, especially at low frequencies where slow surface states can influence the response [27,30]. Modern technology can minimize the effect of surface states, but not fully eliminate them. In order to analyze the behaviour of MIS electrodes we first examined the potential and frequency dependence of insulator/semiconductor electrodes without membranes in aqueous solution at low frequencies. Several different electrode types were studied: oxide on low doping density, float zone Si (fz-Si), nitride and oxide on moderately doped, n-type Si (m-Si), and the m-Si electrodes after annealing in forming gas to passivate surface states (an-Si). Float zone Si was used in this study because the small values of C_e obtained, due to the low doping density, made it easier to observe the full range of behaviour described below within an accessible frequency range. The moderate doping range of the m-Si is typical of the substrate doping density used in device fabrication.

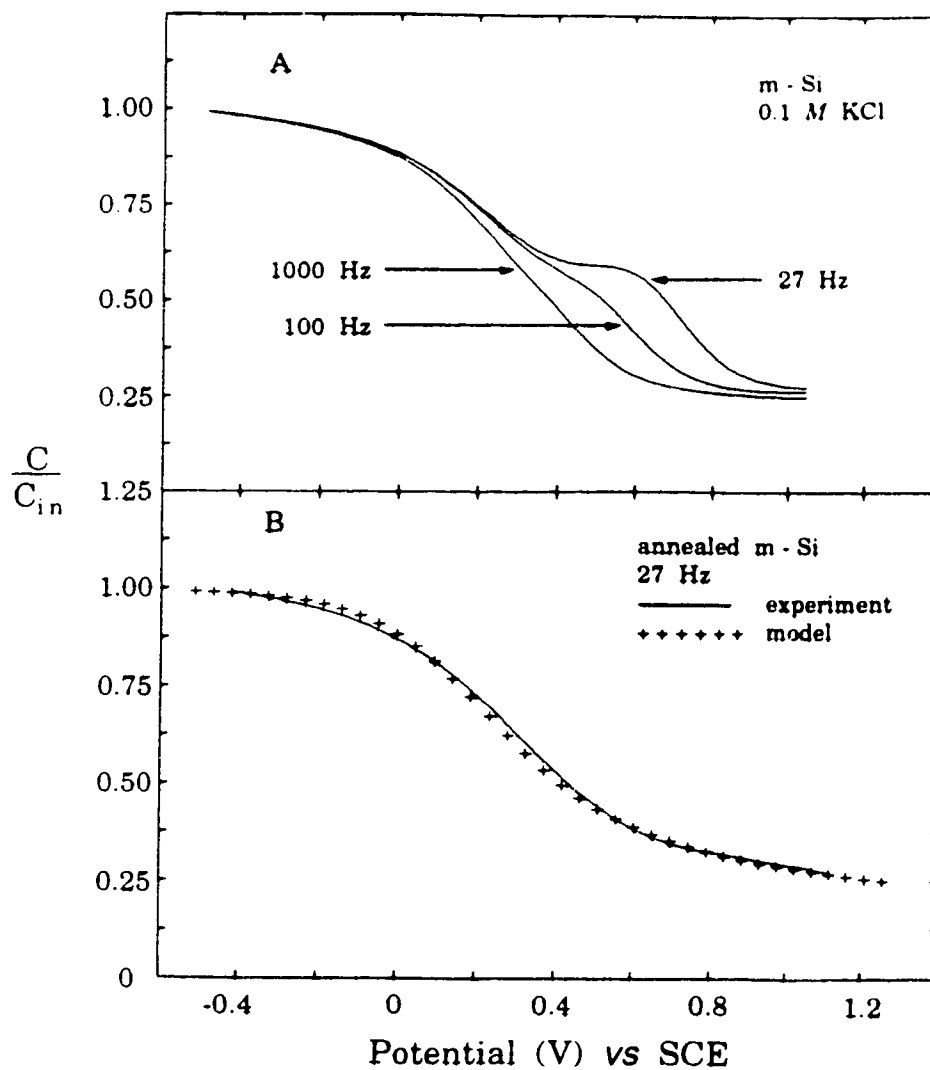


Figure 2.3. Capacitance-voltage curves for a) moderately doped n-type Si, (m-Si), with no membrane coating at three frequencies; b) the same type of Si after annealing in forming gas (an-Si). Model calculations for the annealed electrode are also shown at 27 Hz with the following parameters: $A = 0.12 \text{ cm}^2$, $C_{in} = 5.8 \text{ nF}$, $N_0 = 10^{15} \text{ cm}^{-3}$, $\gamma = 0.34$.

Figure 2.3 shows CV curves for m-Si and an-Si electrodes obtained at 27, 100 and 1000 Hz. The m-Si electrodes showed a significant feature in the CV curve in the transition between accumulation and depletion states as the potential was swept. This ledge-like feature in the curve is strongly frequency dependent and essentially disappears at 1 kHz. The annealed Si does not show a similar feature, however, the CV curve is much broader than a curve for an ideal interface without surface states. This indicates there is a significant, but fairly uniform distribution of inter-gap surface states after annealing. Float zone Si electrodes showed a similar ledge feature at 27 Hz, but it did not completely disappear at 1 kHz. In addition, the maximum and minimum capacitance values for fz-Si were frequency dependent.

For an-Si the effect of surface states was evaluated according to the method of Terman. A plot of ψ_{sc} versus $(V_{ap} - V_{fb})$ was linear for ± 0.25 V around $\psi_{sc} = 0$, or ± 0.7 V around V_{fb} , and the slope gave a value of γ of 0.34. Figure 2.3b shows that this value leads to a good match between the measured and calculated CV curves for an-Si. This value of γ corresponds to a surface state density, D_{it} , of $8.8 \times 10^{10} \text{ cm}^{-2} \text{ V}^{-1}$, calculated using equation 2.11 [30,31],

$$qD_{it} = C_{in}[\gamma^{-1} - 1] - C_{sc} \quad (2.11)$$

This estimate neglects slow states that do not respond within the frequency range studied, and any state present at V_{fb} that affects the electrode capacitance.

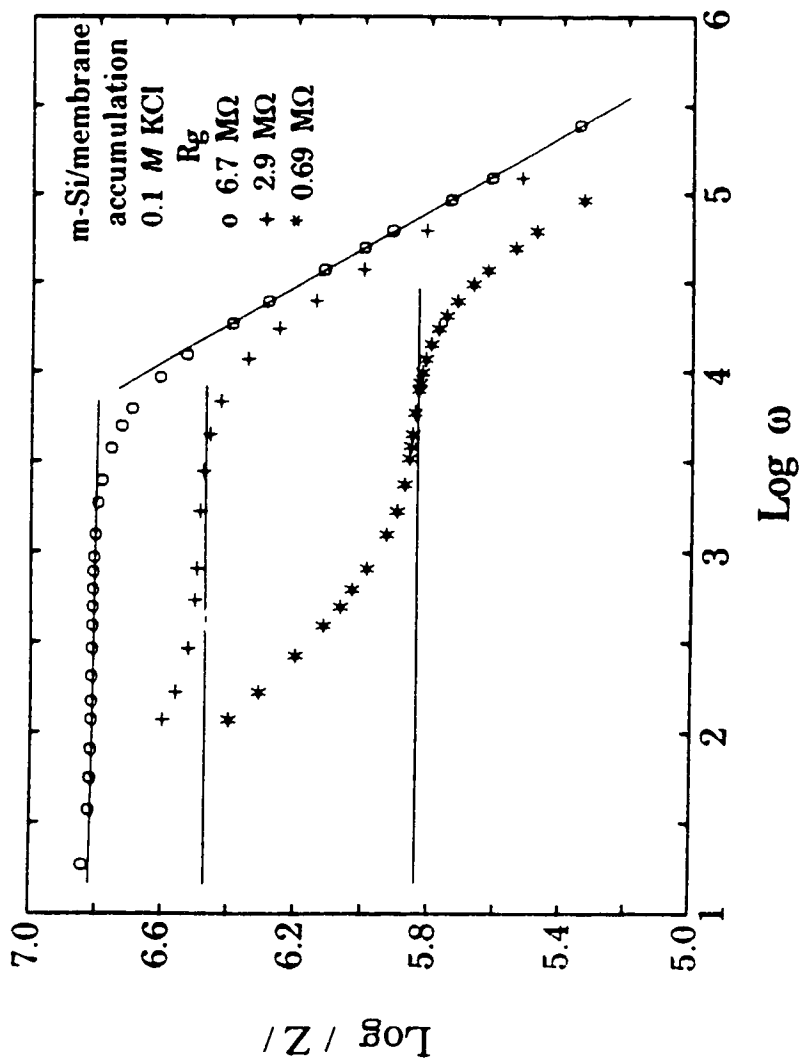


Figure 2.4. Bode plot of the magnitude of impedance ($|Z|$) for an m-Si MIS electrode biased into accumulation in 0.1 M KCl. The electrode was sequentially coated with thicker membranes with resistances, R_g , of (*) 0.69 MΩ, (+) 2.9 MΩ, and (o) 6.7 MΩ. Lines show the expected slope for a pure capacitance, and the limiting value of R_g .

2.4.2 Assignment of MIS Frequency Response Elements

The impedance characteristics of MIS electrodes may be displayed in an impedance plane plot of Z_{im} versus Z_r , known as a Nyquist plot [17-26], or a Bode plot of $\log |Z|$ versus $\log \omega$, where $|Z|$ is the absolute magnitude of impedance (see section 1.5). Figure 2.4 shows Bode plots between 3 Hz and 40 kHz for an MIS (m-Si) electrode with several different membrane thicknesses. At frequencies above 2 kHz a linear curve is seen with a slope very close to -1, but the curve bends over to a plateau of constant impedance at lower frequencies. This is the signature of a parallel RC network. The same data shows a semicircle over this frequency regime when plotted in the impedance plane, again indicative of a parallel RC element. The horizontal lines in Figure 2.4 correspond to the resistance obtained from the real intercept of a Nyquist plot at low frequencies. At still lower frequencies the Bode plot of Figure 2.4 shows the impedance becomes capacitive in nature again, and this corresponds to observation of a rapidly rising tail in a Nyquist plot. This feature is most easily observed with thin membrane coatings, for which the membrane bulk resistance is lower and the capacitance is larger, making the Si impedance more significant relative to the membrane[13].

The parallel RC component at higher frequencies has previously been assigned to the bulk resistance and capacitance of the ion-selective membrane, and this concurs with our present results [13,15,17-20,22]. In support of this the resistance increased with increasing thickness of the membrane coating, the capacitance decreased, while the time constant was approximately independent of thickness. When these

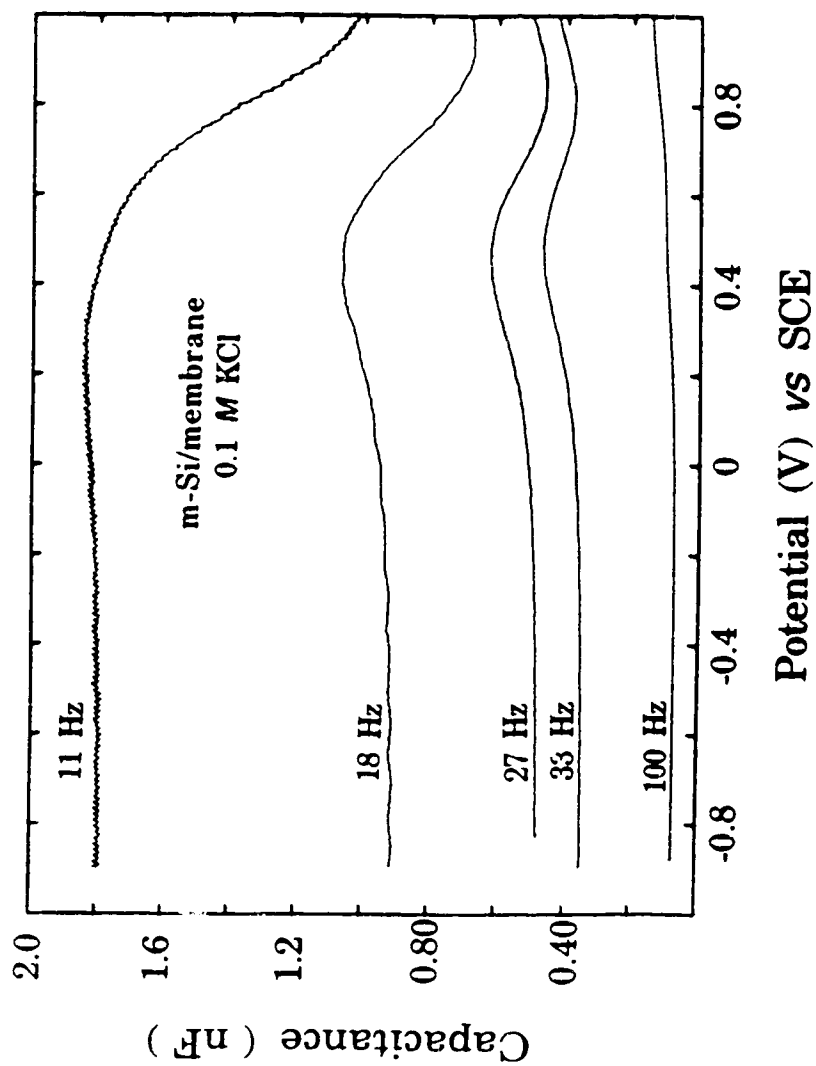


Figure 2.5. Experimental capacitance-voltage curves at several frequencies for an MIS electrode, using an m-Si substrate and a membrane with $R_g = 3.2 \text{ M}\Omega$, $C_g = 20 \text{ pF}$, $A = 0.11 \text{ cm}^2$, $C_{in} = 5.27 \text{ nF}$, $N_0 = 10^{15} \text{ cm}^{-3}$.

membranes are coated on a Pt electrode substrate only a single semicircle, ascribed to the bulk membrane impedance, can be observed. While the effect of the surface impedance of membranes has been observed [18,21], such features are not observed for membranes containing conventional amounts of valinomycin and $\text{KB}(\text{C}_6\text{H}_5)_4$ such as used in this study [18,19,24], and are not observed within the frequency range we have utilized. Similarly, for a $\text{AgBr}/\text{SiO}_2/\text{Si}$ system Buck and Hackleman have shown that when the SiO_2 is thin enough the Si space charge impedance becomes apparent at lower frequencies [13]. Consequently, the lowest frequency feature must arise from the Si electrode. Clearly, the circuit elements arising from the Si space charge and insulator capacitance should lead to a potential dependent response for MIS electrodes at low frequencies.

2.4.3 Qualitative Analysis of MIS Electrode Capacitance

Figure 2.5 shows capacitance voltage curves for an m-Si MIS electrode as a function of frequency. The response is very complex, and resembles a typical semiconductor CV only at the very lowest of frequencies. Plotting the impedance response of such electrodes in a Nyquist format [16] reveals that the typical semiconductor CV response is seen only when the frequency is low enough that the impedance response lies in the rapidly rising tail of the Nyquist plot. The behavior in Figure 2.5 is predicted by the model developed above. Figure 2.6 shows a set of theoretical CV curves calculated for a typical set of m-Si and membrane parameters. At the

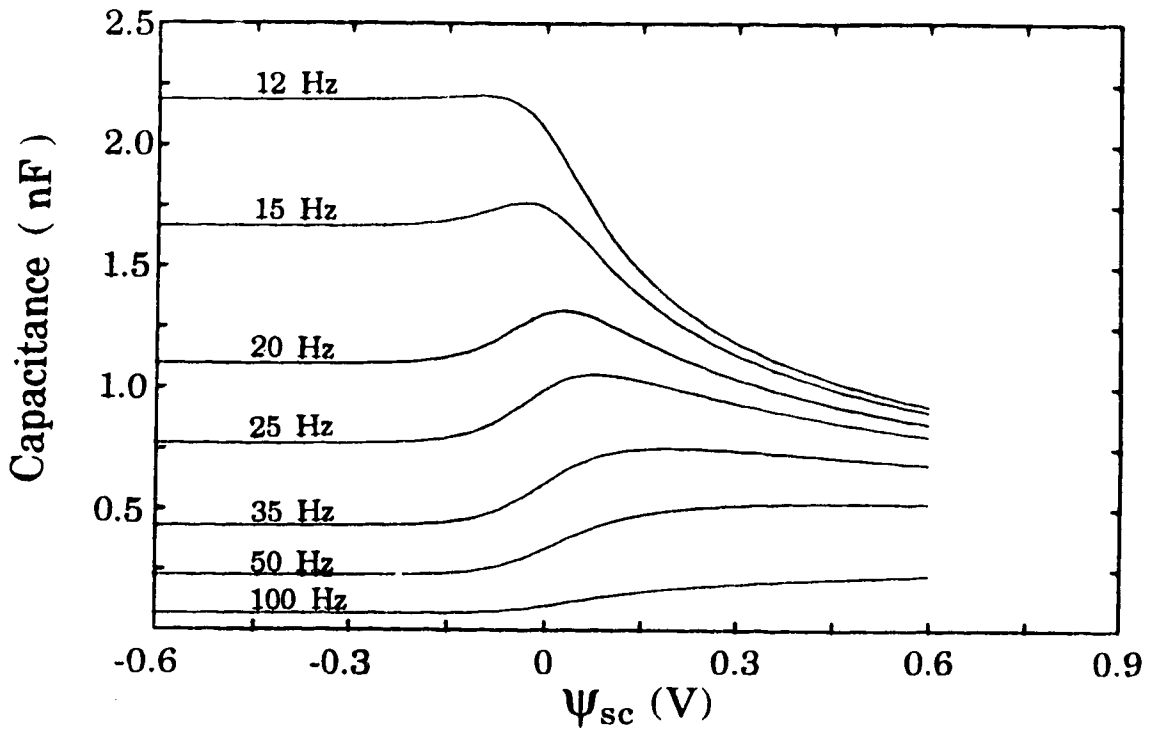


Figure 2.6 Calculated capacitance-voltage curves at several frequencies for an MIS electrode using the following parameters: $R_g = 3 \text{ M}\Omega$, $C_g = 20 \text{ pF}$, $A = 0.1 \text{ cm}^2$, $C_{in} = 5 \text{ nF}$, $N_o = 10^{15} \text{ cm}^{-3}$.

lowest frequency the electrode impedance contributes significantly, but the CV curves are distorted beyond recognition at higher frequencies due to the contribution of the membrane. There is good qualitative agreement between experiment and theory, although the surface state feature that appears at low frequency for the m-Si broadens out the characteristic bump that develops with a membrane coating.

The appearance of the peak, or hump, in the CV response is a strong function of the membrane resistance. This is illustrated by equation 2.9, in which the observed MIS capacitance depends inversely on $\omega C_e R_g^2$. Figure 2.7 shows this effect experimentally for the same fz-Si MIS electrode coated with a low and a high resistance membrane. A calculated curve is also shown for both sets of data, using the same Si electrode parameters and the values of R_g determined from Nyquist plots for the MIS electrodes. The quality of the fit is limited since the effect of surface states is incorporated only as a pure capacitance (or as the factor γ), whereas the actual frequency and potential dispersion of the fz-Si is more complex. This is clearly seen where the presence of the ledge-like feature in the CV is not reproduced by the calculation.

The membrane resistance exhibits a dominant influence on the impedance characteristics of the MIS electrodes at frequencies below 500 Hz. The absolute magnitude of the maximum equivalent capacitance depends strongly on R_g , as well as C_e , but the membrane capacitance, C_g , exerts a minimal influence, even under strong reverse bias conditions. As might be expected from equation 2.9, C_g is influential only at frequencies above about 1 kHz. This strong dependence on R_g is of

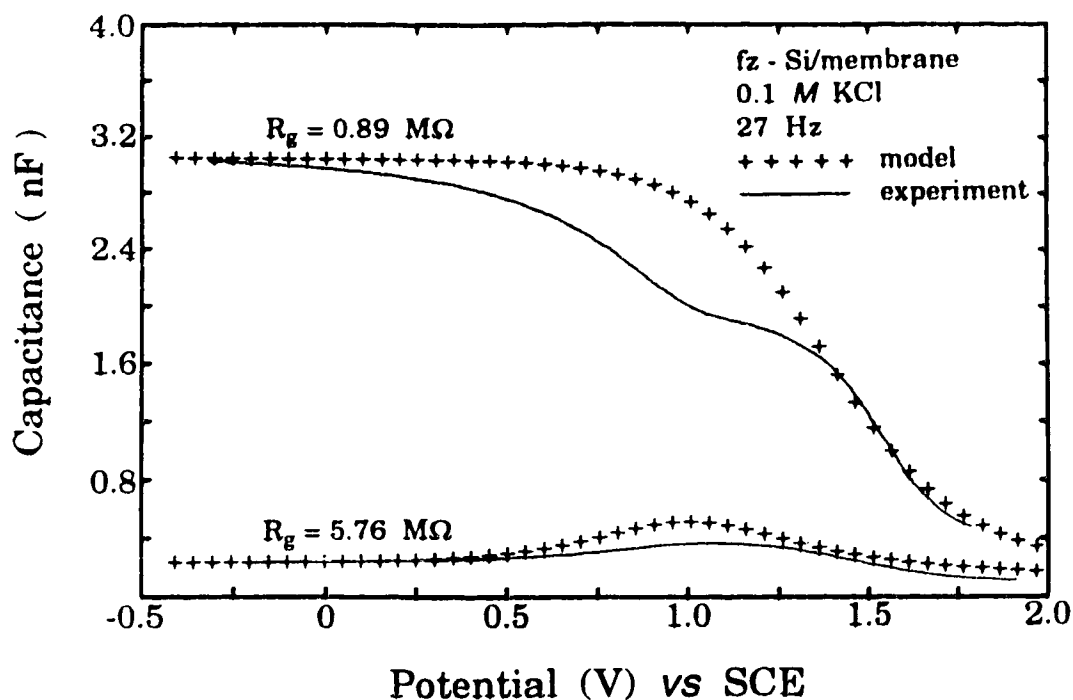


Figure 2.7. Capacitance-voltage curves at 27 Hz for a float zone Si (fz-Si) MIS electrode coated with membranes of two different resistances (R_g). Both (-----) experimental data and (+) calculated curves are shown. Electrode parameters were: $A = 0.11 \text{ cm}^2$, $C_{in} = 4.4 \text{ nF}$, $N_0 = 6 \times 10^{12} \text{ cm}^{-3}$, $\gamma = 0.25$. Membrane parameters were: $R_g = 0.89 \text{ M}\Omega$, $C_g = 40 \text{ pF}$ or $R_g = 5.76 \text{ M}\Omega$, $C_g = 10 \text{ pF}$.

significance for detection schemes based on measuring the equivalent capacitance, or determining shifts in V_{fb} from the CV response. Photovoltage measurements such as are used in the LAPS method would also be susceptible to apparent changes in C_e . Consequently, chemically selective membranes that show changes in resistance with changes in solution conditions are not readily compatible with schemes based on capacitance measurements of MIS style structures.

2.4.4 Quantitative Analysis of MIS Electrode Impedance

Figure 2.8 shows experimental and theoretical CV curves at several frequencies for an an-Si MIS electrode with a thick membrane coating. The membrane resistance was $9.6 \text{ M}\Omega$ for this electrode, as determined from the Nyquist plot for the first semicircle. The calculated curves were obtained using parameters obtained from the CV of the same, uncoated an-Si electrode, and are indicated in the figure caption. The effect of the membrane coating was extreme in this case, causing the CV curves to appear like those of p-type Si, rather than the n-type behaviour that should be observed. However, it can be seen from the theoretical fit that this effect is predicted and described quantitatively by the model we have used. The quality of the fit is much better than in Figure 2.7. This reflects the use of annealed Si as a substrate, for which the surface states are reasonably accurately modeled by use of the factor γ .

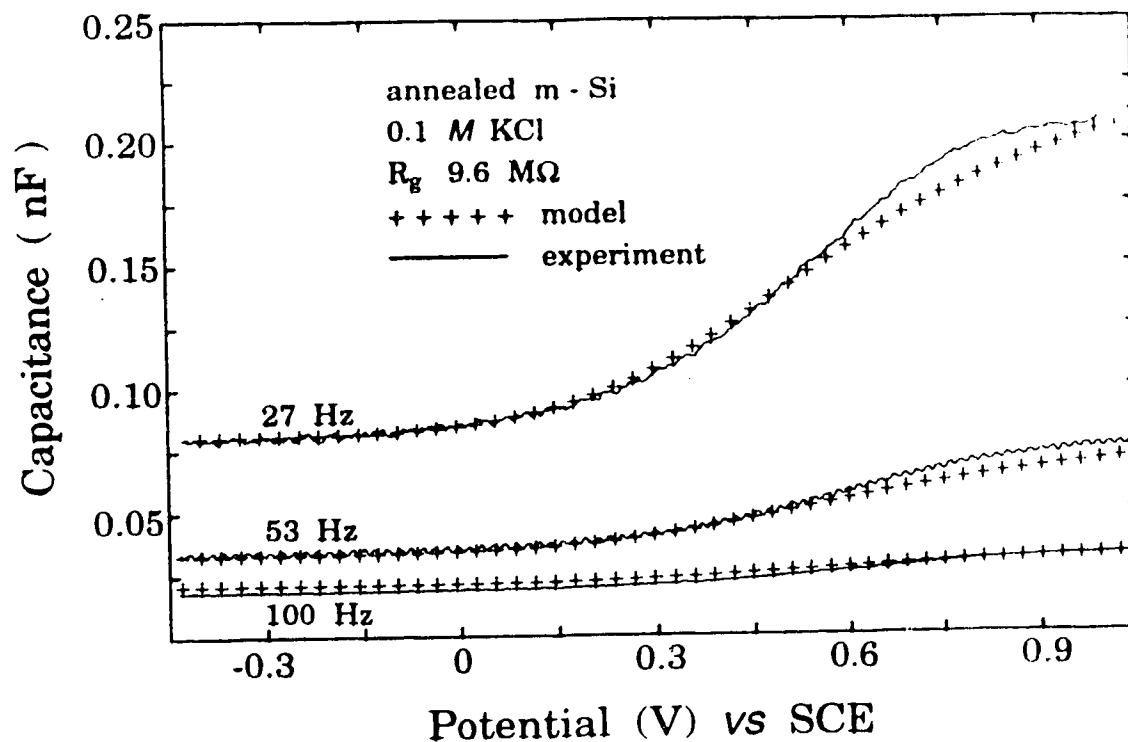


Figure 2.8 Capacitance-voltage curves at several frequencies for an annealed m-Si (an-Si) MIS electrode with a membrane R_g of $9.6 \text{ M}\Omega$, $C_g = 6 \text{ pF}$. Both (—) experimental data and (+) calculated curves are shown, other parameters are as for Figure 2.3b.

2.5 Conclusions

Our results demonstrate that the model can be used to quantitatively describe the impedance of the Si/insulator/membrane/electrolyte structure, so long as the surface states of the Si/insulator structure can be accounted for. Both theory and experiment show that polymeric ion-selective membranes have values of R_g and C_g that tend to dominate the equivalent capacitance of an MIS interface. It is known [25 and ref. cited therein] that the bulk resistance of such membranes is dependent on solution conditions, although the magnitude of this effect appears variable. This greatly complicates the use of capacitance measurements to characterize the expected shifts in flat band potential with solution conditions. Steady state measurements would be less susceptible to such effects, although they can suffer from other difficulties.

The model also suggests desirable parameters for steep capacitance-voltage curves for sensors based on impedance or ac measurements, if membranes are used that do not suffer changes in impedance with solution conditions. For maximum precision the membrane should have low resistivity and high permittivity, the Si doping and surface state density should be low, while the insulator should be thin. These characteristics will ensure CV response dominated by the Si space charge impedance, which is sensitive to changes in the flat band potential induced by changes in the solution composition.

2.6 References

1. Bergveld, P; Sibbald, A. Analytical and Biomedical Applications of Ion-Selective Field-Effect Transistors, in : Comprehensive Analytical Chemistry, XXIII, Svehla, G. (Ed.), Elsevier, New York, 1988.
2. Janata, J. *Anal. Chem.* 1992, 64, 196R.
3. Freiser, H., Coated Wire Ion Selective Electrodes, in: Ion-Selective Electrodes in Chemistry, Freiser, H. (Ed.), vol. 2, Chap. 2, Plenum Press, New York, 1980.
4. Wohltjen, H. *Anal. Chem.* 1984, 56, 87A.
5. Zemel, J.N. *Sens. Actuators* 1981, 1, 31.
6. Hafeman, D.G.; Parce, J.W.; McConnell, H.M. *Science* 1988, 240, 1182.
7. Bousse, L.J.; Mostarshed, S., Hafeman, D. *Sens. Actuators* 1992, B10, 67.
8. Bousse, L.J.; Bergveld, P. *J. Electroanal. Chem.* 1983, 152, 25.
9. Diot, J.L; Joseph, J.; Martin, J.R.; Clechet, P. *J. Electroanal. Chem.* 1985, 193, 75.
10. Siu, W.M.; Cobbold, R.S.C. *IEEE Trans. Electron Dev.* 1979, ED-26, 1805.
11. Barabash, P.R.; Cobbold, R.S.C. *IEEE Trans. Electron Dev.* 1982, ED-29, 102.
12. Fabry, P.; Yvonnou, L.L. *J. Electroanal. Chem.* 1990, 286, 23.
13. Buck, P.R.; Hackleman, D.E. *Anal. Chem.* 1977, 49, 2315.
14. Li, X.; Verpoorte, E.M.J.; Harrison, D.J. *Anal. Chem.* 1988, 60, 493.
15. Smith, R.L.; Janata, J. *J. Electrochem. Soc.* 1980, 127, 1199.

16. Moss, S.D.; Janata, J.; Johnson, C.C. *Anal. Chem.* **1975**, *47*, 2238.
17. Armstrong, R.D.; Horvai, G. *Electrochim. Acta* **1990**, *35*, 1.
18. Armstrong, R.D.; Lockhart, J.C.; Todd, M. *Electrochim. Acta* **1986**, *31*, 591.
19. Armstrong, R.D. *J. Electroanal. Chem.* **1988**, *245*, 113.
20. Armstrong, R.D.; Todd, M. *Electrochim. Acta* **1987**, *32*, 1403.
21. Tóth, K.; Gráf, E.; Horvai, G.; Pungor, E.; Buck, R.P. *Anal. Chem.* **1986**, *58*, 2741.
22. Horvai, G.; Gráf, E.; Tóth, K.; Pungor, E.; Buck, R.P. *Anal. Chem.* **1986**, *58*, 2735.
23. Buck, R.P.; Tóth, K.; Gráf, E.; Horvai, G.; Pungor, E. *J. Electroanal. Chem.* **1987**, *223*, 51.
24. Chan, A.D.C.; Li, X.; Harrison, D.J. *Anal. Chem.* **1992**, *64*, 2512.
25. Harrison, D.J. *J. Electroanal. Chem.* **1990**, *278*, 193.
26. Verpoorte, E.M.J.; Harrison, D.J. *J. Electroanal. Chem.* **1992**, *325*, 153.
27. Goetzberger, A.; Klausmann, E.; Schulz, M.J. *CRC Crit. Rev. Solid State Sci.* **1976**, *6*, 1.
28. Garrett, C.G.B.; Brattain, W.H. *Phys. Rev.* **1955**, *99*, 376.
29. Terman, L.M. *Solid-St. Electron.* **1962**, *5*, 285.
30. Sze, S.M. *Physics of Semiconductor Devices*, 2nd ed., Wiley, New York, **1981**.
31. Nicollian, E.H.; Brews, J.R. *MOS (Metal Oxide Semiconductor) Physics and Technology*, Wiley, New York, **1982**.
32. Berman, A.; Kerr, D.R. *Solid-St. Electron.* **1974**, *17*, 735.

Chapter 3

Electrochemical Impedance Study of the Adsorption of SDS⁻ onto an ODS Silanized Surface

3.1 Introduction

Adsorption of surfactants from solution on to the solid-liquid interface attracts scientific interest in such diverse areas as separation, detergents, flotation, toxic waste management, pharmaceuticals, and enhanced oil recovery. The nature of the adsorption of surfactants at the solid-solution interface is controlled by the characteristics of the adsorbing species itself, the properties of the solid adsorbent and the composition of the solution. Reverse phase chromatographic separation columns of octadecylchlorosilane bonded to silica substrates have been used in ion pair chromatography, both for ion pair separations [1] and for separations clearly based on the hydrophobic interaction of the surfactant and the stationary phase [2,3]. Alkyl sulfonates and sulfates have been separated on reversed phase stationary phases because of their hydrophobic interaction [4]. Some of the possible mechanisms for ion pair chromatography have been mentioned briefly in Section 1.4. It was stated there that retention of the ion pairing agents would be accompanied by double layer formation at the stationary phase. Ion pairing agents are

surfactants containing a hydrophilic segment that is a conjugate base or acid of a strong acid or base respectively. Consequently, they exist in the ionized form in aqueous solutions. The adsorption of the ion pairing agent on the surface of a stationary phase therefore can determine the double layer potential at the interface. It is possible to simulate the reverse phase by silanizing the SiO₂ surface of silicon substrate electrodes. One can then measure the potential change of the surface upon adsorption of a surfactant in situ using the AC impedance technique.

One aspect of the study of adsorption of surfactants or ion pairing agents is determining the amount adsorbed on the solid-liquid interface. The traditional bulk methods for studying adsorption generally involve bringing the solid adsorbent in powder form in contact with the solution, letting the system equilibrate, and then separating the slurry and the solution. The amount adsorbed is determined by analyzing the residual solution. Another way is "washing-off" the adsorbed component with an eluent and determining the amount from the collected volume. These techniques cannot be conducted in situ and do not directly measure the surface potential. Consequently, the determination of the adsorbate may suffer some degree of uncertainty. Moreover, the adsorbed sample not only has to be charged, but has to meet the requirements of the detection technique employed. AC impedance technique does not have these limitations and is suited to the study of potential changes caused by charged species adsorption at the electrolyte-silanized SiO₂/Si electrode. It does not provide a direct measure of the total mass of adsorbate, however.

Below, the organization of this chapter is briefly outlined. The AC impedance technique has already been discussed in the foregoing chapters.

The measured parameter that leads to discerning the potential due to SDS⁻ adsorption is the capacitance of the semiconductor as the applied voltage is varied. Section 3.2.1 describes how the double layer potential shift is evaluated from CV measurements in general. This is followed by a description of the structure and potential distribution of the double layer according to the most complete double layer model, the Gouy-Chapman-Stern-Graham (GCSG) model. In Section 3.3 the relationship between the double layer potential and the amount of adsorbed charge, i.e. SDS⁻ is established. The remainder of the chapter is devoted to estimating the mass of adsorbed SDS⁻ from surface potential data.

3.2.1 Introductory theory

The measured property of all chemical sensors based upon the field effect principle is dependent on the surface potential of the semiconductor. The distribution of the applied voltage and the thermodynamic basis for the measurement of double layer potential change, and subsequently the adsorbed charge from the capacitance-voltage study of the electrolyte-oxide-semiconductor (EOS) is outlined below. The discussion is obtained from a lucid exposition given by Bousse [5]. The electrochemical cell represented by equation 3.1 is used to explain the basis of the method of measurement. Introducing additional layers and liquid junctions between electrolytes is not critical to the theory. Therefore, the cell is represented by a minimum number of interfaces for simplicity.



In such a cell current flow is maintained by charge flow through the reference to the back side of the Si as the thick SiO₂ is a perfect insulator. The flow of current stops when the electron energy (the electrochemical potential of the electron) in the lead metals M'' and M' are equal. That is

$$\tilde{\mu}_e^{M''} = \tilde{\mu}_e^{M'} \quad (3.2)$$

Extending the same thermodynamic equilibrium condition at the M''/SCE and M'/Si interfaces gives:

$$\tilde{\mu}_e^{Ref} = \tilde{\mu}_e^{Si} \quad (3.3)$$

When external bias potential is applied the electron energy between the reference and the blocked working electrode are displaced by the same amount as the applied potential.

$$V_{app} = \frac{1}{q} [\tilde{\mu}_e^{Si} - \tilde{\mu}_e^{Ref}] \quad (3.4)$$

where $\tilde{\mu}_e^i$ is the electrochemical energy per particle of species "i" and q is the magnitude of the electron charge. Splitting the electrochemical potential into potential work function and chemical potential terms (see Section 1.3) equation 3.4 can be expressed by;

$$V_{\text{app}} = \frac{1}{q} \mu_e^{\text{Si}} - \frac{1}{q} \mu_e^{\text{Ref}} + (\Phi_b^{\text{Ref}} - \Phi_b^{\text{Si}}) \quad (3.5)$$

Where Φ_b^{Ref} , Φ_b^{Si} are the inner or Galvani potentials of the bulk reference and bulk Si respectively. In equation 3.5 and the discussion hereafter the chemical potential of "i" is expressed per particle. Defining the absolute potential of the reference electrode with respect to the solution, $\text{abs}V_{\text{Ref}}$, in terms of the electrochemical potential difference of an electron in the metal and the solution gives:

$$\text{abs}V_{\text{app}} = -\frac{1}{q} \mu_e^{\text{Ref}} + \frac{1}{q} \mu_e^{\text{Sol}} + (\Phi_b^{\text{Ref}} - \Phi_b^{\text{Sol}}) \quad (3.6)$$

μ_e^{Sol} is the chemical solvation energy of the electron which is not dependent on the particular reference electrode considered, but only on the nature of the solvent. For all electrodes in aqueous solutions, μ_e^{Sol} will be constant. So, for two electrodes in a cell this term will cancel out in the expression for potential difference and the reference potential may be given as;

$$V_{\text{Ref}} = -\frac{1}{q} \mu_e^{\text{Ref}} + (\Phi_b^{\text{Ref}} - \Phi_b^{\text{Sol}}) \quad (3.7)$$

Substituting equation 3.7 into equation 3.5 gives:

$$V_{\text{app}} = V_{\text{Ref}} + \frac{1}{q} \mu_e^{\text{Si}} + (\Phi_b^{\text{Sol}} - \Phi_b^{\text{Si}}) \quad (3.8)$$

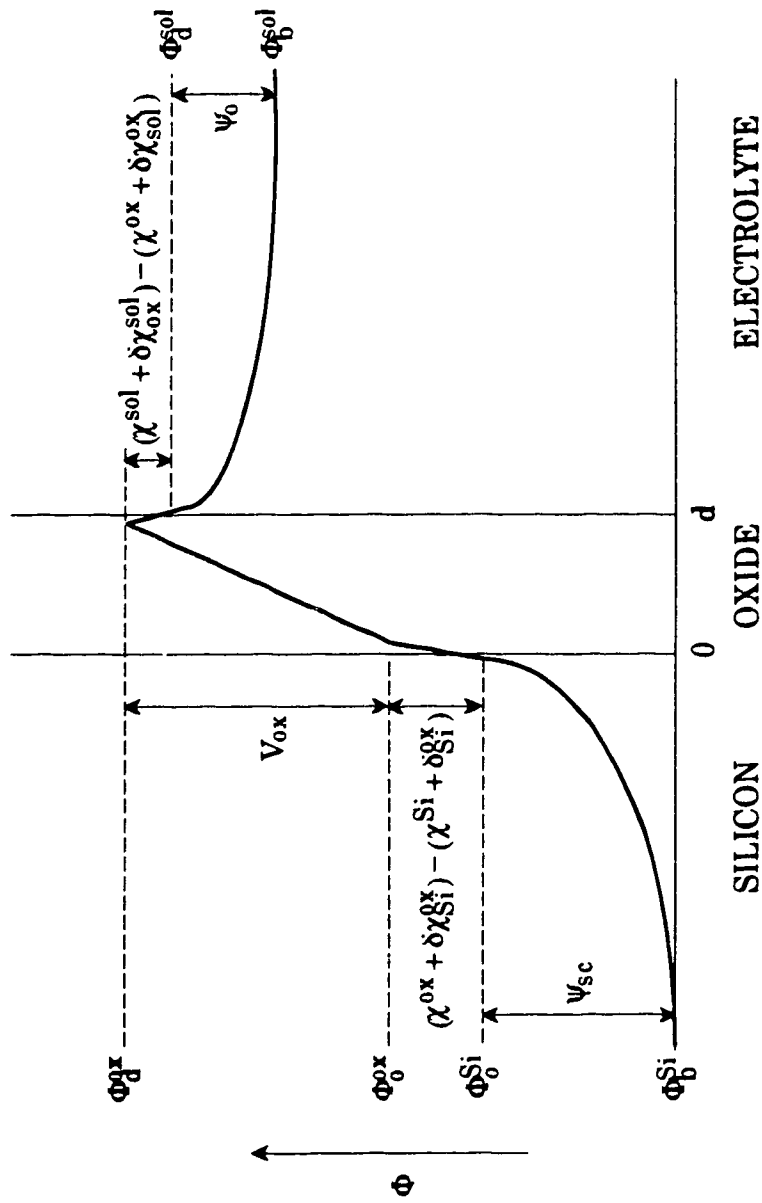


Figure 3.1 Potential distribution in the electrolyte/SiO₂/Silicon system.

The difference in inner potential between solution bulk and Si bulk can be split up as follows:

$$\left(\Phi_b^{\text{Sol}} - \Phi_b^{\text{Si}}\right) = \left(\Phi_b^{\text{Sol}} - \Phi_d^{\text{Sol}}\right) + \left(\Phi_d^{\text{Sol}} - \Phi_d^{\text{ox}}\right) + \left(\Phi_d^{\text{ox}} - \Phi_o^{\text{ox}}\right) + \left(\Phi_o^{\text{ox}} - \Phi_o^{\text{Si}}\right) + \left(\Phi_o^{\text{Si}} - \Phi_b^{\text{Si}}\right) \quad (3.9)$$

Figure 3.1 adopted from reference 5 identifies the position of the different potential terms. The terms on the right hand side of equation 3.9 can be interpreted as follows:

1- $\left(\Phi_b^{\text{Sol}} - \Phi_d^{\text{Sol}}\right) = -\psi_o$, where ψ_o is the double layer potential of the oxide surface relative to the potential of the electrolyte bulk.

2- $\Phi_d^{\text{ox}} - \Phi_o^{\text{ox}} = V_{\text{ox}}$ is the potential drop across the oxide.

3- $\Phi_o^{\text{Si}} - \Phi_b^{\text{Si}} = \psi_{\text{sc}}$ where ψ_{sc} is the surface potential.

4- $\Phi_d^{\text{sol}} - \Phi_d^{\text{ox}} = \left(\chi^{\text{sol}} + \delta\chi_{\text{ox}}^{\text{sol}}\right) - \left(\chi^{\text{ox}} + \delta\chi_{\text{sol}}^{\text{ox}}\right)$, $\delta\chi_b^a$ is the change in χ potential that phase "a" undergoes by being brought into contact with phase "b" while χ^a is the surface dipole potential of phase "a" in contact with vacuum.

Similarly;

$$5- \Phi_o^{\text{ox}} - \Phi_o^{\text{Si}} = \left(\chi^{\text{ox}} + \delta\chi_{\text{Si}}^{\text{ox}}\right) - \left(\chi^{\text{Si}} + \delta\chi_{\text{ox}}^{\text{Si}}\right).$$

The first three terms of equation 3.9 are in principle measurable, as they are potential differences within the same phase. The other two terms are inner potential differences across the oxide/silicon and the solution/oxide interfaces due to polarization and orientation of molecules (see Section 1.3). Replacing some of the terms by their commonly used representations, equation 3.8 becomes:

$$V_{\text{app}} = V_{\text{Ref}} - \left(\frac{1}{q} \mu_e^{\text{Si}} - \chi^{\text{Si}} \right) + V_{\text{ox}} + \Psi_{\text{sc}} - \Psi_o + \chi^{\text{sol}} + \left(S\chi_{\text{ox}}^{\text{sol}} - \delta\chi_{\text{sol}}^{\text{ox}} \right) + \left(\delta\chi_{\text{Si}}^{\text{ox}} - \delta\chi_{\text{ox}}^{\text{Si}} \right) \quad (3.10)$$

χ^{sol} is the surface potential characteristic of the solution in contact with vacuum. From surface reactivity [6,7], radio tracer [8] and impedance measurements [9], it has been shown that the chemical interactions between SiO₂ and the electrolyte are limited to surface reactions. Also, because of the unavailability of electrons for conduction, $(\delta\chi_{\text{ox}}^{\text{sol}} - \delta\chi_{\text{sol}}^{\text{ox}})$ of the insulator-electrolyte interface is insignificant [5]. This term is therefore dropped from subsequent equations. However, the corresponding term for the metal-electrolyte interface can not simply be neglected [5,10].

The electrochemical and outer potential of a species are measurable quantities. The difference between the two values expressed per particle

$$\mathfrak{Z}_i^\alpha = \bar{\mu}_i^\alpha - q_i \Psi^\alpha \quad (3.11)$$

called the real potential should be a measurable quantity too. \mathfrak{Z}_i^α measures the work required to move species "i" from the interior of α to a point just outside the range of the surface effects. It is also equal to the total potential energy change associated with entry of the charged particle from infinity into the medium when the latter is in an uncharged state. Hence, $(\mu_e^{\text{Si}}/q - \chi^{\text{Si}})$ in equation 3.10 is the work function of Si to be represented by W_{Si}/q .

Unlike colloids, in which electroneutrality must be achieved in the double layer, in EOS the charge is open to flow and redistribution amongst

the semiconductor, the electrolyte and the electrolyte-insulator interface. Disregarding other possible types of charges:

$$\sigma_o + \sigma_d + Q_{ox} + Q_{sc} = 0 \quad (3.12)$$

Where σ_o is the surface adsorbed charge at the electrolyte-insulator interface, σ_d is the charge in the electrolyte including the diffuse layer, Q_{ox} is the equivalent integral oxide charge that is taken to reside at the SiO₂/Si interface, and Q_{sc} is the space charge inside Si. The capacitance of the space charge (excluding surface trap effects) is a unique function of ψ_{sc} in the depletion region. It is possible to treat the space charge region in Si analytically using what is known as the delta-depletion approximation model. This model may seem coarse but has proven to be surprisingly accurate [11]. The approximation states that under depletion condition the transition from the neutral region to the space charge region occurs at a sharp boundary in the silicon substrate. It also assumes that the space charge density in the region lying between the boundary of the space charge and the oxide layer is constant, and is fixed by the dopant density. The space charge density in this case is then given by;

$$Q_{sc} = -qN_oX_{sc} \quad (3.13)$$

and the relationship between space charge capacitance, C_{sc} , and space charge potential, ψ_{sc} , is expressed by [11]:

$$\psi_{sc} = \frac{q\epsilon_o\epsilon_s N_o}{2C_{sc}^2} \quad (3.14)$$

Also, the width of the space charge layer, X_{sc} , is

$$X_{sc} = \left(\frac{2\epsilon_s \epsilon_0 \psi_{sc}}{qN_o} \right)^{0.5} \quad (3.15)$$

Here ϵ_0 is the permittivity of free space, ϵ_s is the relative dielectric constant of silicon, and N_c is its doping density. The voltage drop across the oxide may be expressed by the parallel plate capacitance equation;

$$V_{ox} = \frac{Q_{ox} + Q_{sc}}{C_{ox}} \quad (3.16)$$

Expressing Q_{sc} by the term obtained using equation 3.15 in equation 3.13 and then replacing ψ_{sc} by the term from equation 3.14;

$$V_{ox} = \frac{1}{C_{ox}} \left(Q_{ox} - \frac{q\epsilon_0\epsilon_s N_o}{C_{sc}} \right) \quad (3.17)$$

Substituting ψ_{sc} and V_{ox} in equation 3.10 by equations 3.14 and 3.17 respectively, we get;

$$V_{app} = V_{Ref} - \frac{W}{q} - \psi_o + \chi^{sol} + \frac{Q_{ox}}{C_{ox}} + \frac{q\epsilon_0\epsilon_s N_o}{C_{sc}} \left(\frac{1}{2C_{sc}} - \frac{1}{C_{ox}} \right) + (\delta\chi_{Si}^{ox} - \delta\chi_{ox}^{Si}) \quad (3.18)$$

The only term in equation 3.18 that would exhibit a significant solute dependence is ψ_o . The potential difference measured at constant electrode capacitance, ΔV_{app} , between a blank solution that has a supporting

electrolyte only, V'_{app} , and another that in addition also contains a surface active adsorbate, V''_{app} , is obtained from equation 3.18, considering all the terms that will be constant. This gives:

$$\Delta V_{app} = V''_{app} - V'_{app} = -(\psi''_0 - \psi'_0) \quad (3.19)$$

It should here be interjected that the applied potential following the convention of solid state physicists is defined relative to the Si substrate (equation 3.4). Electrochemists measure potential relative to the reference electrode rather than the indicator electrode. To conform with our experimental conditions in which the applied potential is measured relative to the saturated calomel electrode:

$$V = \frac{1}{q} [\bar{\mu}_e^{Ref} - \bar{\mu}_e^{Si}] \quad (3.20)$$

Equation 3.20 is the same as equation 3.4 except one is the negative of the other. Consequently ΔV in our experiment is given by:

$$\Delta V = \psi''_0 - \psi'_0 \quad (3.21)$$

This equation clearly shows that the difference in the applied voltage at an arbitrary constant depletion region capacitance between two sets of electrolytes is equal to the difference of the interfacial potentials' of the two samples.

Employing more exact equations than the delta-depletion approximation model would not alter the above conclusion since the

relationship between the three parameters of Q_{sc} , C_{sc} , and ψ_{sc} is one to one in the depletion region, where the voltage change is to be measured. The above description establishes the ground on which we were able to measure the potential change due to SDS⁻ adsorption from CV measurements.

3.2.2 The Gouy-Chapman-Stern-Grahame (GCSG) model

In order to relate the bulk SDS⁻ concentration to the amount of SDS⁻ adsorbed on the ODS surface, a relation between the voltage shift and charge has to be formulated. Several models have been proposed to describe the double layer region formed at an interface [12-14]. Colloid and surface scientists have used these models in the pH titration experiments of colloid particles [15,16], as well as mineral oxide titration with metal ions [16-18]. The choice of a particular model is governed by its ability to simulate the titration behavior of the oxide surfaces. It is, however, not seldom that basic constants have been treated as fit parameters [19, 20]. There are times when different models have been made to represent the same set of adsorption data equally well, with corresponding constants taking on quite different values [21]. The absence of independent information about the chemical species on the different planes of the interface, and several of the associated physical constants demonstrates the limitation of this approach. These kinds of technicalities decrease the confidence in the adequacy of a chosen model. However, there is no way around using model dependent interpretations.

The major difference among models, in terms of the expression for potential-charge relationships stems from the geometric description of the charge elements. If different ions are considered to adsorb on, or react with the surface at different surface planes, based on their chemical nature or on their size, then different potentials must be defined for each of the adsorption planes. A surface charge must be calculated for each plane and a capacitance determined for each plane. We break down this procedure for the GCSG model into two consecutive steps. First the planes of charge, their capacitances and their potentials are defined. The double layer theory is then used to yield surface charge-potential expressions. The GCSG model is the most general double layer model. It can generate the other double layer models under certain limiting conditions. Therefore, the basic features of this model are described below.

A reversed phase such as ODS does not have its own ionizable groups. It is the adsorption of charged species from solution which confers charge to it. This process dictates the interfacial potential difference. The adsorbing ion is therefore referred to as the potential determining ion (PDI). The charge density owing to the PDI is represented by σ_0 , as shown in Figure 3.2. The closest the finite sized, hydrated, non-adsorbing counter ions and co-ions can approach the PDI is the outer Helmholtz plane (OHP). The OHP is the plane where the diffuse double layer starts. The layer between the plane of the PDI and the plane of the OHP is referred to as the Stern layer. The capacitance of this layer is given by the Stern layer capacitance; C_{Stern} . In oxide surface studies the Stern layer is often divided into two layers. The first layer referred to as the inner Helmholtz plane (IHP) extends from the surface of the PDI to a layer formed by

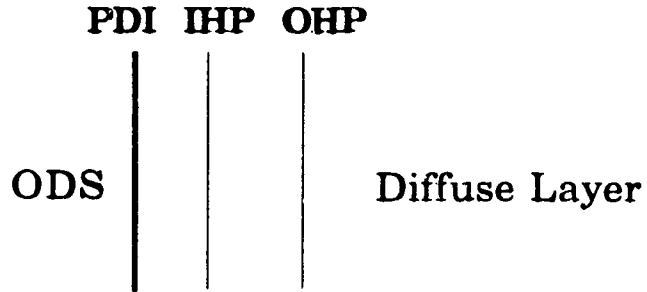
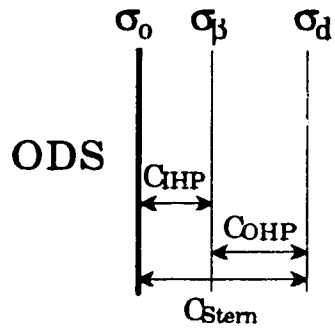
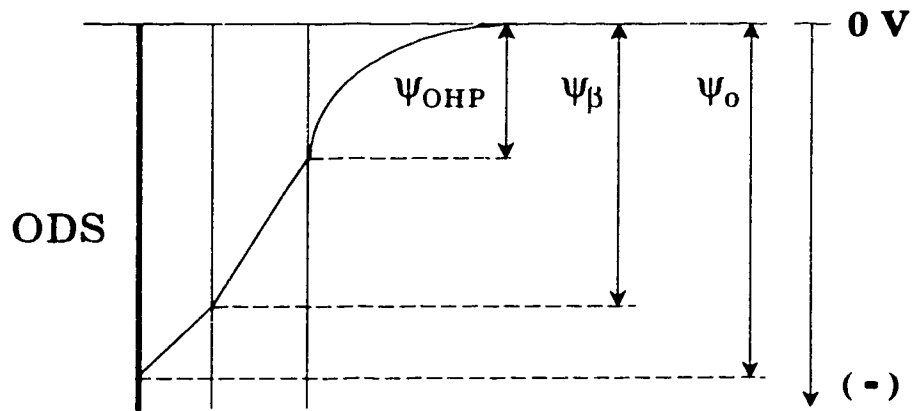
Model Planes*Charge Distribution**Potential Distribution*

Figure 3.2 Schematic representation of the GCSG model.
The potential distribution shown is for a negatively charged PDI.

"surface complexing" ions. The capacitance of the IHP is represented by C_{IHP} . The second layer extends from the IHP to the OHP. Except for the change of nomenclature, the "surface complexing" ions are equivalent to what is known in electrochemical studies as specifically adsorbed ions. The corresponding potentials of the various charged planes is shown in Figure 3.2.

Every plane of charge from the PDI upto the OHP is separated from its closest one by a region in which charge is absent. This separation of charge allows use of the conventional parallel plate capacitor model to relate charge density to potential gradient.

$$\psi_0 - \psi_\beta = \frac{\sigma_o}{C_{IHP}} \quad (3.22)$$

$$\psi_\beta - \psi_{OHP} = \frac{-\sigma_d}{C_{OHP}} \quad (3.23)$$

Where

$$\frac{1}{C_{Stem}} = \frac{1}{C_{IHP}} + \frac{1}{C_{OHP}} \quad (3.24)$$

In these equations C_{IHP} and C_{OHP} are the integral capacitance values. When the integral and differential capacitances are equal it is possible to write equation 3.24. However, when there is charge present in the IHP equation 3.24 may not hold. Adding equations 3.22 and 3.23 and then rearranging yields equation 3.25.

$$\psi_0 = \frac{\sigma_o}{C_{IHP}} - \frac{\sigma_d}{C_{OHP}} + \psi_{OHP} \quad (3.25)$$

Equation 3.25 states that the total potential difference across the double layer is the sum of the potential drops across the layers that are connected in series. The name "triple layer model" often used in colloid science to refer to the GCSG model is a recognition of the fact that three layers are involved. From charge neutrality:

$$\sigma_o + \sigma_\beta + \sigma_d = 0 \quad (3.26)$$

When equation 3.24 is valid then applying the charge neutrality condition to equation 3.25 gives:

$$\psi_o = \psi_{OHP} - \frac{\sigma_d}{C_{Stern}} - \frac{\sigma_\beta}{C_{IHP}} \quad (3.27)$$

The last two terms on the right hand side of equation 3.27 are potentials given by the charge on the capacitor plates. An expression relating ψ_{OHP} with the diffuse layer charge is known as the Gouy-Chapman equation [12, 14]. For a symmetrical electrolyte of charge Z ;

$$\psi_{OHP} = \frac{2RT}{ZF} \sinh^{-1} \left\{ \sigma_d \left(\frac{500\pi}{\epsilon_o \epsilon' RTC} \right)^{0.5} \right\} \quad (3.28)$$

Here ϵ' is the relative dielectric constant of the diffuse layer, C is the ionic strength of the supporting electrolyte, and the rest of the terms have their usual meaning. For a 1:1 electrolyte, concentration of C mol/L, and a temperature of 25 °C the Gouy-Chapman equation reduces to [12,14];

$$\psi_{\text{OHP}} = \frac{1}{19.47} \sinh^{-1} \left(\frac{\sigma_d}{11.77 C^2} \right) \quad (3.29)$$

If one only has potential measurements and the desired quantity is the density of the PDI or vice versa, equation 3.27 has to be reduced into a one variable equation. This is usually done by assigning values for the different capacitances and most importantly also defining the relation between σ_β and σ_d .

Equation 3.27 can also describe the charge-potential relationship in the absence of "surface complexation". This means there is no charge at the IHP. This double layer model is commonly known as the Stern-Gouy-Chapman (SGC) model. In this condition [12,14];

$$\sigma_o = -\sigma_d \quad (3.30)$$

The double layer potential as a function of σ_d is then given by :

$$\psi_o = - \left(\frac{\sigma_d}{C_{\text{Stern}}} + \psi_{\text{OHP}} \right) \quad (3.31)$$

Equation 3.31 has only the diffuse charge parameter. The adsorbed charge density can easily be calculated from double layer potential values.

3.2.3 Multiple layer blocking interface

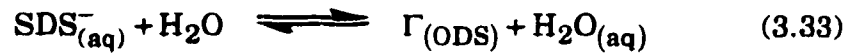
For the cell of Section 3.11, the Si is covered by only one type of blocking layer, namely SiO₂. In order to meet different requirements several layers have been interposed between the Si and the solution (see Section 1.2.3). The voltage drop across the blocking, multiple layers is expressed by equation 3.16, with the oxide layer replaced by the equivalent capacitance of the multiple layers. The residual charge density at constant pH of the SiO₂/ODS-electrolyte interface is constant. This charge resides right at the oxide surface and can be regarded as part of the Q_{ox}. The ODS layer itself as was discussed in Section 1.1 is an "inert" blocking layer. Thus, the effect of having the extra ODS layer on top of the oxide in the Si/SiO₂/ODS system is to modify the capacitance of the region between the Si and the solution part according to the equation:

$$\frac{1}{C_{in}} = \frac{1}{C_{ox}} + \frac{1}{C_{ODS}} \quad (3.32)$$

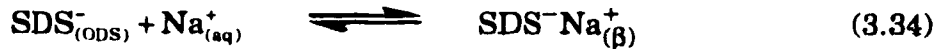
Where C_{ODS} is the capacitance of the ODS layer and C_{in} is the equivalent capacitance of the series arrangement of SiO₂ and ODS layers. Because the thickness of the ODS is normally a lot smaller than the SiO₂ layer, C_{in} can actually be approximated by C_{ox}.

3.3 SDS⁻ as the PDI

The potential that is developed at the ODS-electrolyte interface is mainly ascribed to the adsorption of SDS⁻ as represented in equation 3.33:



In addition to this, surface complexation can occur if the PDI associates with the supporting electrolyte sodium ion.



The equilibrium expressions for the adsorption and complexation processes respectively are:

$$K_{\text{ad}} = \frac{[\Gamma_{(\text{ODS})}]}{[\text{SDS}_{(\text{aq})}^{-}]} \quad (3.35)$$

and

$$K_{\text{Na}^{+}} = \frac{[\text{SDS}^{-}\text{Na}_{(\beta)}^{+}]}{[\text{SDS}_{(\text{ODS})}^{-}][\text{Na}_{(\text{aq})}^{+}]} \quad (3.36)$$

Here $[\text{SDS}_{(\text{ODS})}^{-}]$ and $[\text{SDS}^{-}\text{Na}_{(\beta)}^{+}]$ are the activities of adsorbed unbound SDS⁻ and surface complexed adsorbed SDS⁻ respectively. The subscript β is added to indicate the possibility of the Na⁺ ion being at a different plane from the PDI. $[\text{Na}_{(\text{aq})}^{+}]$ is the activity of Na⁺ in the aqueous phase which will be replaced by C mole/L in the following equations. K_{ad} and $K_{\text{Na}^{+}}$ are

the equilibrium constants of the adsorption and surface complexation processes respectively.

The total amount of PDI at the ODS plane, consists of both the free and bound SDS^- . That is

$$\Gamma_{(\text{ODS})} = [\text{SDS}_{(\text{ODS})}^-] + [\text{SDS}^- \text{Na}_{(\beta)}^+] \quad (3.37)$$

Combining equations 3.36 and 3.37;

$$\Gamma_{(\text{ODS})} = [\text{SDS}_{(\text{ODS})}^-] \left(1 + C * K_{\text{Na}^+} \right) \quad (3.38)$$

The activities of the $[\text{SDS}_{(\text{ODS})}^-]$ and $[\text{SDS}^- \text{Na}_{(\beta)}^+]$ can be expressed in a variety of units. Any one type chosen would change neither the value of K_{Na^+} , nor its units. In this particular case irrespective of the units of these two species, K_{Na^+} will have the inverse bulk sodium ion concentration unit such as $(\text{mole/l})^{-1}$. Since our analysis for the determination of the amount of adsorbed substance is based on the GCSG or SGC model, it is more convenient that surface concentrations be expressed in units of charge per unit area. This will allow a direct visualization of the correspondence between charge representations as σ_o , σ_β , σ_d and surface concentrations $\Gamma_{(\text{ODS})}$, $[\text{SDS}_{(\text{ODS})}^-]$ and $[\text{SDS}^- \text{Na}_{(\beta)}^+]$. Anyway, converting charge units in to other desired units is straight forward. For example, dividing the adsorbed charge density that is in Coul/cm^2 by the Faraday constant (i.e. 96487 Coul/equivalent) will give the adsorption density in moles/cm^2 for a singly charged adsorbent. However, care must be taken to consider the sign of the charge, since concentrations can't be negative.

Equation 3.38 allows the calculation of the total amount of SDS⁻ adsorbed from a knowledge of the unbound adsorbed SDS⁻ and the coordination constant K_{Na^+} . Combining equations 3.36 to 3.38 and rearranging gives:

$$\frac{1}{[\text{SDS}_{(\text{ODS})}^-]} = \frac{1}{K_{\text{ad}}[\text{SDS}_{(\text{aq})}^-]} + \frac{C \cdot K_{Na^+}}{K_{\text{ad}}[\text{SDS}_{(\text{aq})}^-]} \quad (3.39)$$

This equation shows that a plot of $1/[\text{SDS}_{(\text{ODS})}^-]$, the adsorbed charge due to uncomplexed SDS⁻ on the surface, will be linear in the concentration of Na⁺ ion if the activity of SDS⁻ is kept constant. For greater accuracy the activity of the Na⁺ should be considered. The slope and intercept of such a plot will yield K_{ad} and K_{Na^+} . The charge in the diffuse layer counterbalances the unbound surface adsorbed SDS⁻. Therefore

$$[\text{SDS}_{(\text{ODS})}^-] = -\sigma_d \quad (3.40)$$

Equation 3.40 is valid when superequivalent adsorption is not involved, that is, there is less Na⁺ in the IHP than there is Γ_{SDS^-} . σ_d can be calculated from the measured interfacial potential difference using one of the appropriate double layer models discussed in Section 3.12. The models, while presenting a physical representation of the system do not specify what values the various elements such as the C_{IHP} , C_{OHP} should be, or where the position of the surface coordinated Na⁺ is. Therefore, depending on the values used the same potential difference can be interpreted to give

different amounts of adsorbed charge, unless the capacitance values are known.

3.4 Experimental Section

SDS was purchased from Sigma Chemical and used without further purification. Its purity was reported to be approximately 99%. The pH buffer solutions were prepared from glacial acetic acid (BDH) or monochloroacetic acid (Fisher Scientific). NaOH (BDH) solution was used for the adjustment of pH. pH measurements were done by a combination Fisher glass electrode and a Fisher Model 810 Accumet pH meter. NaCl (BDH) was used to maintain the required ionic strength of solutions. All of the above reagents were of analytical grade. The water used was distilled, deionized and redistilled from alkaline KMnO_4 . Solutions were prepared as described below.

Constant ionic strength, constant pH and varying SDS concentration solutions were prepared from two stock solutions. One of the stock solutions was prepared from weighed amounts of SDS and NaCl containing acetic acid. Before the volume of the solution was adjusted, its pH was adjusted to 5 with very dilute NaOH solution. A second diluting stock solution having the same NaCl ionic strength and acetate buffer solution as the first stock solution and whose pH was similarly adjusted to pH 5 was also prepared. This second stock solution that did not contain SDS was used to dilute the first stock solution in order to prepare constant ionic strength, constant pH but varying SDS concentration solutions.

Aliquots were taken from three stock solutions of a) X M SDS, 1 mM buffer (pH=5); b) 1.25 M NaCl, 1 mM buffer (pH=5); c) 1 mM buffer (pH=5) and then mixed to prepare constant activity, constant pH but varying ionic strength solutions. The buffer was 1 mM in the sum of acetate anion and acetic acid concentrations. X was 0.47 mM for the 0.1 mM activity and 1.41 mM for the 0.3 mM activity of SDS study. The activity coefficients of SDS were calculated using the extended Debye-Huckel equation with the ion size of SDS⁻ equal to 5 picometer.

pH effect studies were carried out using just one stock solution of 2 mM acetate buffer and 0.03 M NaCl solution containing either 0.3 mM or 0.6 mM SDS. The pH was changed by adding NaOH from a relatively concentrated solution. The slight change in ionic strength and SDS activity introduced by the dilution due to the volume of NaOH added was neglected. For pHs below 4 the acetate buffer was made from monochloroacetic acid while for pHs between 4 and 7 acetic acid was used.

The three electrode electrochemical system was used to obtain CV data. The counter electrode was a platinum wire gauze electrode. Potentials were measured relative to a saturated sodium chloride calomel electrode. The reference electrode was isolated with a frit glass tipped double junction filled with a blank solution of the same ionic strength and pH as the test solution. All measurements were done at room temperature. Regular 50 ml size beakers were used as electrochemical cells. A separate beaker was reserved for blank solutions. All glassware used were cleaned after being kept in persulfate acid bath or ethanol base bath.

Semiconductor electrodes were prepared from float zone n-Si (International Wafer Services) having a resistivity of 400-800 Ω -cm, (100)

face and diameter of 3 inch. Thermal oxide was grown to 850 Å thickness at the Alberta Microelectronic Center (Edmonton, Canada). The silanization steps were first completed before making electrodes.

A piece about 0.5 cm by 3 cm was taken from the Si/SiO₂ float zone wafer. It was cleaned in H₂O, CH₃OH, trichloroethylene, CH₃OH and H₂O, followed by a 30 seconds etch in 5% HF. It was then rinsed with H₂O and surface hydroxyl formation encouraged by refluxing for 3 to 4 hours in H₂O. After about 12 hours of drying at 60 °C it was silanized with ODS (Petrarch Systems Inc.). The silanization was carried out by refluxing the Si/SiO₂ piece for 24 hours in excess of ODS (at least 0.14 M) dissolved in analytical grade toluene (Fisher Scientific). The toluene was dried by being kept over phosphorus pentoxide (General Intermediates of Canada). The same piece was refluxed for a third time in 10 ml trimethylchlorosilane (General Intermediates of Canada), 30 ml dried toluene for another 24 hours so that any remaining accesible surface silanol groups were endcapped. Both of the silanizing reagents were used as received. Monochlorosilanes can react with only one silanol group and therefore the Si/SiO₂ surface was covered with no more than one molecular layer of ODS.

After the silanization procedure was completed, the non-polished back side of about 0.2 cm² piece was abraided using a diamond pen in the presence of gallium-indium eutectic to form a very highly doped, degenerate spot for ohmic contact. It was then contacted to a coiled end of about 15 cm long lead copper wire using silver epoxy and kept in the oven below 60 °C for 12 hours during which time the silver epoxy cured. The copper lead was isolated from solution by a 0.4 cm internal diameter glass tube and the Si/SiO₂-copper contact including some part of the front edge of the silanized

surface was covered with Chem-grip® (Norton performance plastics). The only part of the electrode that was in contact with solution was the front silanized Si/SiO₂ surface.

Capacitance-voltage data were obtained using the same instruments described in the previous chapter. A single 1000 Hz sine wave, peak-to-peak amplitude of 10 mV was used throughout the CV measurements. For each test solution, triplicate CV measurements covering the inversion and depletion regions were made. The "median" CV curves of the test solutions and reference solution were plotted together in the same plot. A depletion capacitance of about 25% relative to the maximum (accumulation region) capacitance of the electrode was then selected for comparison. The difference in voltage at the chosen capacitance between the CV of the reference solution and that of the test solutions were used to obtain the voltage shifts. The constant depletion capacitance of the electrode was chosen away from any ledge that is normally caused by surface traps (see Section 2.4.1).

3.5 Results and Discussion

The potential shift required to maintain a constant depletion capacitance of the electrode with changing solution conditions has been shown to measure the change in the double layer potential. The potential shift measurement at constant electrolyte conditions including pH but changing activity of a charged adsorbate, as discussed below, measures the surface potential change due to adsorption of the PDI. By correlating the

measured surface potential to the adsorbed charge density the adsorption isotherm of the PDI can be worked out. In the following sections we present the results of the SDS⁻ adsorption on the ODS surface and finish by determining the adsorption isotherm of SDS⁻.

3.5.1 pH of point of zero charge of the ODS surface

Octadecyldimethylchlorosilane is a monofunctional silane that results in a monomeric alkane on an SiO₂ surface. It does not contribute additional silane silanols to the phase [22,23]. Because of steric hindrance silanization with ODS optimally leads to reaction with about 50% of the surface silanol groups present on the oxide surface [23,24]. Trimethylchlorosilane, which is a small silanizing agent, was used to end-cap the remaining accessible silanols. Even after this procedure there will be some unbonded silanols left. A good fraction of the residual silanols are shielded from any reaction. Nonetheless, a limited number of ionizable sites normally remains on the surface.

The sign and net charge density due to ionizable silanols remaining on the silanized surface is dependent on the reactive site density, pH of the experiment, and the pH of the point of zero charge (pH_{pzc}) [25-27]. The pH_{pzc} represents the pH and electrolyte conditions at which the net surface charge of an amphoteric surface is zero. The potential status of the surface relative to the bulk solution remains unknown unless the isoelectric point (iep) is known. At the iep the surface plus the Stern charge is zero and the diffuse layer potential is zero. In the absence of specific adsorption there is

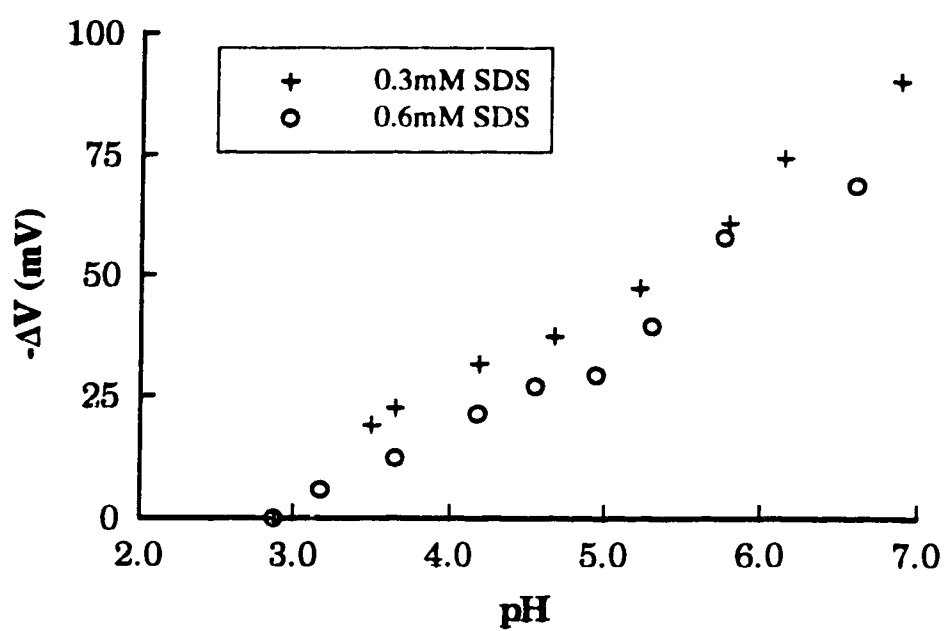


Figure 3.3 Potential shift-pH measurements of 0.03 M NaCl; 2mM acetate buffer; at two constant SDS activities, where ΔV is measured relative to the 2.87 pH solution.

no distinction between pH_{pzc} and the iep. Oxides have silanol densities that depend on the surface structure, crystallographic orientation, stoichiometry, degree of hydration and previous heat treatment [28,29]. As a result, the range of the pH_{pzc} reported for ostensibly the same type of oxide is large. The pH_{pzc} of silicon dioxide is reported to be between 2 and 3.5 [28,30]. It has been reported that amorphous SiO_2 begins to obtain negative charge at pH values near a pH of 7.0 [31], indicating that the pH_{pzc} is close to 7.0. There are not many reports about the pH_{pzc} of a silanized surface. Oxides with a large silanol site density show Nernstian behavior to pH change [25-27], while the effect of reducing silanol density, either by chemical bonding of apolar groups or vacuum heating of the oxide, is a lowered sensitivity to pH [25,32-34]. The silanized oxide we prepared shows about 20 mV shift per pH unit. This is evidence that the accessible, residual silanol, surface charge density is reduced on a silanized surface.

Figure 3.3 shows a plot of $-\Delta V$ versus pH of a silanized electrode in 0.03 M NaCl at SDS concentrations of 3 and 6×10^{-4} M. The potential shifts are measured relative to the 2.87 pH solution. To avoid hydrolysis of the silanized surface, the experiments were done at pH values below 7. In addition, higher pH media are known to give less reproducible measurements [33]. ψ_0 / pH characteristics of insulators of differing exchangeable ion densities have been estimated [35,36]. It has been shown that the ψ_0 / pH plot has the smallest sensitivity around the pH_{pzc} [33-36]. Bousse *et al.* [33] have used the minimum in the slope of the electrode potential versus pH plot as the criterion to determine the pH_{pzc} . This should be true even in the presence of SDS^- as discussed below. The inflection point of the slopes in the Figure suggests the pH_{pzc} may lie in a pH range of 4.5 to 5.

However, the inflection point is not strong, so this may not be a very reliable estimate.

3.5.2 The resolution of residual charge and SDS⁻ charge from CV studies

The analysis for the determination of the amount of SDS⁻ adsorbed is based on the measurement of the potential shift of the CV as the SDS⁻ bulk concentration is varied from a fixed reference solution. Equations 3.18 and 3.30 express the applied potential-capacitance curve in the depletion region. The very fact that Figure 3.3 shows pH dependence shows some silanol groups remain active. Their presence and effect must be accounted for in the analysis of the effect of SDS⁻ on potential.

The mathematically simplest way of considering the presence of residual silanol charge in the model presented above is to assume it is present in the same plane as the adsorbed SDS⁻. The error introduced by this assumption will be discussed in detail later. In the absence of SDS⁻ the surface potential ψ_0 will be a function of the charge due to ionized silanols, σ_{SiOH} . In the presence of SDS⁻, ψ_0 reflects the total charge due to $\sigma_0 = \sigma_{\text{SDS}^-} + \sigma_{\text{SiOH}}$, where σ_0 is the total ionized charge. The SGC equation for ψ_0 as a function of σ_0 given in equation 3.31 is a non-linear function when σ_0 is large. This means that the potential difference measured in the presence and absence of SDS⁻ does not generally give a potential due to the effect of SDS⁻ alone, i.e.,

$$\psi_0(\sigma_{\text{SDS}^-} + \sigma_{\text{SiOH}}) - \psi_0(\sigma_{\text{SiOH}}) \neq \psi_0(\sigma_{\text{SDS}^-}) \quad (3.41)$$

However, when σ_0 is sufficiently small the hyperbolic sine function in equation 3.28 is approximately linear, so that equation 3.41 does become an equality.

Using the SGC equation it is possible to estimate the fraction of the potential that drops across the compact, or Stern layer, and the fraction of potential appearing across the diffuse layer. The model requires the Stern layer capacitance in equation 3.31 so that the adsorbed charge density can be calculated from the measured surface potential. Not enough is known about the value of the C_{Stern} of a hydrophobic surface or for that matter, of the well studied oxide-electrolyte interface [37]. The capacitance of an oxide solution interface is much larger than that of the classical surfaces of silver halide sols and mercury [38-41]. On the basis of values encountered on noble metal electrodes, a value of $20 \mu\text{F}/\text{cm}^2$ is often used for C_{OHP} . Values well in excess of $100 \mu\text{F}/\text{cm}^2$, as high as $348 \mu\text{F}/\text{cm}^2$ [42] have been used for the C_{IHP} . There are no systematic rules for determining the C_{IHP} . It is invariably treated as an adjustable experimental parameter [19,20]. As a result best fit experimental data are ill matched to theoretical predictions of IHP capacitance based on ion size and dielectric constant [37]. C_{OHP} is generally assumed to be lower than C_{IHP} . We have used $20 \mu\text{F}/\text{cm}^2$, and $100 \mu\text{F}/\text{cm}^2$ for C_{OHP} and C_{IHP} respectively. These values were chosen simply because they seem to have gained the concensus of use. Given the condition of ionic strength used in this study about 70% of the interfacial potential should fall across the Stern layer. Since the Gouy-Chapman equation is a linear function for potentials across the diffuse layer of up to

about 25 mV, a total ψ_0 value of up to about 100 mV will allow equation 3.41 to be treated as an equality.

Figure 3.3 shows how $-\Delta V$ changes as function of pH at two different activities of SDS^- . The electrode potential at pH 2.87 was taken as the reference potential. The curves for the two concentrations are very close to overlapping, indicating that linearization of the Gouy-Chapman equation is possible under these conditions, so that equation 3.41 can be treated as an equality. The Figure also indicates the potential shift due to pH is about -20 mV per pH unit. The offset of the points at the two activities is significantly smaller than that observed with SDS^- .

As previously mentioned the inflection point in Figure 3.3 suggests pH_{pzc} is at about 4 to 5. Consequently, experiments varying the SDS^- activity or concentration were performed at pH 5 where σ_{SiOH} should be very small. However, the reported value of pH_{pzc} for uncoated SiO_2 is about 2 to 3, so it is possible that a reasonable oxide charge is present. The impact of oxide surface charge on the use of ΔV to evaluate σ_{SDS^-} can be estimated. This effect is illustrated by considering the worst case condition in which the pH_{pzc} is taken at the lowest reported pH_{pzc} , 2.

The effect of a pH_{pzc} of 2 on experiments performed at pH 5 would be to induce a surface potential due to oxide charge of about -60 mV given a 20 mV/pH response to pH. The value of σ_{SiOH} calculated from equation 3.28 for this surface potential is $-0.708 \mu\text{C}/\text{cm}^2$; given an ionic strength of 0.03 M, $C_{\text{IHP}} = 100 \mu\text{F}/\text{cm}^2$ and $C_{\text{OHP}} = 20 \mu\text{F}/\text{cm}^2$.

When SDS^- is adsorbed the surface potential ψ_0 will become more negative. Table 3.1 compares the value of σ_{SDS^-} obtained from applying equation 3.31 to the total value of ψ_0 , with the value σ'_{SDS^-} estimated for

adsorbed SDS⁻ from the $\Delta\psi$ value that is experimentally accessible from ΔV . The potential difference was calculated from the potential in the presence of SDS⁻ relative to the potential in its absence, assuming $\sigma_{\text{SiOH}} = -0.708 \mu\text{C}/\text{cm}^2$. The table shows that at a value of $\Delta V = -150 \text{ mV}$ the error in estimating σ_{SDS^-} is less than 4%. This is within experimental error, so that the approximation

$$\Delta V = \psi(\sigma_{\text{SDS}^-}) = \psi(\sigma_{\text{SDS}^-} + \sigma_{\text{SiOH}}) - \psi(\sigma_{\text{SiOH}}) \quad (3.42)$$

is a reasonable one for the data range studied.

The point of zero charge is the pH at which the net charge is zero, however, both positively and negatively charged oxide sites will probably be present at the pH_{pzc} . Consequently, changes in ionic strength in solution could shift the pH_{pzc} by affecting the activity of ions in solution or on the surface, as well as by shifting the potential distribution in the double layer. Figure 3.4 shows also a plot of $-\Delta V$ versus ionic strength in the absence of SDS⁻. The reference potential was taken as the value in the highest ionic strength solution. The electrode surface potential shifted negative by less than 6 mV as the ionic strength was changed from 250 to 0.6 mM NaCl concentration. Because of the way the solutions were prepared the changes in ionic strength would have shifted the activity of the buffer ions slightly. Using the extended Debye-Huckel equation the effect of this shift was estimated to shift pH by about 0.11 pH units from the lowest to highest ionic strength. This should have caused a ΔV of -2 mV, given a -20 mV slope, in reasonable agreement with the observed shift. The standard deviation of the potential shift for triplicate measurements of the same

Table 3.1 Charges calculated for given values of potential in order to test the the validity of equation 3.42.

$-\Psi_{\text{SDS}/\text{SiOH}}$ (mV)	$-\sigma_0$ $\mu\text{C}/\text{cm}^2$	$-\sigma_{\text{SDS}^-}$ $\mu\text{C}/\text{cm}^2$	$-\Delta\Psi_0$ (mV)	$-\sigma'_{\text{SDS}^-}$ $\mu\text{C}/\text{cm}^2$	% error charge
70	0.828	0.120	10	0.118	-1.7
80	0.948	0.240	20	0.235	-2.1
100	1.192	0.484	40	0.471	-2.7
120	1.437	0.729	60	0.709	-2.7
140	1.688	0.98	80	0.949	-3.2
160	1.941	1.233	100	1.192	-3.3
190	2.329	1.621	130	1.562	-3.6
210	2.592	1.884	150	1.814	-3.7

$\Psi_{\text{SDS}/\text{SiOH}}$ is a hypothetical surface potential due to the adsorbed SDS^- and silanol charge, $\Delta\Psi_0$ is the difference in potential that would be measured if the SDS^- and silanol charge potentials were additive, σ_0 and σ'_{SDS^-} are the respective charges calculated using equation 3.28. $\sigma_{\text{SDS}^-} = (\sigma_0 - 0.708)$, and the error in the estimated charge due to the linear potential approximation is given as a % error.

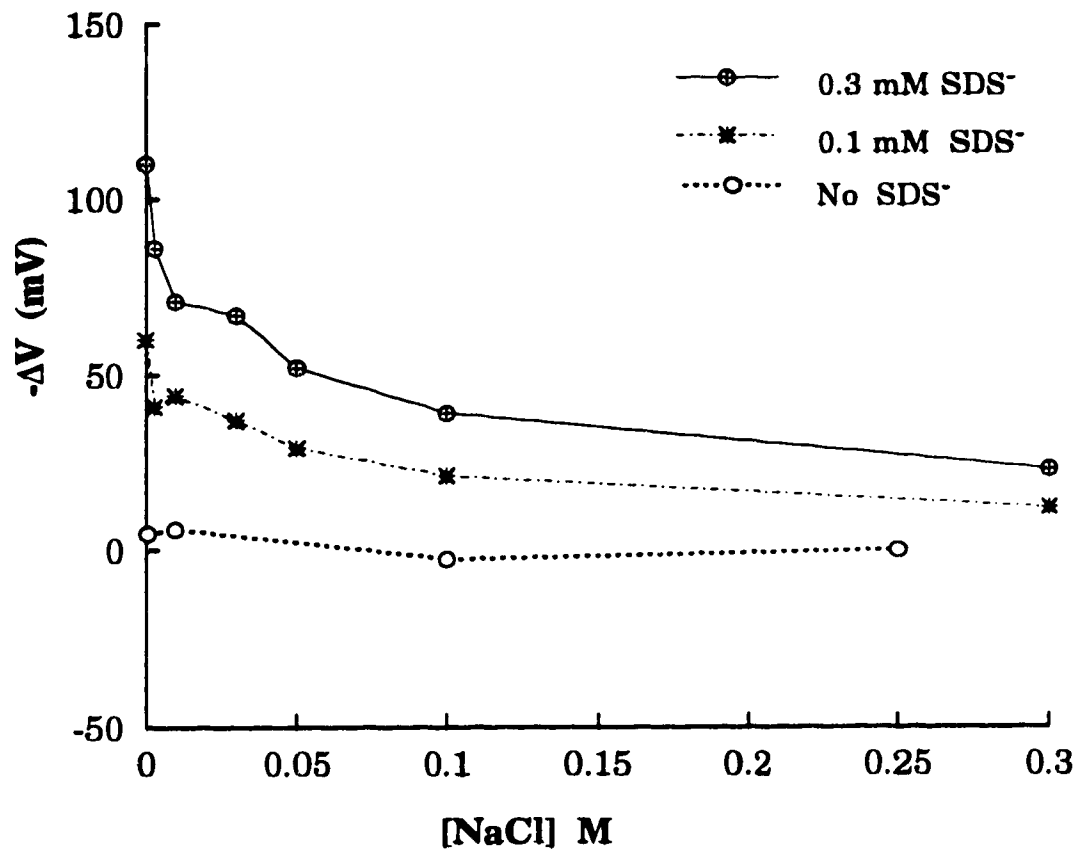


Figure 3.4 Plot of the variation of ψ_0 as a function of ionic strength at two SDS⁻ constant activities of 0.1 mM and 0.3 mM and without SDS⁻. The pH of the solution is kept at 5 by a 1 mM acetate buffer in all cases.

solution was less than ± 2 mV. Consequently, the -6 mV shift measured is slightly larger than might be expected but lies on the limit of experimental error. Regardless, the shift is certainly small. The result in Figure 3.4 in the absence of SDS^- shows that the surface potential due to the oxide charge is not strongly dependent on ionic strength.

The model incorporating surface silanols described above assumed σ_{SiOH} and σ_{SDS^-} were in the same plane. It is more likely they are separated by the ODS layer. If the silanol sites were accessible to H_2O , but not to ions, then the ODS layer would act as an insulating dielectric, effectively decreasing the value of C_{Stern} by the thickness of the ODS layer. Since $V = q/C$ across a parallel plate capacitor this means that the potential drop across this region would represent a larger fraction of ψ_0 . Consequently, the potential across the diffuse layer induced by the σ_{SiOH} would be even smaller than if σ_{SiOH} and σ_{SDS^-} occupied the same plane. As a result the equality of equation 3.42 would be valid to even higher surface potentials.

If the ODS layer separates σ_{SDS^-} from σ_{SiOH} , but the ODS layer is permeable to ions, then the surface may be treated as having separate regions of exposed silica surface and other regions coated by ODS onto which SDS^- adsorbs. Assuming C_{Stern} is the same for both surfaces then the situation will essentially be the same as the case where σ_{SDS^-} and σ_{SiOH} are treated as lying in the same plane.

3.5.3 Adsorption saturation of SDS⁻

In Figure 3.5 is given the potential shifts measured at constant pH and three constant ionic strengths as the SDS⁻ concentrations were varied. The Figure shows initial sharp rising voltage shifts that plateau at higher SDS⁻ concentrations.

It has been demonstrated that the amount of surfactant adsorbed on a stationary phase is constant at concentrations above the CMC [43,44]. This is similar to the physical properties of surfactant solutions which normally depend upon the number of solute molecules per unit volume of solution. Often a discontinuity of these properties is exhibited at the CMC. Below the CMC they act as normal electrolytes, but above the CMC such colligative properties as the osmotic pressure, boiling point, turbidity, vapor pressure, etc. show little or no change. The simplest model for such behavior is that above the CMC a phase equilibrium exists between the monomer surfactant and its micelle with a constant activity of the surfactant in the micellar phase. The activity of free SDS⁻ (PDI) remains unchanged above the CMC [45]. Below we discuss whether the plateau effect shown by SDS⁻ adsorption is a result of reaching the CMC, or arises from adsorption saturation. This was evaluated by determining the CMC of SDS⁻ as a function of NaCl concentration.

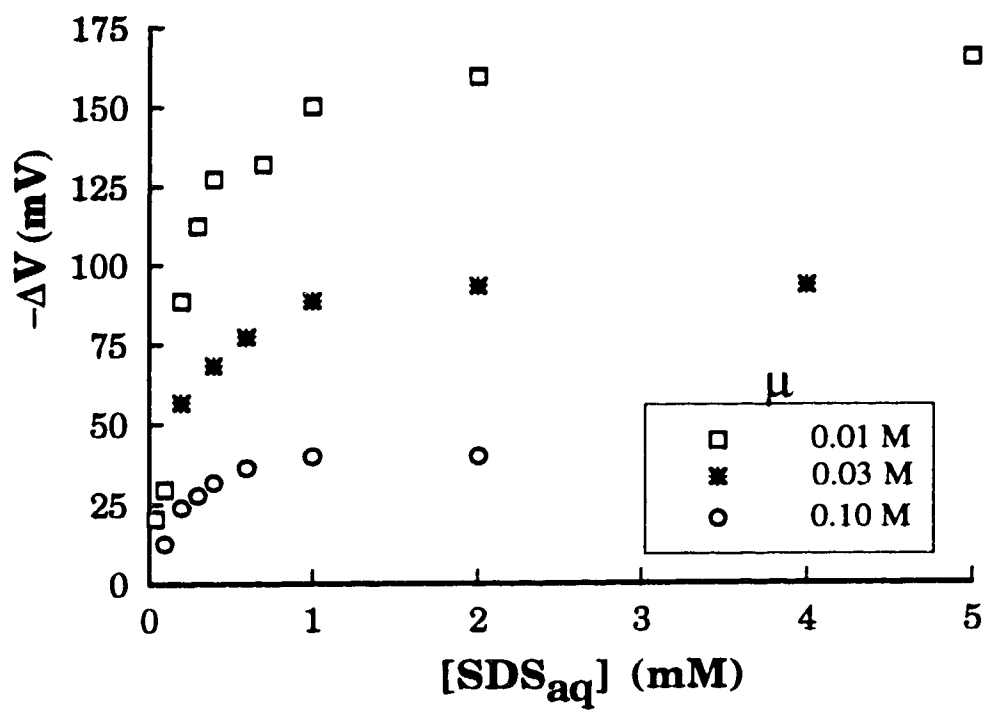


Figure 3.5 Plot of the variation of $-\Delta V$ as a function of SDS^- at three ionic strengths (μ) of 0.01, 0.03 and 0.1 M. The pH of the solution is kept at 5 by a 1 mM acetate buffer in all cases.

3.5.4 Critical Micelle Concentration of SDS

SDS is a well studied surfactant. It has characteristic hydrophobic and hydrophilic segments (Diagram 3.6). The solubility of surfactants as single molecules or ions in aqueous media results from the presence of the polar (or ionic) group. The hydrophobic part, when interacting with the aqueous

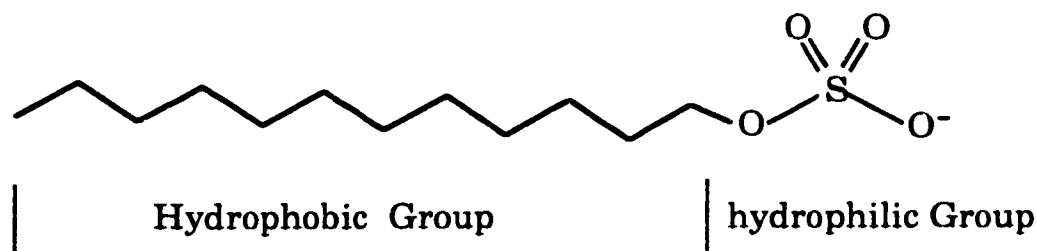


Diagram 3.6 Schematic structure of SDS⁻ molecule.

solvent, restricts the orientation of the H₂O molecules in solution, and consequently affects the entropy of the system. When the chemical potential of the monomer reaches an appropriate level, it wants to escape from the water layer. Adsorption at interfaces, as at the liquid/gas or liquid/solid interfaces, is one way of avoiding the entropically unfavorable contact between water and the hydrophobic part, while maintaining the aqueous hydrophilic part's contact. Another alternative is self-association

into aggregates of structures having an inner hydrophobic core and an outer hydrophilic surface of the head groups, called micelles.

The concentration at which surfactant micelles emerge, referred to as the critical micelle concentration (CMC), depends on the balance between the factors promoting micellization and those opposing it. The CMC of SDS⁻ is lowered by the addition of an indifferent electrolyte. In water the CMC of SDS⁻ is 8.1 mM and decreases to 0.52 mM in 0.4 M NaCl [45]. The Corrin-Harkin empirical equation [46]:

$$\log(\text{CMC}) = -a * \log(C) + b \quad (3.43)$$

relates the CMC of a surfactant to the indifferent electrolyte concentration in equivalents per liter, C. "a" and "b" are constants specific to the head group. We find that a plot of the inverse square root of the NaCl concentration against the SDS CMC is linear as shown in Figure 3.7. The best least squares equation of this plot is:

$$\text{CMC} = 10^{-4} \left(\frac{6.108}{\sqrt{C}} - 4.946 \right) \quad (3.44)$$

Re-writing equation 3.43:

$$\text{CMC} = \frac{10^b}{C^a} \quad (3.45)$$

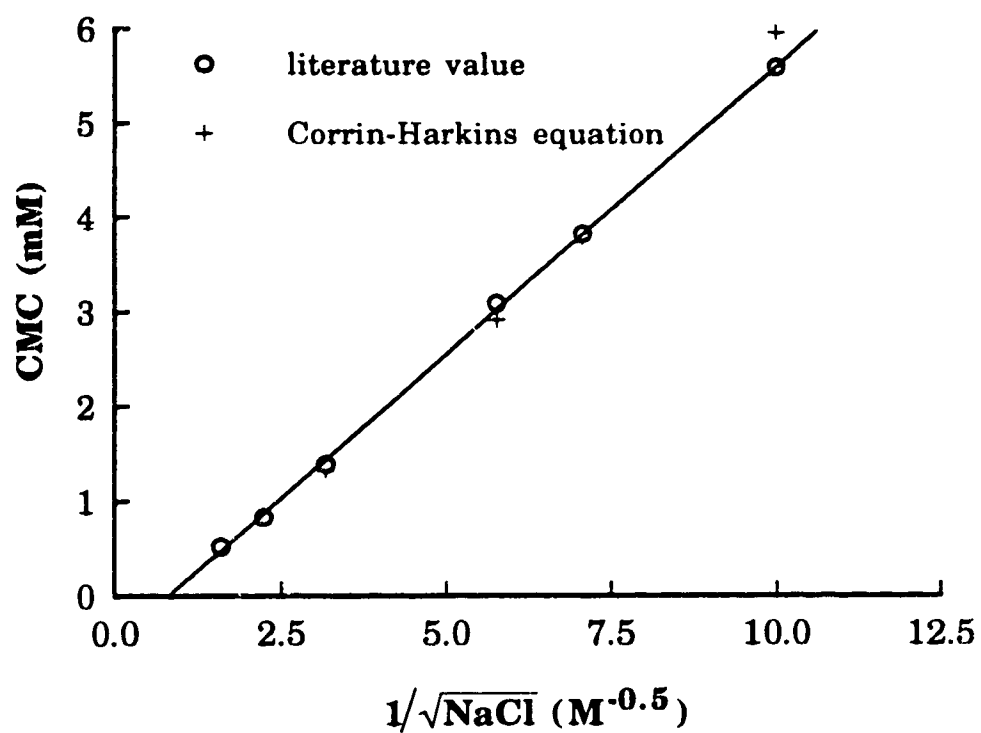


Figure 3.7: Plot of literature values of the CMC of SDS vs $[NaCl]^{-0.5}$. Points generated from the Corrin-Harkins relationship for the identical data are shown by +.

By letting "a " be equal to 0.5, equation 3.45 does not reduce to equation 3.43. Therefore equations 3.43 and 3.44 are not different forms of the same expression. As far as SDS is concerned, a better fit and correlation is obtained from the inverse square root of NaCl versus CMC plot that we propose (Figure 3.7). A log-log plot in general tends to be linear, and small variations in the slope of such a plot may introduce relatively large variations when extrapolated to other regions. At the low ionic strength end, both equations predict close values. The proposed equation predicts the CMC reaches zero at ionic strengths close to 1.5 M which is probably not a reasonable expectation. The disparity between the two empirical equations increases with increasing ionic strength. We do not have data, particularly around the 1 M region, to check which of the two equations gives a better prediction.

As can be calculated based on the empirical expressions the lowest CMC occurs at the highest indifferent ionic strength solution, which in our experiments of constant ionic strength was 0.1 M. The CMC of SDS⁻ in 0.1 M NaCl is about 1.5 mM. The plot of $-\Delta V$ versus SDS⁻ of Figure 3.5 plateaus at less than 1 mM of SDS⁻ concentration at all ionic strengths. Therefore the plateauing of SDS⁻ adsorption in this work is only due to adsorption saturation as it occurs before the CMC is reached. In the adsorption experiment shown in Figure 3.4 the highest ionic strength was 0.3 M and the highest SDS activity (0.3 mM) was below 0.62 mM which is the CMC of SDS at this ionic strength.

3.5.5 The estimation of K_{Na^+}

An effect such as that shown in Figure 3.4 is predicted by the analysis presented in Section 3.2, if there is an interaction between SDS^- adsorbed on the ODS layer and $Na^+_{(aq)}$. This interaction could be interpreted as arising from Na^+ occupying the IHP, essentially forming a contact ion pair with $SDS^-_{(ODS)}$. Alternatively, it may be thought of as arising from spherical coordination by an average of one Na^+ ion around an $SDS^-_{(ODS)}$ head group. That is, the Na^+ ion is not constrained to lie on a plane as it would be at a true solid surface. Rather the SDS^- head group extends away from the ODS plane far enough that no one plane can be clearly defined for the Na^+ counter ion. In this case, Na^+ simply neutralizes an SDS^- on the surface and C_{IHP} can be taken as very large, or approaching infinity.

The data in Figure 3.4 shows the changes in surface potential as the ionic strength was varied in solution. Two constant activities of SDS^- at pH 5 were used. The value of ΔV was calculated relative to the signal measured in 0.3 M ionic strength and pH 5. The data clearly show that the surface potential varies substantially as the ionic strength is varied, even though the activity of SDS^- is held constant. The effect is much greater in the presence of SDS^- than in its absence, so that the role of any residual surface oxide is virtually negligible.

The analysis of Section 3.2 yields equation 3.39, which predicts that a plot of $1/[SDS^-_{(ODS)}]$ versus the Na^+ activity should be linear. If we take C_{IHP} to be infinite, as discussed above, then $\sigma_o = -\sigma_d$ and the amount of uncompensated charge due to $SDS^-_{(ODS)}$ ($[SDS^-_{(ODS)}]$) will be equal to $-\sigma_d$. The diffuse layer charge was calculated using equations 3.28 and 3.31 to

obtain $[\text{SDS}_{(\text{ODS})}^-]$ as a function of ψ_o . Figure 3.8 shows a plot of $1/[\text{SDS}_{(\text{ODS})}^-]$ versus Na^+ activity for the data shown in Figure 3.4. A linear relationship is observed, with slopes of $1.4 \times 10^{15} \text{ cm}^5/\text{mole}^2$, $6.6 \times 10^{14} \text{ cm}^5/\text{mole}^2$, and intercepts of $1.8 \times 10^{11} \text{ cm}^2/\text{mole}$ and $1.0 \times 10^{11} \text{ cm}^2/\text{mole}$ for the 0.1 and 0.3 mM $\text{SDS}_{(\text{aq})}^-$ activities, respectively. These give values of K_{ad} of $5.6 \times 10^{-5} \text{ cm}$ and $3.2 \times 10^{-5} \text{ cm}$ at the two ionic strengths. The interaction with Na^+ , K_{Na^+} , was 7.8 and 6.3 lt/mole for 0.1 and 0.3 mM SDS^- , respectively.

The data indicate a decrease in K_{ad} as $[\text{SDS}_{(\text{aq})}^-]$ increases. This is consistent with the non-linear behaviour of the adsorption isotherm indicated by the data in Figure 3.5. Another model for adsorption is discussed later.

The values of K_{Na^+} are in reasonable agreement given experimental error, and the fact that changes in activity of surface adsorbed species with ionic strength are not incorporated in the model. The binding constant is quite small, consistent with the fact that little or no ion pairing is reported for aqueous SDS^- . However, the constant does indicate that some of the SDS^- adsorbed on the ODS layer will be neutralized by Na^+ from solution. This means that methods used to determine the total mass of an adsorbate such as SDS^- on a surface will overestimate the potential generated by the adsorbed material, unless charge compensation is taken into account.

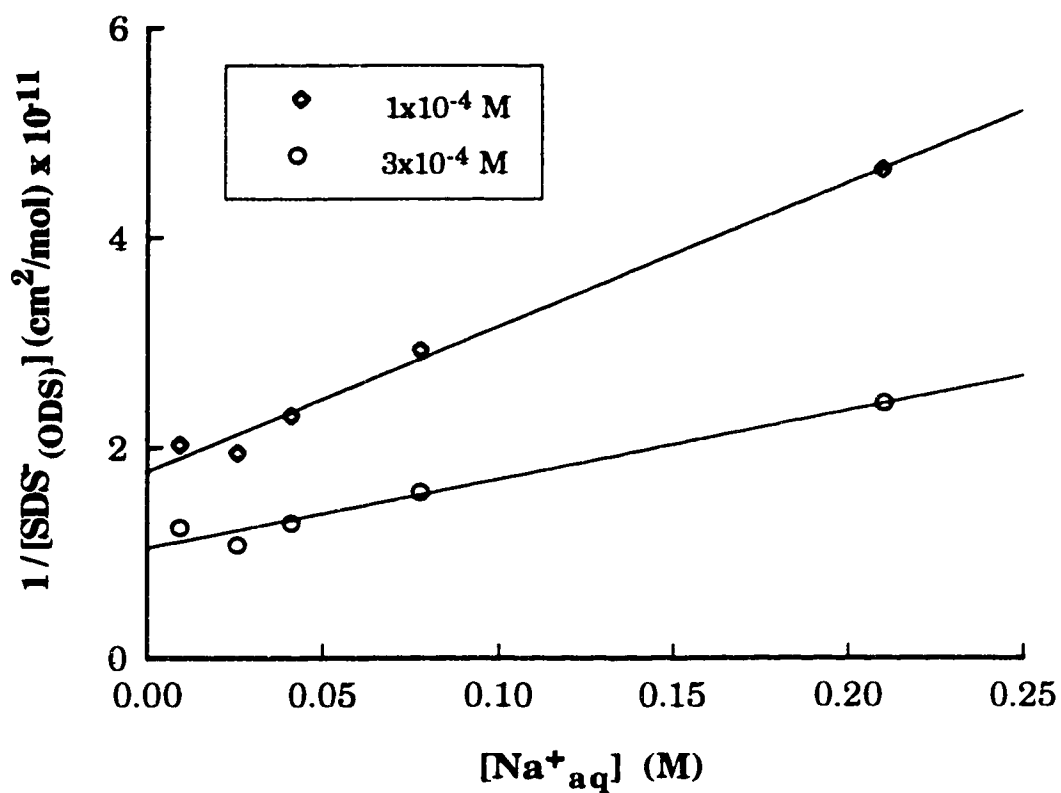


Figure 3.8 Plot of inverse adsorbed SDS^- concentration versus activity of Na^+ ; at two constant aqueous phase activities of SDS^- equal to 1 and $3 \times 10^{-4} \text{ M}$.

3.5.6 Adsorption Isotherms of SDS⁻

The potential at the electrolyte-ODS interface is a consequence of the larger amount of SDS⁻ (the adsorbate) found at the ODS surface (the adsorbent) relative to the bulk electrolyte. This process in which an excess of the substance is accumulated on the surface of a solid is known as adsorption. The equilibrium adsorbate distribution is presented in the form of an adsorption isotherm.

Figure 3.9 shows the adsorption isotherms of SDS⁻. First the amount of adsorbed unbound SDS⁻ is determined from equation 3.31 assuming equation 3.40 is valid. The total amount adsorbed, $\Gamma_{(ODS)}$, is then calculated using equation 3.38. The value of K_{Na^+} used, 7 lt/mole is the average of the constants obtained from constant SDS⁻ activity analysis discussed in 3.2. The isotherms are linear at lower concentrations of SDS⁻. Such an isotherm in which the amount adsorbed increases linearly with the adsorbate activity is called Henry's adsorption isotherm by analogy with the solubility of gases in liquids. At sufficiently high concentrations the adsorption assumes a constant value. There are no breaks in the isotherms before they reach the plateau, and since the adsorption maximums occur below the CMC, multi-layered adsorption is unlikely. The adsorption process of equation 3.33 that results in an L shaped isotherm is well described by the Langmuir adsorption isotherm.

$$\beta = \frac{\Gamma_{(ODS)}}{(\Gamma_m - \Gamma_{(ODS)}) [SDS_{(aq)}^-]} \quad (3.46)$$

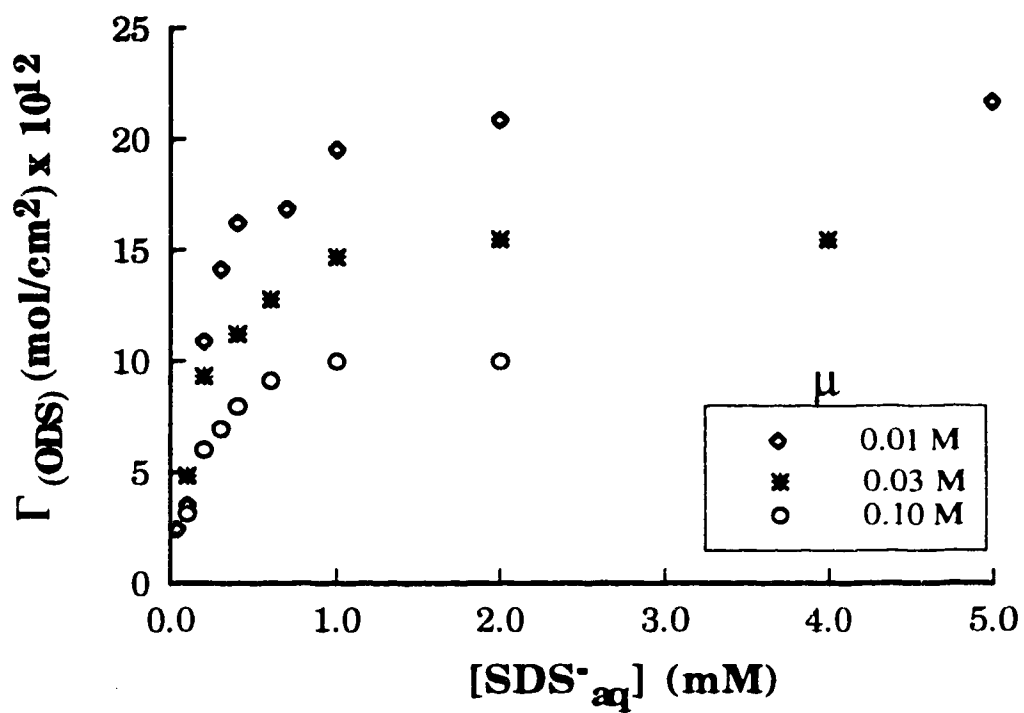


Figure 3.9 Adsorption isotherms of SDS⁻ for the data presented in Figure 3.5. $K_{\text{Na}^+} = 7 \text{ lt/mol}$; $C_{\text{Stern}} = 20 \text{ } \mu\text{F/cm}^2$.

Here Γ_m is the surface density of SDS^- at maximum coverage, $(\Gamma_m - \Gamma_{(\text{ODS})})$ is the concentration of the surface sites not occupied by SDS^- , and β is another form of the adsorption equilibrium constant. Equation 3.46 can be transformed into linear Langmuir adsorption isotherm forms:

$$\frac{[\text{SDS}_{(\text{aq})}^-]}{\Gamma_{(\text{ODS})}} = \frac{1}{\Gamma_m \beta} + \frac{[\text{SDS}_{(\text{aq})}^-]}{\Gamma_m} \quad (3.47)$$

or

$$\frac{\Gamma_{(\text{ODS})}}{[\text{SDS}_{(\text{aq})}^-]} = \beta (\Gamma_m - \Gamma_{(\text{ODS})}) \quad (3.48)$$

or

$$\frac{1}{\Gamma_{(\text{ODS})}} = \frac{1}{\Gamma_m} + \frac{1}{\Gamma_m \beta [\text{SDS}_{(\text{aq})}^-]} \quad (3.49)$$

The plots of $[\text{SDS}_{(\text{aq})}^-]/\Gamma_{(\text{ODS})}$ versus $[\text{SDS}_{(\text{aq})}^-]$, $\Gamma_{(\text{ODS})}/[\text{SDS}_{(\text{aq})}^-]$ versus $\Gamma_{(\text{ODS})}$, or $1/\Gamma_{(\text{ODS})}$ versus $1/[\text{SDS}_{(\text{aq})}^-]$ are, when Langmuir's equation is applicable straight lines, permitting the calculation of the constants β and Γ_m . Equation 3.49 involves two reciprocal quantities subject to experimental error. We use equation 3.47 which has the advantage of giving β and Γ_m directly from the slope and intercept of the least squares line, eliminating the need for further calculations. More exactly, from the plot of $[\text{SDS}_{(\text{aq})}^-]/\Gamma_{(\text{ODS})}$ versus $[\text{SDS}_{(\text{aq})}^-]$:

$$\Gamma_m = \frac{1}{\text{slope}} \quad (3.50)$$

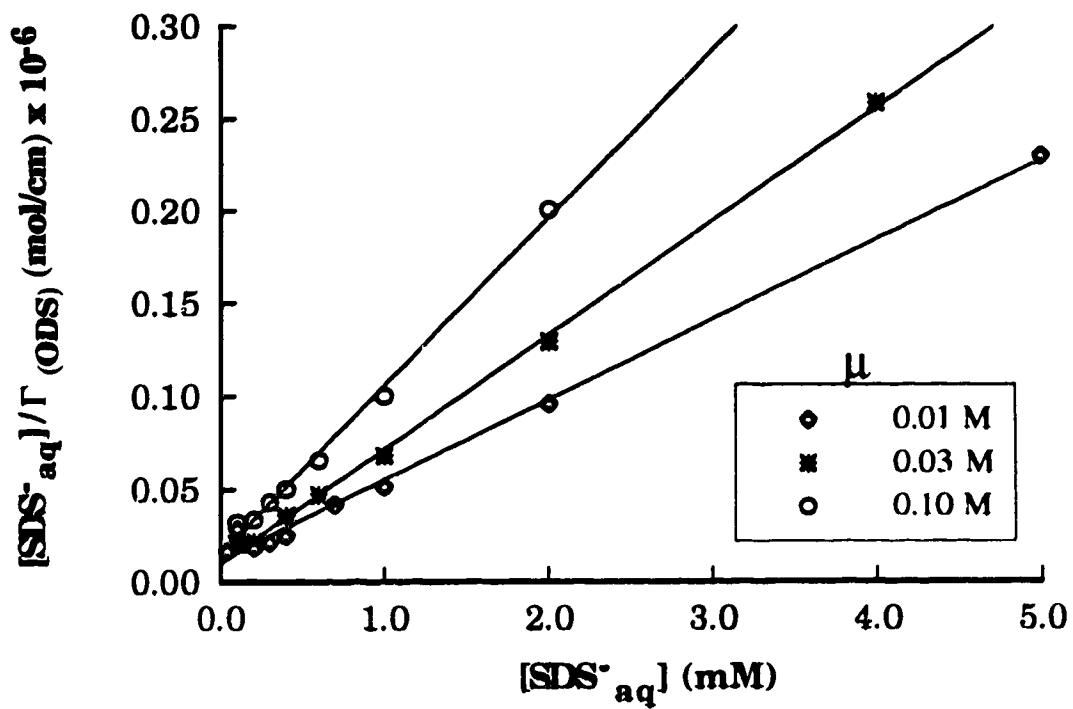


Figure 3.10 Linear Langmuir isotherm plots of Figure 3.9.

and

$$\beta = \frac{\text{slope}}{\text{int ercept}} \quad (3.51)$$

Fits of the adsorption isotherms of Figure 3.9 to the linear form of the Langmuir adsorption isotherm (equation 3.47) are shown in Figure 3.10. The correlation coefficient was better than 0.99 for each curve.

3.5.7 Adsorption free energy of SDS⁻

Since the distribution of the SDS at the interface can be correlated to the degree of coverage directly, it is preferable to express the equilibrium constant of equation 3.33 in mole fraction units.

$$K_{\text{ad}}^{\text{x}} = \frac{X_{\text{ODS}}^{\text{SDS}^-}}{X_{\text{aq}}^{\text{SDS}^-} X_{\text{ODS}}^{\text{H}_2\text{O}}} \quad (3.52)$$

The Xs refer to the mole fractions, the superscripts refer to the adsorbate, the subscripts refer to the phase, and K_{ad}^{x} is the conditional mole fraction adsorption equilibrium constant. The quantity of SDS⁻ and water at the ODS surface is not expected to exceed one nano mole. The total number of moles for dilute solutions can be approximated by the number of moles of solvent. For example, the error introduced by this approximation for a 0.1 M aqueous solution is acceptably less than 0.2 %. The mole fraction equilibrium constant is then given by

$$K_{ad}^x = \frac{55.56\Gamma_{(ODS)}}{\left[SDS_{(aq)}^-\right]\left[H_2O_{(ODS)}\right]} \quad (3.53)$$

The concentration at the ODS surface and the fraction of coverage are proportional. This allows equations 3.52 and 3.53 be written in terms that contain the adsorption isotherm directly.

$$K_{ad}^x = \frac{55.56\Gamma_o}{\left[SDS_{(aq)}^-\right](\Gamma_m - \Gamma_o)} \quad (3.54)$$

or

$$K_{ad}^x = 55.56\beta \quad (3.55)$$

The Gibbs free energy change of the adsorption process can therefore be estimated from equation 3.55.

$$\Delta G_{ad}^x = -RT \ln K_{ad}^x \quad (3.56)$$

The adsorption free energy of SDS⁻ we so obtain from Figure 3.10 are -47.4, -48.7 and -48.6 kJ/mole at ionic strengths of 0.01, 0.03 and 0.1 M respectively. This is higher than the -37 kJ/mole adsorption free energy of SDS⁻ on an AgI surface [47], but that would be expected due to the hydrophobic interactions of SDS⁻ and ODS. The adsorption free energy of SDS⁻ compiled by Rosen for the organic-aqueous interface are higher than our value by about 10 kJ/mole [48]. This could be a result of the difference between a surface confined ODS system and freely moving bulk hydrocarbon interface.

The area per molecule at surface saturation are ionic strength dependent as shown in Figure 3.9. We calculate areas of 7, 10 and 15 nm² at ionic strengths of 0.01, 0.03 and 0.1 M respectively. The cross sectional area of a perpendicular aliphatic chain is 0.20 nm² [49]. The area for a closely packed monolayer of SDS⁻ is given to be 0.27 nm² [47]. The areas per molecule at surface saturation at all ionic strengths indicate that the adsorption of SDS⁻ does not represent a closed-packed arrangement normal to the aqueous layer-ODS interface. The cross sectional area of a -CH₂-group lying flat at the interface is about 0.07 nm². With the area of the hydrated head group included, the area of a flat lying SDS⁻ molecule can be estimated to be about 1.34 nm². This area is also smaller than the smallest area we estimate. Therefore adsorption saturation due to steric limitation is not congruent with our results, which give larger areas and areas at adsorption saturation that are ionic strength dependent. This suggests coulombic effects may be involved and that is consistent with the fact that the results are ionic strength dependent.

3.6 Conclusions

The adsorption of SDS⁻ onto an ODS silanized SiO₂/Si electrode surface was examined using the impedance analysis technique. While the method has been used quite extensively in the investigation of bare gate pH sensitive ISFETs or membrane/insulator/semiconductor systems, this is the first instance in which it was specifically employed to determine the density of

adsorbed charge density from solution onto a nonionic adsorbent of a reversed phase surface.

From its response to pH the silanized surface was found to have accessible silanol groups. However, approximating that it was additive to the potential due to the PDI was within experimental error. The voltage shift at constant depletion capacitance of the electrode was shown to be equal to the double layer potential change. It was observed that at equal concentrations or activities of SDS⁻ the double layer potential decreased with increasing ionic strength of NaCl. This phenomena was rationalized by the interaction between the PDI and the sodium cation. Therefore, the double layer was considered using the GCSG model, taking into account the sodium cation interaction with the surface adsorbed SDS⁻ in the form of ion pair formation. The plane of the PDI was relaxed from the rigid two dimensional surface, allowing the use of equation 3.31 to calculate $\Gamma_{\text{SDS}^-_{\text{(ODS)}}$ and subsequently $\Gamma_{\text{(ODS)}}$.

Increasing ionic strength of NaCl gave decreased $\Gamma_{\text{(ODS)}}$ at the plateau of adsorption. This trend is not in agreement with many studies on the adsorption of charged species on different kinds of surfaces, where adsorption increases with increasing ionic strength. However, Luey *et al.* used ellipsometry to show there is a decreasing amount of protein adsorption onto a dichlorodimethylsilane silanized silicon wafer surface with increasing ionic strength [50]. In addition to a few other works cited in reference 50, Van de Steeg *et al.* have also observed that increasing ionic strength decreases protein adsorption onto crystalline cellulose around its pH_{pzc} [51].

We have also observed that the surface potential was a function of ionic strength at constant activities of SDS⁻. It is often assumed that the surface potential at constant bulk phase activity of the PDI will remain constant, however, the results of our study do not support this assumption. Our observation is readily explained by a form of ion-pairing or "charge shielding" in which some of the adsorbed species is charge compensated by supporting electrolyte. The present study has not fully resolved observed discrepancies between measurements of surface potential versus measurements of total adsorbed mass, in terms of the effect of ionic strength. Other experiments that could help to further resolve these issues are proposed in chapter 5.

The adsorption onto ODS was observed to follow a Langmuir type of relationship with SDS⁻ concentration. Based on the Langmuir adsorption isotherm the free energy of adsorption of SDS⁻ was 48.2 ± 0.7 kJ/mole. Although the isotherms level off, all do not go to the same limiting value. The area per molecule at adsorption saturation was calculated to be 7, 10 and 15 nm² at ionic strengths of 0.01, 0.03 and 0.1 M respectively. The large area and its ionic strength dependence indicates that the surface is not fully covered by SDS⁻ at the plateau of adsorption. The ionic strength seems to change the density of adsorbate but not the energy of adsorption.

3.7 References

1. *Ion Pair Chromatography: Theory and Biological and Pharmaceutical Applications*; Hearn, M.T.W., Ed.; Marcel Dekker: New York, 1985.
2. *High Performance Liquid Chromatography: Advances and Perspectives*; Horvath, C., Ed., Academic Press: Toronto, 1980; vol.1.
3. Hough, D. B., Rendall, H. M., in *Adsorption from Solution at the Solid/Liquid Interface*; Parfitt, G. D., Rochester C. H., Eds.; Academic Press, Toronto, 1983, Chapter 6.
4. Zhou, D., Pietrzyk, D. J., *Anal. Chem.* 1992, 64, 1003.
5. Bousse, L. *J. Chem. Phys.* 1982, 76, 5128.
6. Fung, D. C.; Cheung, P. W., Ko, W. H. *IEEE Trans. Electron. Devices* 1986, ED-33, 8.
7. Siu, W. M.; Cobbold, R. S. C. *IEEE Trans. Electron. Devices* 1978, ED-26, 1805.
8. Smit, W.; Holten, C. L. M.; Stein, H. N.; De Goeij, J. J. M.; Theelen, H. M. *J. Colloid Interface Sci.* 1978, 63, 120.
9. Barabash P. R.; Cobbold, R. S. C. *IEEE Trans. Electron. Dev.* 1982, ED-29, 102.
10. Trasatti, S. in *Comprehensive Treatise of Electrochemistry*, Bockris, J. O. M.; Conway, B. E.; Yeager, E, (Eds.); Plenum Press, New York, 1980, vol. 1, p 45-81.
11. Grove, A. S. *Physics and Technology of Semiconductor Devices*: Wiley, New York, 1967, Chapter 9.

12. Bard, A. J.; Faulkner, L. R. *Electrochemical Methods: Fundamentals and applications*, Wiley, New York, 1980, Chapter 12.
13. Grahame, D. C. *Chem. Rev.* **1947**, *41*, 441.
14. Hunter, R. J. *Foundations of Colloid Science*, Oxford University Press, New York, 1987; vol. 1. Chapter 6.
15. Hayes, K. F.; Redden, G.; Ela, W.; Leckie, J. O. *J. Colloid Interface Sci.* **1991**, *142*, 448.
16. Anderson, M. A.; Ruben, A. J. (Eds.) *Adsorption of Inorganics at Solid-Liquid Interface*, Ann Arbor Sciences, MI, 1981
17. Hayes, K. F.; Leckie, J. O. *J. Colloid Interface Sci.* **1987**, *115* 564.
18. Schindler, P. W. *Pure App. Chem.* **1991**, *63*, 1697.
19. Huang, T. L.; Tsai, P.; Wu, C. T.; Lee, C. S. *Anal. Chem.* **1993**, *65*, 2887.
20. Hayes, K. F.; Redden, G.; Ela, W.; Leckie, J. O. *J. Colloid Interface Sci.* **1991**, *142*, 448.
21. Westhall, J.; Hohl, H. *Adv. Colloid Interface Sci.* **1980**, *12*, 265.
22. Varlez, M.; Mussche, P. *J. Chrom.* **1983**, *254*, 117.
23. Sander, L. C.; Wise, S. A.; *CRC Crit. Rev. Anal. Chem.* **1987**, *18*, 299.
24. Berndsen, G. E.; Pikaast, K. A.; de Galan, L. *J. Liq. Chromatogr.* **1980**, *189*, 299.
25. Bergveld, P.; Sibbald, A.: *Analytical and Biomedical Applications of Ion Selective Field Effect Transistors*, in: *Comprehensive Analytical Chemistry; XXIII*, Svehla, G., Ed., Elsevier, New York, 1988
26. Harame, D. L.; Bousse, L. J.; Schott, J. D.; Meindl J. D. *IEEE Trans. Electron Dev.* **1987**, *ED-34*, 120.
27. Fung, C. D.; Cheung, P. W.; Ko, W. H.; *IEEE Trans. Electron Dev.* **1986**, *ED-33*, 8.

28. Hunter, R. J. *Zeta potential in Colloid Science*, Academic Press, New York, 1981, pp 228.
29. Iler, R. K. *The Chemistry of Silica*, Wiley, New York, 1979.
30. Bousse, L. J.; Mostafashed, S.; Hafeman, D. *Sensors and Actuators*, 1992, B10, 67.
31. Sposito, G. *The Surface Chemistry of Soils*, Oxford University Press, New York, 1984, pp 75.
32. Bergveld, P.; Reinhoudt, D. N.; Sudholter, E. J. R. *Sensors and Actuators*, 1985, 5, 129.
33. Bousse, L. J., de Rooij, N.F.; Bergveld, P. *IEEE Trans. Electron Dev.* 1983, ED-30, 1263.
34. Clechet, P. *Sensors and Actuators*, 1991, B4, 53.
35. Matsuo, T.; Nakajima, H. *Sensors and Actuators*, 1984, 5, 293.
36. Bousse, L. J.; de Rooij, N. F.; Bergveld, P. *Surf. Sci.* 1983, 135, 479.
37. Bousse, L. J.; Meindl, J. D. in: *Geochemical Processes at Mineral Surfaces*; Davis, J. A.; Hayes, K. F.; Eds. ACS, 1986, 323, 79.
38. Yates, D. E.; Levine, S.; Healy, T. W. *J. Chem. Soc. Faraday Trans. I* 1979, 70, 1807.
39. Davis, J. A.; James, R. O.; Leckie, J. O. *J. Colloid Interface Sci.* 1978, 63, 480.
40. Stumm, W.; Huang, C. P.; Watillon, A. *J. Colloid Interface Sci.* 1976, 55, 678.
41. Hunter, J. R. *Zeta Potential in Colloid Science*, Academic Press, New York, 1981, pp 296.
42. Smit, W., Holten, C. L. M. *J. Colloid Interface Sci.* 1980, 78,1.

43. Yarmchuck, P.; Weinberger, R.; Hirsh, R. F.; Cline, L. J. *Anal. Chem.* **1982**, *54*, 2233.
44. Dorsey, J. G.; Khaledy, M. G.; Landy, J. S.; Lin, J. L. *J. Chrom.* **1984**, *316*, 183.
45. Hiementz, P. C. *Principles of Colloid and Surface Chemistry* 2nd ed.; Marcel Dekker: New York, **1986**, Chapter 8.
46. Corrin, M.; Harkins, W. *J. Am. Chem. Soc.* **1947**, *69*, 683.
47. Hunter, R. J. *Zeta Potential in Colloidal Science*, Academic Press, New York, **1981**, pp 312.
48. Rosen, M. J. *Surfactants and Interfacial Phenomenon*, 2nd Ed., Wiley, New York, **1989**, Chapter 2.
49. Kuha, H; Mobius, D. in: *Physical Methods in Chemistry*; Weissberger, A., Rossiter, B. Eds.; Wiley, New York, **1972**; Part IIIB, Vol. 1, pp 577.
50. Luey, J.K, McGuire, J.; Sproull, R.D. *J. Colloid Interf. Sci.* **1991**, *143*, 488.
51. Van de Steeg, H.G.M.; de Keizer, A.; Stuart, M.A.C.; Bijsterbosch, B.H. *Colloid Surfaces A: Physiochem. Eng. Aspects* **1993**, *70*, 77.

Chapter 4

Characterization of Extremely low Defect Density Hexadecanethiol Monolayers on Hg Surfaces

4.1 Introduction

Self-assembled monolayers have offered a convenient method to chemically modify the properties of a surface [1,2]. Silanes such as octadecyltrichlorosilane have been shown to readily self-assemble as a monolayer on various substrates [3,4]. However, these monolayers are not uniform or stable enough for extensive electrochemical study, or to form a blocking layer, effective in isolating the underlying substrate from solution [5,6]. Self-assembly of thiols and their derivatives on gold surfaces has provided a route to well ordered, oriented, monolayer films, and extensive studies of these films have been made [7-12]. The presence of defects in the thiol films has been recognized and they are identified as pinholes and regions in which the coating is thinner, due to packing defects [5,9,12-14]. The evidence for these comes primarily from the observation of electrochemical leakage currents for various redox species in solution, and redox processes of the Au surface. The magnitude of these currents depends on the packing density of the thiols on the surface, and the density of defect sites [9,12,13]. The microscopic roughness of Au, and the presence of surface steps and kinks in the Au lattice [15], plays a

significant role in establishing defects in the films [12,13]. In addition there is uncertainty about the effect of the Au lattice in determining the thiol chain packing [9]. Strong and Whitesides [16] have concluded from electron diffraction studies on Au (111) that the film formed is not commensurate with the crystal lattice, while others suggest the monolayer is epitaxial [9,17]. A further complication comes from the fact that the Au surface appears to reconstruct as a function of applied potential and contacting medium [18,19].

The case of preparing close-packed thiol monolayers on gold has made them an ideal substrate on which to study electron transfer and electron tunneling processes of compounds either in solution or bound to the film [5,12,13,20-24]. It has been found necessary to make corrections for the presence of pinholes and more subtle defects in the films [5,20]. However, such analyses are subject to some uncertainty since the small tunneling current is measured in the presence of a large background. Clearly, more defect-free films would be desirable for characterizing the intrinsic properties of the films, and many applications could also benefit.

Mercury, as a liquid metal has a homogeneous, featureless, defect free surface. Unlike Au or Pt there is no need to condition the electrode prior to use. The likelihood of forming blocked, dense films is increased if the packing is controlled by the coating molecules and not the crystal lattice surface [9], and so a liquid Hg substrate could give denser films. These characteristics, in addition to the very high affinity of mercury for thiols [25] makes it an ideal substrate to consider for the study of the properties of spontaneously self-assembled monolayers of thiol. However, we note that Li and Weaver [23] found the films formed by short thiol

chains on Hg were more permeable than those formed on Au. This was thought to be due to the fluidity of the Hg surface. In this report we demonstrate that long chain thiol films do form on Hg, as would be anticipated, and that they appear to be extraordinarily impermeable and free of defects.

4.2 Experimental Section:

Reagents. Hexadecanethiol (HDT) (Aldrich, 99.99%), methyl viologen dichloride (Aldrich), Ru (NH₃)₆Cl₃ (Strem Chemicals), Pb (NO₃)₂ (Fisher Scientific, certified), p-benzoquinone (BDH, 98%), K₃Fe (CN)₆ (Amachem, reagent grade), KCl (BDH, analytical reagent), NaF (Fisher Scientific, certified) were used as received. Hg was triply distilled in-house. n-Hexadecane (Aldrich, 99%) was passed through a grade one alumina (Fisher Scientific) column. All aqueous solutions were prepared from distilled, deionized water, redistilled from alkaline permanganate. Electrolyte solutions were purged with N₂ for 15 min before use, and were kept under a N₂ blanket.

Electrode Preparation. A Pt wire (0.51mm diameter.) sealed in soft glass was mechanically polished, sonicated and finally electrochemically cleaned by holding it at 1.90 V vs SCE for 4 minutes, followed by potential cycling at 0.1 V/sec, between -0.28 and 1.10 V for 30 minutes in 0.5 M H₂SO₄. To avoid Pt oxide formation, which is poorly wet by Hg [26], the Pt tip was contacted with Hg in the H₂SO₄ solution at a reducing potential. On the average 3 milligrams of Hg was delivered to the Pt surface with a

Metrohm microburette E410 electrode, creating a static mercury drop electrode (SMDE). Electrode areas were determined from the capacitance at -0.5 V in 0.1 M NaF, and were typically $8 \times 10^{-3} \text{ cm}^2$ ($\pm 5\%$).

Self-assembled thiol monolayers were formed by immersing the SMDE in a 20 % (by volume) solution of HDT in n-hexadecane or in neat HDT for 2 sec to 30 min. They were then rinsed with n-hexadecane to remove unadsorbed HDT. Both soaking solutions and all soaking times gave identical results, but 30 min in a 20% solution was the most common procedure.

Electrochemical Measurements . An Amel potentiostat and Kipp and Zonen BD-90 xy recorder with a Hokuto Denko HG-III function generator were used for cyclic voltammetry. The electrochemical instrumentation for AC impedance and capacitance-voltage (CV) measurements was previously described [27], except that the Hokuto function generator was used for a dc ramp (5 mV/s), and a Wavetek Model 23 computer programmed function generator provided the 10 mV peak to peak AC perturbation (113 Hz). A large area Pt mesh counter electrode and a KCl saturated calomel electrode (SCE) in 0.1 M NaF double junction solution, isolated by a fritted glass disc were used, and housed in a faraday cage. The frequency dependence of the impedance was measured with the electrode potential adjusted to its rest potential *vs* the SCE. The impedance measurements were independent of the style of the reference electrode, or the presence of the double junction.

4.3 Results and Discussion

It was expected that hexadecanethiol (HDT) would adsorb on the surface of a Hg electrode. However, the nature of the film formed relative to the self-assembled, compact monolayers formed on gold surfaces was uncertain. We have characterized HDT films on Hg electrochemically, by measuring their permeability to redox species in solution, and the effect of the adsorbed HDT film on the capacitance of the Hg-electrolyte interface. Film formation occurs by immersion of a Hg electrode in neat HDT, or a solution of HDT in n-hexadecane. No kinetic study was performed on the rate of deposition of HDT on Hg, however, based on the permeability of the films to redox species, adsorption is complete within 2 to 10 sec. This is fast compared to the formation of self-assembled monolayers of mercaptans on Au, which is reported to require exposure for a period of 30 to 60 min to approach equilibrium, while overnight exposure appears to have become routine [2,7,10,13,14]. The HDT films formed on Hg are quite stable, the characteristics described below were unchanged during 36 h of storage in 0.1 M NaF solution. Normal handling of the static Hg drop electrode (SMDE) coated with HDT such as rinsing, mounting in a cell, or stirring the solution with a stir bar, did not change the film properties.

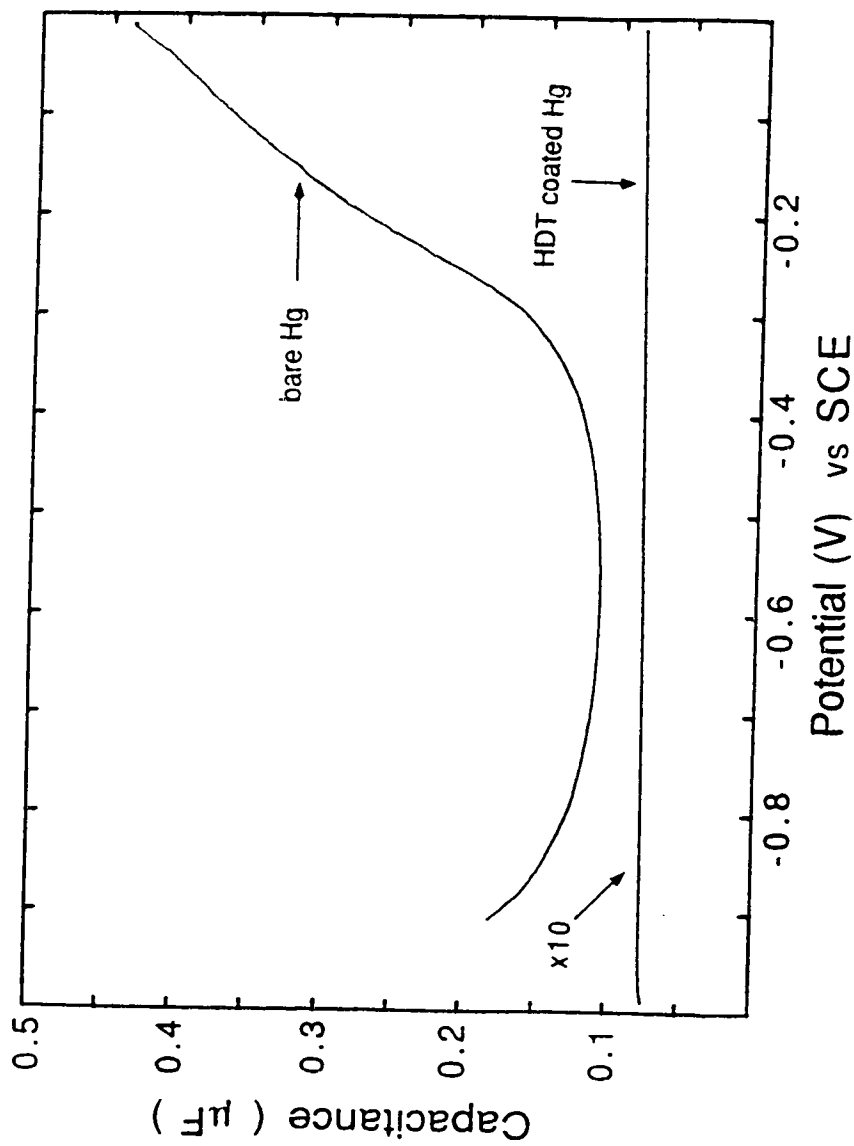


Figure 4.1. Differential capacitance as a function of potential at a bare static Hg drop electrode, and a thiol coated electrode. C for the coated electrode is multiplied by 10 for clarity.

4.3.1 Differential Electrode Capacitance.

The capacitance of the static Hg drop electrode in NaF is potential dependent, in agreement with the behavior of the dropping Hg electrode [28]. Figure 4.1 shows this behavior between 0 and -0.9 V. In the non-specifically adsorbing electrolyte NaF the potential of zero charge (pzc) is close to -0.1 V [28]. The double-layer capacitance is at a minimum around -0.5 V due to dielectric saturation [24], arising from the effect of the potential on the orientation of H₂O molecules in the double layer. Unlike bare Hg, the capacitance of Hg with adsorbed thiol is independent of potential, as shown in Figure 4.1. In addition, the capacitance of the HDT coated surface is about 50 times smaller at -0.1 V and 15 times smaller at -0.5 V than on naked Hg.

The insulating HDT film will act as a capacitor, C_f , in series with the double layer capacitance, C_{dl} , to give a total capacitance C . This will be in series with the solution resistance, R_s . For such a lumped element network the impedance, Z , of the system can be expressed by

$$Z = R_s - \frac{j}{\omega C} \quad (1.20)$$

where j is the imaginary number, and ω is the radial frequency ($\omega = 2\pi f$, where f is the oscillation frequency of an applied potential). For this network a Bode plot of $\log |Z|$, where $|Z|$ is the modulus of Z , versus $\log \omega$ should exhibit a linear region at low ω , with a slope of -1 and an intercept of $-\log C_f$ (see section 1.5). At high frequencies $|Z|$ should be

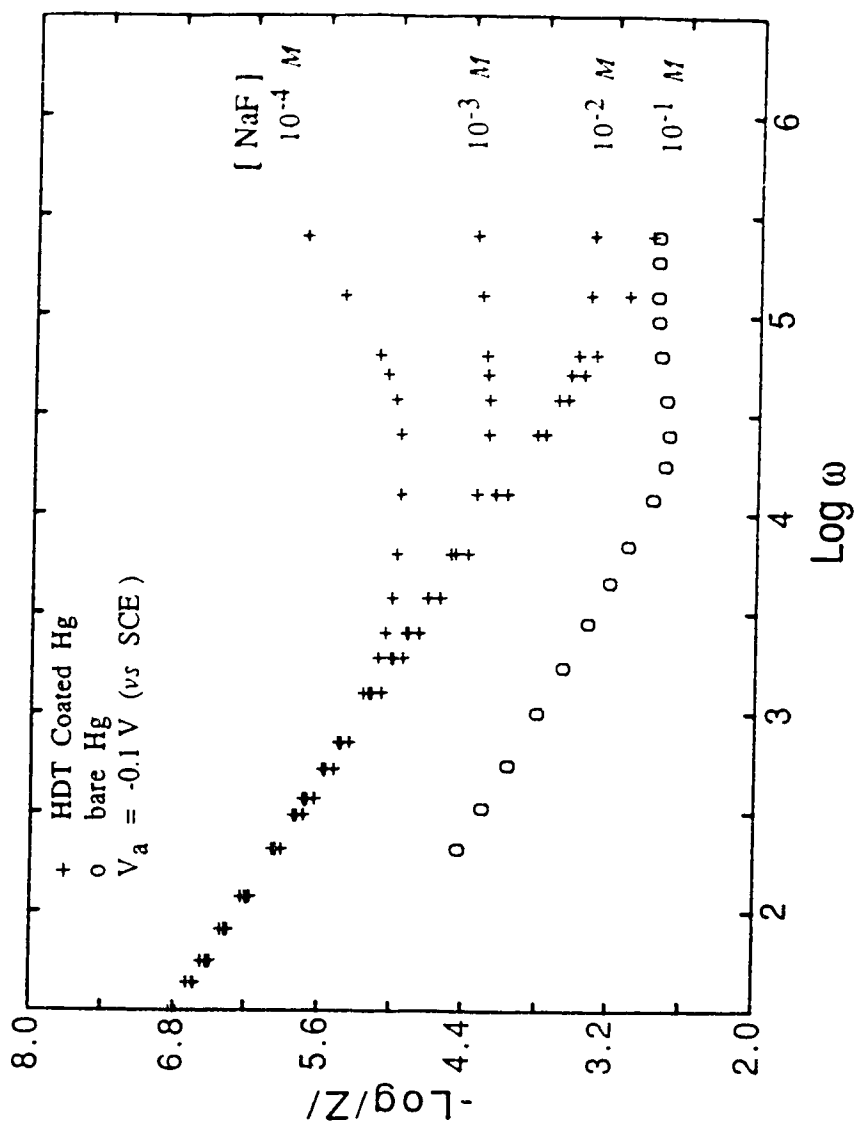


Figure 4.2. Bode plot of $\log |Z|$ vs $\log \omega$ for a bare SMDE (O) in 0.1 M NaF, and for an HDT coated SMDE (+) at several NaF concentrations.

independent of frequency and the Bode plot should give a horizontal line with a magnitude of $\log R_s$ (Figure 1.6). The experimental results of this behavior is shown in Figure 4.2 for both a bare SMDE and an electrode coated with HDT. Both electrodes exhibit the same kind of response, but the magnitude of C is substantially different.

The small value of C on the coated electrode indicates that it is dominated by C_f . To confirm this the dependence of C on the ionic strength of the solution was examined, since the double layer capacitance at Hg is known to be a function of ionic strength [30]. Figure 4.2 shows that the capacitance of the HDT coated electrode is independent of ionic strength across a wide range, while the variation in R_s with ionic strength is observed in the plateau region at higher frequency. This result is consistent with the formation of an impermeable, pinhole-free layer on the Hg surface. Using Grahams' Hg capacitance data in 0.1 M NaF, $14.4 \mu\text{F}/\text{cm}^2$ at -0.5 V vs SCE [28], to determine the area of the bare SMDE surface, the thickness of an HDT coating on the same SMDE could be calculated from the reduction in C . Taking a dielectric constant of 2.3 for HDT, which is similar to that of polyethylene [8,9,31], gave a thickness of 20 Å. This is in agreement with the thickness of HDT monolayers on Au, as determined by ellipsometry [7,32], and indicates a monolayer film is formed on Hg.

The decrease in capacitance observed when HDT is adsorbed on Hg, and then aged by limited potential scanning (*vide infra*), is larger and more reproducible than we have obtained with HDT on Au. Other author's have also noted that the capacitance of self-assembled monolayers on Au often varies between 50 and 90 % of the theoretical value

expected for a compact film [5]. In contrast, for HDT on Hg we find values are typically 95 to 100 % of the expected value. This value is based on an estimate of the dielectric constant and is not proof of a maximally dense film, but does indicate the greater reproducibility of film formation on Hg relative to Au.

4.3.2 Redox Active Probes.

The potential window of Hg extends from about 0.4 V to about -2.0 V vs SCE in 0.1 M NaF electrolyte [28]. In studying the response to redox couples the upper potential excursion was limited to +0.1 V, to avoid any complications due to oxidation of the Hg electrode. A number of redox species of differing charge and lipophilicity were used as probes. The coating may totally block access of a specific redox couple, or may cause a significant increase in the separation of the peak potentials for a species that can permeate it [3,5,8,9,12-14,20,21,33]. The presence of film defects causes a decrease in the blocking ability of the film. Figure 4.3 shows the cyclic voltammetry of Ru (NH₃)₆³⁺ and methyl viologen (MV²⁺) in 0.1 M NaF at a bare, and an HDT coated, Hg electrode. Less than 0.005% of the current measured on a bare electrode is observed at a coated one. The current observed on a coated Hg electrode was proportional to the scan rate between 0.1 and 2 V/sec, demonstrating that the current is capacitive not faradaic. Figure 4.3 shows that the film is almost completely blocking to the two redox species within the potential range examined. The results contrast with those found at

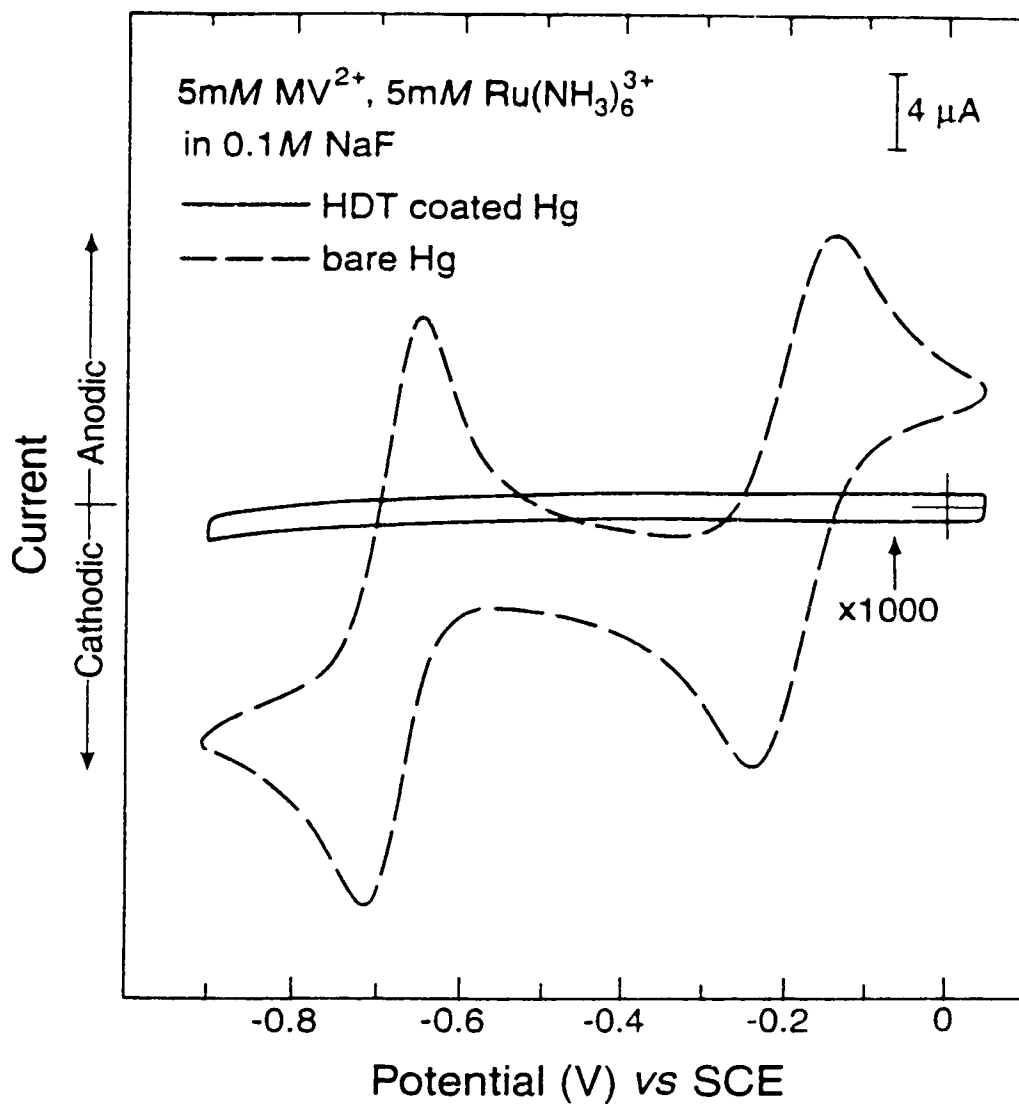


Figure 4.3 Cyclic voltammogram at 100 mV/s of 5 mM MV^{2+} and 5 mM $Ru(NH_3)_6^{3+}$ in 0.1 M NaF at a bare SMDE (---), and an HDT coated SMDE (—). The latter curve is increased 1000-fold in sensitivity for clarity.

HDT films coated on Au, for which a significant current is still observed for Ru(NH₃)₆³⁺ [9,12,14]. Cyclic voltammetric studies (not shown) of the reduction of benzoquinone in 0.1 M KCl, and ferricyanide in 0.1 M NaF showed that these species were blocked by the HDT film on Hg, and only essentially capacitive currents were observed.

There has been considerable interest in using self-assembled thiol films to study electron tunneling effects across the film for impermeable species. However, it has been recognized that defects can significantly influence the observation of such effects [9,12–14,29,30]. Comparing the results in Figure 4.3 to those for thiol films on Au [8,9,14] shows that the leakage currents observed at high overvoltage (about -0.7 V) for Ru(NH₃)₆³⁺ and for MV²⁺ are not present at HDT coated Hg. The redox couples we have examined cover the range from anions and cations to neutral species, and vary from hydrophilic to moderately hydrophobic. Our results indicate the HDT film formed is compact and pinhole free, consistent with a highly perfect self-assembled monolayer.

Data such as that in Figure 4.3 do allow for an estimation of the standard rate constant for electron transfer k_{ap} . A detailed study is underway by S. Tsai in our group, but we present here an upper limit estimate of k^* for Ru(NH₃)₆³⁺ at HDT coated Hg. From the curve for the coated SMDE in Figure 4.3 it can be seen the current dips cathodically at negative potentials. If we assume that this is due to a Faradaic process then the difference in current between -0.5 V, where the curve is flat, and -0.9 V provides an estimate of the apparent rate constant through equation 4.1.

$$i_f = n F A C^* k_{ap} \quad (4.1)$$

Here i_f is the faradaic component of current at -0.9 V in a solution of 5 mM $\text{Ru}(\text{NH}_3)_6^{3+}$, 0.1 M NaF, F is the Faraday constant, A is the electrode area, C^* is the redox species concentration, and k_{ap} is apparent rate constant [34]. If we assume Butler-Volmer kinetics [34] then the apparent standard rate constant at zero overpotential is given by equation 4.2

$$k_{ap} = k_{ap}^0 \exp(-\alpha n \eta F/RT) \quad (4.2)$$

where α is the electron transfer coefficient, assumed to be 0.5, n is one electron, η is the overpotential, $E-E''$, and R and T have their usual meanings. The formal potential, E'' , was approximated by the average of the anodic and cathodic peak potentials of a cyclic voltammogram on a naked electrode.

In $\text{Ru}(\text{NH}_3)_6^{3+}$ the current at -0.5 V was linear (1.000 correlation coefficient) between 10 and 2000 mV/s. The value of i_f calculated from the observed current at -0.9 and -0.5 V was independent of sweep rate and typically about 0.75 nA. This is consistent with a kinetically controlled current with no diffusion control. For $\text{Ru}(\text{NH}_3)_6^{3+}$ we obtain a value of k_{ap}^0 of 3×10^{-13} cm/s, more than twelve orders of magnitude lower than 1.8 cm/s reported at a bare Au electrode [5]. This is also much lower than has been reported for other redox couples at thiol films on Au [20,21,24] and indicates a considerable barrier to electron transfer.

Tunneling current is expected to depend exponentially on film thickness [20,23,35,36] according to equation 4.3

$$k_{ap} = k'' \exp(-\beta d) \quad (4.3)$$

where k'' is the standard state constant at a naked electrode, β is a tunneling parameter, and d is the film thickness determined from the capacitance of the HDT film. We estimate a value of β of 1.5 \AA^{-1} assuming k'' at Hg is the same as at Au. For a rectangular barrier, β gives a measure of the barrier height through the equation [37],

$$\beta = \frac{4\pi}{h} \sqrt{2mE_B} \quad (4.4)$$

Where m is the free electron mass, h is planck's constant, and E_B is the height of the barrier in electron volts. Substituting the values of the constants in equation 4.4 [20,36,37],

$$\beta = 1.025 E_B^{1/2} \quad (4.5)$$

We estimate E_B to be equal to 2.1 eV. These values are in reasonable agreement with those of Li and Weaver [23] for tunneling across relatively thin films on Au, and are somewhat higher than those recently reported for longer chain thiol films on Au [21].

We wish to stress that these calculations are estimates of k_{ap} , β and E_B , and that more detailed studies will be required to determine if equation 4.2 is followed over a ~ 0.7 V overvoltage, and whether α is 0.5.

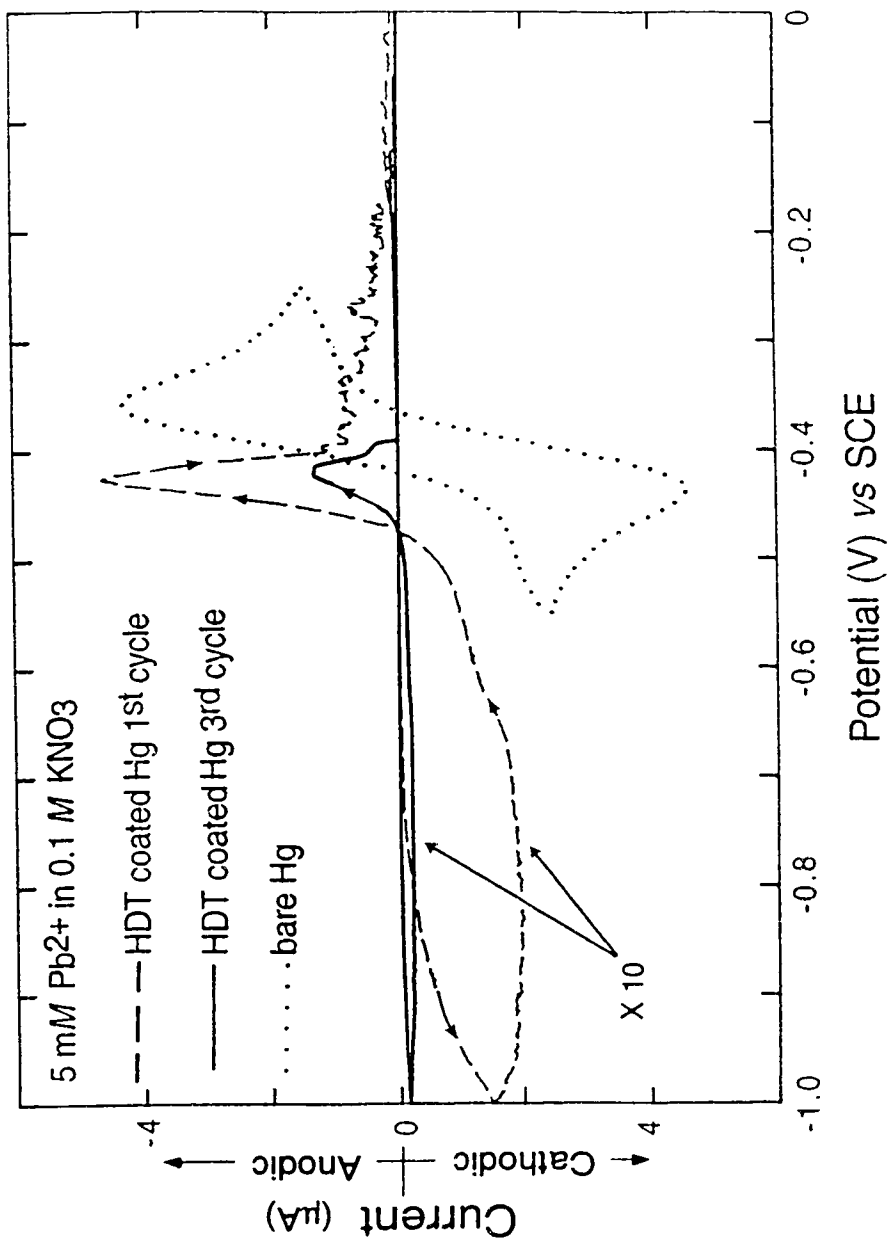


Figure 4.4 Deposition and stripping waves at 100 mV/s for 5 mM Pb²⁺ in 0.1 M KNO₃ at (•••) bare Hg, and at HDT coated on the Hg (---) first cycle, and (—) third cycle. The coated electrode currents are magnified tenfold.

In addition, not all the excess current at -0.9 V may be due to the added redox couple. As discussed below a trace current is observed in this potential regime with new electrodes in redox couple free solutions.

To further probe the permeability of these films the reduction and stripping of 5 mM Pb^{2+} in 0.1 M KNO_3 was examined. Unlike the other species it was much easier to reduce Pb^{2+} at the HDT coated SMDE, with current onsetting at about -0.65 to -0.75 V *vs* SCE. On the first cathodic sweep the maximum current is typically 4% of that seen at a bare Hg electrode, and a stripping wave is also observed, as shown in Figure 4.4. On subsequent sweeps the current decreased substantially, usually stabilizing after the third or fourth sweep. The return sweep showed an increase in current such as is seen in a typical nucleation process. This suggests the metal is depositing as islands in or on the HDT film, since the deposition wave at the naked Hg surface is essentially Nernstian. Since the same electrodes showed no current for the other redox couples examined the results are unlikely to be due to pinholes. Instead it appears that the Pb^{2+} ion either has a greater permeability in 0.1 M KNO_3 than the other species do in 0.1 M NaF, or that the current arises from a reduced barrier to electron tunnelling across the film [21]. Further study of this process is underway by S. Tsai.

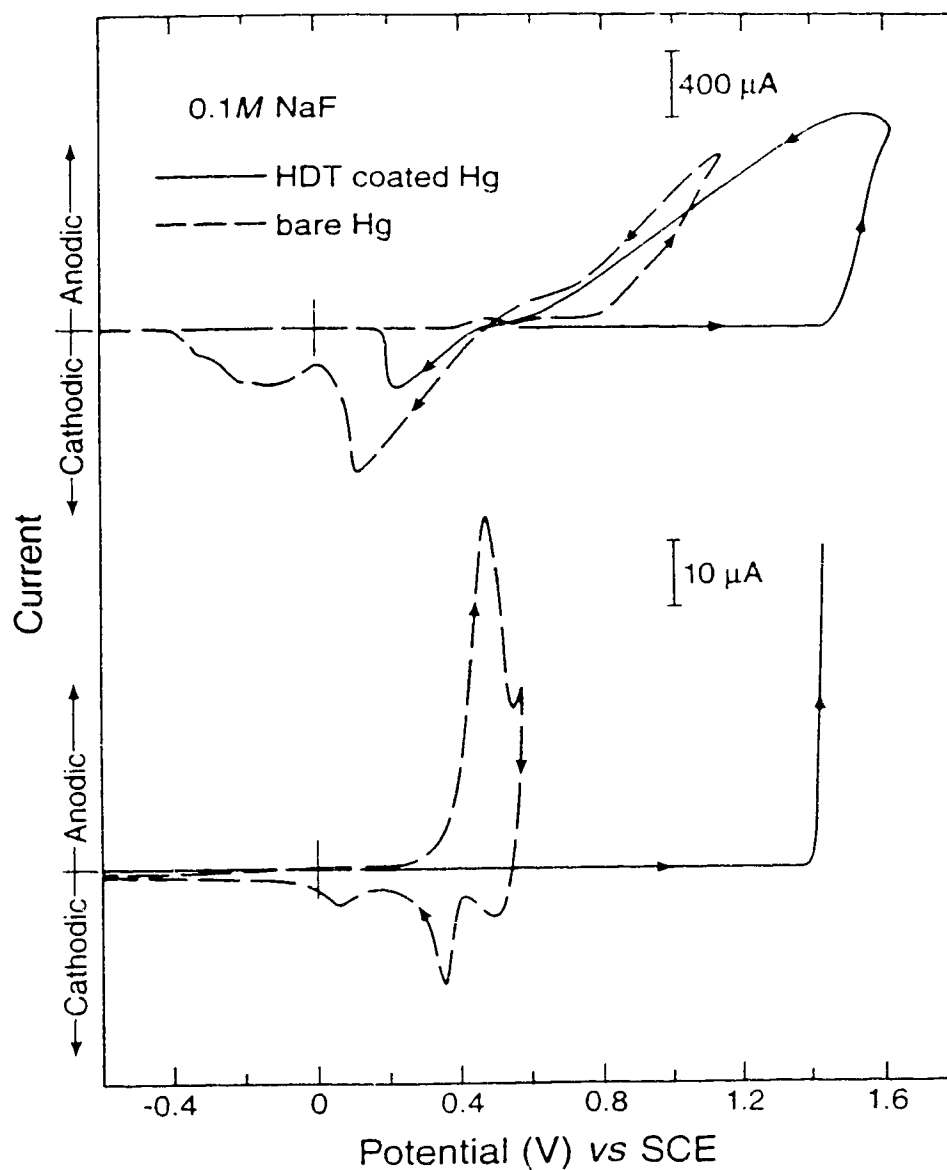


Figure 4.5. Current for Hg oxidation *vs* potential in 0.1 M NaF for both bare (---) and HDT coated (—) SMDE obtained at 100 mV/s. The upper traces show the same data as the lower trace on a 40-times less sensitive scale.

4.3.3 Processes at the Hg Surface.

Figure 4.5 illustrates the rather striking effect that HDT coating has on the oxidation of a SMDE. The lower figure shows that while Hg oxidation onsets at about 0.4 V *vs* SCE on a bare electrode in 0.1 M NaF, there is no oxidation of a coated electrode until about 1.4 V. The top figure indicates that substantial Hg oxidation occurs at a bare electrode at about 0.8 V, while this is shifted to 1.5 V on a coated electrode. However, once oxidation begins the film is destroyed, since the return sweep for the coated electrode becomes similar to that for the bare electrode. The 1.0 V anodic shift in the onset of Hg oxidation illustrates that the HDT film is extremely free of pinholes and highly impermeable, and so substantially alters the interaction between the electrode and solution.

It has been reported that cycling the potential of an HDT coated Au electrode sufficiently cathodic causes the film to be partially stripped off [9,12,38]. We observe this behavior at HDT coated Hg electrodes in 0.1 M NaF, with a stripping peak potential of -1.23 V *vs* SCE, as shown in Figure 4.6a. While much of the film remains after a single cathodic excursion, the film becomes increasingly permeable to solution redox couples with each excursion. In addition to this effect, when a coated electrode's potential is limited to excursions between 0 and -1.1 V there is a very small cathodic current observed, which is at a maximum on the first scan for a new electrode, and decreases thereafter, as shown in Figure 4.6b. This cycling does not measurably change the permeability of the film to the redox couples studied, however, there is a significant

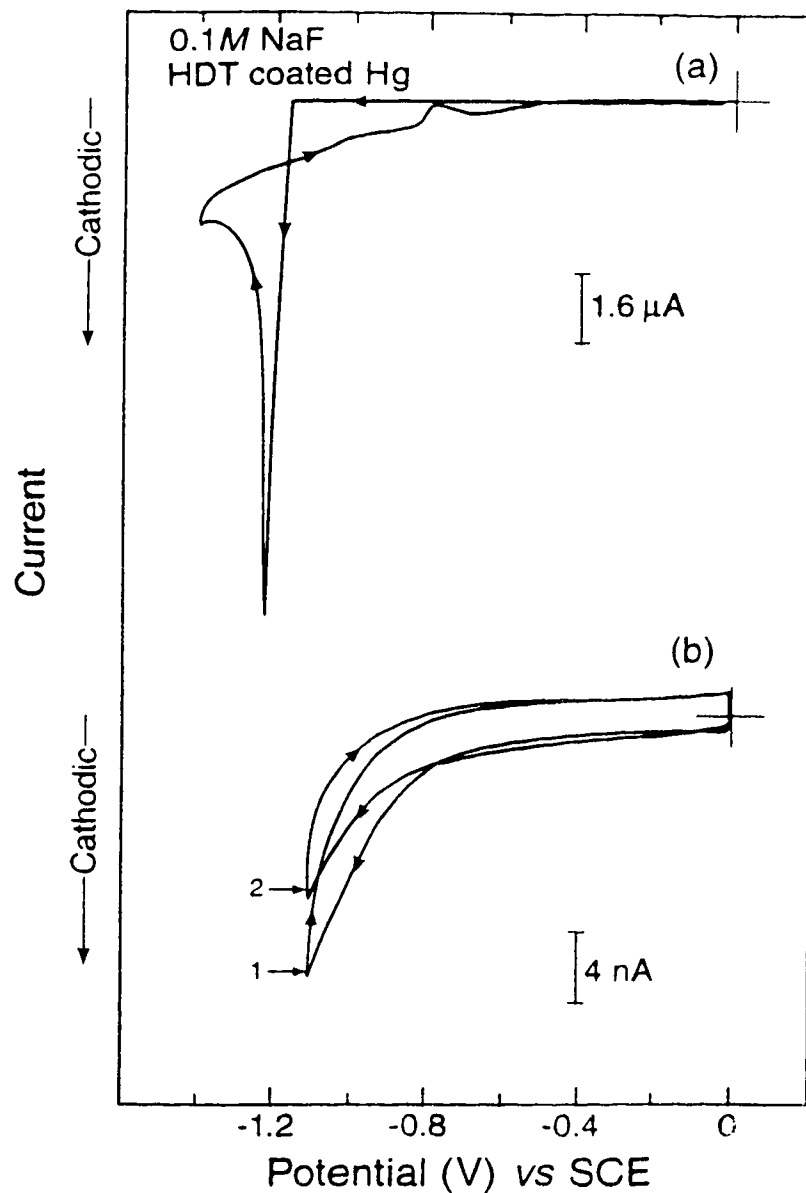


Figure 4.6. (a) Reduction current at 100 mV/s observed during stripping of an HDT film from an Hg surface in 0.1 M NaF. (b) Reduction current observed at 100 mV/s between 0 and -1.1 V at a virgin HDT coated SMDE during the first and second scans. Note the high current sensitivity.

change in the capacitance of the film. Figure 4.7 shows that C decreases with cycling over a potential range of 0 to -1.1 V. When the potential is initially cycled between 0 and -0.5 V there is only a small change in C , and this appears to be time dependent rather than potential dependent. However, the first excursion to -1.1 V results in a large decrease of the capacitance. A typical relative change of the capacitance with cycling to -1.1 V is shown for two electrodes in the inset in Figure 4.7 as the ratio C/C_i , in which C_i is the initial electrode capacitance and C is the observed capacitance after cycling. The largest decreases occur during the first few scans, and the effect then progressively diminishes. The change in C coincides with the change in current flow in this potential regime shown in Figure 4.6, suggesting the processes are correlated.

The 20 to 40 % change in capacitance observed indicates that there is some type of irreversible reorganization of the film occurring as a result of the applied potential. The variability in the extent of change in C for different electrodes is significant, and a little surprising given the very low permeability and pin-hole density observed for all the SDME electrodes coated with thiol. Figure 4.7 shows that the capacitance does decrease slowly over time, and it is possible that the potential excursion to -1.1 V simply accelerates the same process. If this is so, then the difference in the relative change observed upon cycling may be due to differences in the initial state of aging before the cycling begins, which might arise due to the electrode preparation process. We note that the final values of C obtained are usually in good agreement with the value predicted for a monolayer film.

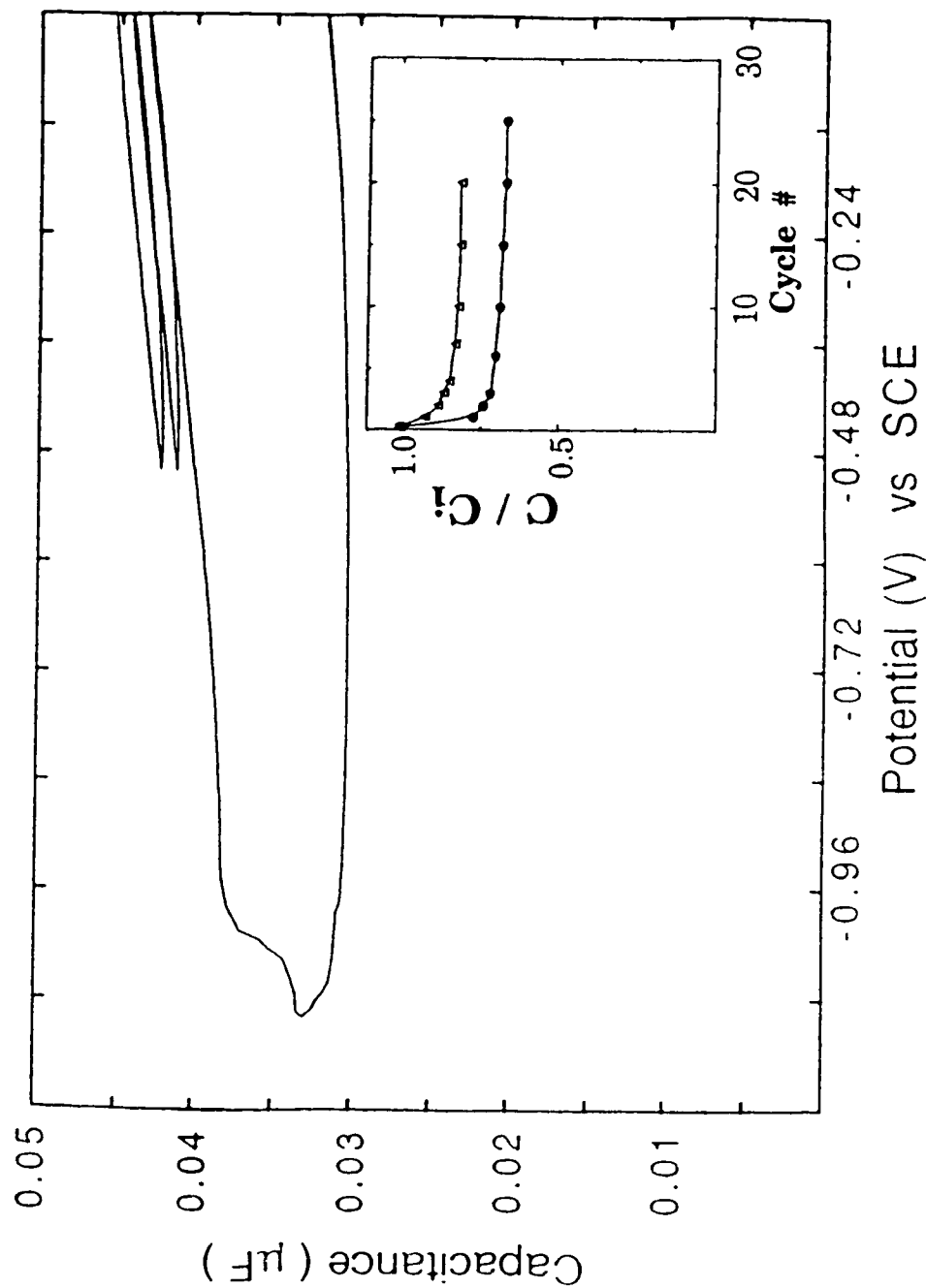


Figure 4.7. Change in differential capacitance as a function of potential for a virgin HDT coated SMDE during cycling from 0 to -0.5 V and then to -1.1 V. The inset shows the ratio of C observed to initial C_i , following each potential sweep from 0 to -1.1 V for two typical electrodes.

The data in Figures 4.6 and 4.7 do not identify the nature of the processes occurring and we do not have a definitive explanation for the phenomenon. It is interesting that the abrupt decrease in C is not observed on Au electrodes during potential cycling. This may suggest that the effect is in part due to a reorganization of the Hg-thiol contacting layers, in a manner unique to the Hg surface. However, it is also possible that such behavior is not observed on Au because the greater density of defect sites masks the effect [5]. The effects may be due to potential induced desorption of water or other contaminants. The capacitance of organic film monolayers on alumina in vacuum has been observed to decrease about 10% relative to that in air due to the evaporation of retained water [39], and the incorporation of water in thiol films has previously been suggested as the reason that the film dielectric constant was 13 % higher than expected [8]. Alternatively, the effect may be due to reorientation of the HDT film induced by the applied field. It is recognized that the orientation of molecular species on an electrode can be a function of potential [40-42], and changes in the capacitance of adsorbed phospholipids on Hg at about -1.2 V have been correlated with changes in the films permeability [41].

The observations presented here demonstrate the very high impermeability of HDT films on Hg. The ease of formation and reproducibility of the films generated makes this an attractive substrate for the study of the properties of self-assembled thiol monolayers if a minimum of defects is required.

4.4 Conclusions

Organized organic monolayers are an ideal medium to investigate the effects of both length and structural parameters of the bridge on electron transfer, because their organization ensures a well defined length and conformation. In this chapter we have demonstrated that HDT forms a well organized self-assembled monolayer on an Hg surface. The results indicate that Hg is a viable option on which alkane thiols can be assembled as it does not suffer some of the problems encountered on solid metal surfaces such as the often used Au.

HDT film formation on Hg is completed in less than 1 minute. The onset of Hg oxidation in 0.1 M NaF is shifted anodically by 1.0 V when coated with HDT. On the cathodic side no significant Faradaic current is observed up to -1.1 V vs SCE on HDT coated Hg. This gives a relatively large potential window of about 2.5 V in which electron transfer studies over blocked films can be carried out.

The chain length calculated based on capacitance measurements agrees with ellipsometric measurements indicating an organized, monolayer film that is found with the alkane vertically positioned. The current for $\text{Ru}(\text{NH}_3)_6^{3+}$, methyl viologin, benzoquinone, and $\text{Fe}(\text{CN})_6^{3-}$ reduction at an HDT coated SMDE is <0.005% of that at a bare electrode, and is principally due to capacitive effects. Thus the film is blocking to charged and uncharged species in solution with the exception of Pb^{+2} which is able to permeate the HDT film. Using the electron tunneling theory we estimate an apparent electron transfer coefficient for $\text{Ru}(\text{NH}_3)_6^{3+}$ of 3×10^{-13} cm/s at a coated electrode. This represents 12

orders drop in the electron transfer rate compared to a bare electrode. Such a decrease of rate is in agreement with that predicted by Moser et. al. for electron exchange across a 20 Å chain sigma bond [43]. Being a generic thiol, it is evident that extending it to other thiols should result in a similarly well-organized self-assembled films on Hg.

4.5. References

1. Ulman, A. *An Introduction to Ultrathin Organic Films: From Langmuir-Blodgett to Self-Assembly*; Academic press: Boston, 1991.
2. Colvin, V.L.; Goldstein, A.N.; Alivisatos, A.P. *J. Am. Chem. Soc.* **1992**, *114*, 5221.
3. Moaz, R.; Sagiv, J. *Langmuir*, **1987**, *3*, 1034.
4. Tillman, N.; Ulman, A.; Schildkraut, J.S.; Penner, T.L. *J. Am. Chem. Soc.* **1988**, *110*, 6136.
5. Sabatani, E.; Rubenstein, I.J. *Phys. Chem.* **1987**, *91*, 6663.
6. Finklea, H.O.; Robinson, L.R.; Blackburn, A.; Allara, A.; Bright, T. *Langmuir* **1986**, *2*, 239.
7. Troughton, E.B.; Bain, C.D.; Whitesides, G.M.; Nuzzo, R.G.; Allara, D.L.; Porter, M.D. *Langmuir* **1988**, *4*, 365.
8. Porter, M.D.; Bright, T.B.; Allara, D.L.; Chidsey, C.E.D. *J. Am. Chem. Soc.* **1987**, *109*, 3559.
9. Chidsey, C.E.D.; Loiacono, D. *Langmuir* **1990**, *6*, 682.
10. Laibinis, P.E.; Whitesides, G.M. *J. Am. Chem. Soc.* **1992**, *114*, 1990.
11. Fabiankowski, W.; Coyle, L.C.; Weber, B.A.; Granata, R.D.; Castner, D.G.; Sadownik, A.; Regen, S.L. *Langmuir* **1989**, *5*, 35.
12. Finklea, H.O.; Avery, S.; Lynch, M.; Furtsch, T. *Langmuir* **1987**, *3*, 409.
13. Creager, S.E.; Hockett, L.A.; Rowe, G.K. *Langmuir* **1992**, *8*, 854.
14. Creager, S.E.; Collard, D.M.; Fox, M.A. *Langmuir* **1990**, *6*, 1617.

15. Barth, J.V.; Brune, H.; Ertl, G.; Behm, R.J. *Phys. Rev.* **1990**, *B42*, 9307.
16. Strong, L.; Whitesides, G.M. *Langmuir* **1988**, *4*, 546.
17. Camillone, N.; Chidsey, C.E.D; Liu, G.Y.; Putvinski, T.M.; Scoles, G. *J.Chem. Phys.* **1991**, *94*, 8493.
18. Ross, P.N.; D'Agostino, A.T. *Electrochim. Acta.* **1992**, *37*, 615, and references cited therein.
19. Wang, J.; Davenport, A.J.; Isaacs, H.S.; Ocko, B.M. *Science* **1992**, *255*, 1416.
20. Finklea, H. O.; Hanshew, D. D. *J. Am. Chem. Soc.* **1992**, *114*, 3173.
21. Becka, A. M.; Miller, C. J. *J. Phys. Chem.* **1992**, *96*, 2657.
22. Chidsey, C.E.D. *Science* **1991**, *251*, 919.
23. Li, T.T.T.; Weaver, M.J. *J. Am. Chem. Soc.* **1984**, *106*, 6107.
24. Miller, C.; Bratzel, M. *J. Phys. Chem.* **1991**, *95*, 5225.
25. Chambers, J.Q. In *Encyclopedia of Electrochemistry of Elements*; Bard, A.J., Ed.; Marcel Dekker: New York; **1973**, Vol. *XII*, pp 329.
26. Vydra, F.; Stulik, K.; Julakova, E. *Electrochemical Stripping Analysis*; Ellis Horwood Ltd.: Sussex, England, **1976**, pp142.
27. Li, X.; Verpoorte, E.M.J.; Harrison, D.J. *Anal. Chem.* **1988**, *60*, 493.
28. Grahame, D.C. *Chem. Rev.* **1947**, *41*, 441.
29. Bockris, J. O'M; Jeng, K.T. *Adv. Coll. Interf. Sci.* **1990**, *33*, 1.
30. Bockris, J. O'M; Reddy, A.K.N. *Modern Electrochemistry* Vol. 2; Plenum Press: New York, **1970**; pp 725.
31. Lanza, V.L.; Herrman, D.B. *J. Polym. Sci.* **1958**, *28*, 622.
32. Bain, C.D.; Troughton, E.B.; Tao, Y-T.; Evall, J.; Whitesides, G.M.; Nuzzo, R.G. *J. Am. Chem. Soc.* **1989**, *111*, 321.

33. Amator, C.; Saveant, J.M.; Tessier, D. *J. Electroanal. Chem.* **1983**, *147*, 39.
34. Bard, A.J.; Faulkner, L.R. *Electrochemical Methods: Fundamentals and Applications*, Wiley: New York, **1980**, pp 91-95.
35. Marcus, R.A.; Sutin, N. *Biochim. Biophys. Acta* **1984**, *811*, 265.
36. Miller, C.; Cuendet, P.; Gratzel, M. *J. Phys. Chem.* **1991**, *95*, 877.
37. Hartman, T.E. *J. Appl. Phys.* **1964**, *35*, 3283.
38. Widrig, C. A.; Chung, C.; Porter, M.D. *J. Electroanal. Chem.* **1991**, *310*, 335.
39. Polymeropoulos, E.E.; Sagiv, J. *J. Chem. Phys.* **1978**, *69*, 1836.
40. Christensen, P.A.; Hammett, A.; Blackham, I. *J. Electroanal. Chem.* **1991**, *318*, 407.
41. Moncelli, M.R.; Guidelli, R. *J. Electroanal. Chem.* **1992**, *326*, 331.
42. Nelson, A.; Auffret, N. *J. Electroanal. Chem.* **1988**, *248*, 167.
43. Moser, C.C.; Keske, J.M.; Warncke, K.; Farid, R.S.; Dutton, P.L. *Nature*, **1992**, *355*, 796.

Chapter 5

Conclusion

The use of integrated potentiometric sensors such as ISFETs involves a chemically specific sensing layer that is placed between the sample and a blocking layer of insulator and/or semiconductor. Another construction of semiconductor based chemical sensors is the membrane/insulator/semiconductor (MIS) capacitor devices. Both types detect the potential change at the electrolyte-membrane interface by capacitive coupling with the semiconductor space charge. We chose to study the MIS because it is easy to make in the laboratory and has fewer variables than the ISFET. At the same time the conclusions derived from the investigation of the MIS could be a basis for ISFETs as well.

As explained in the introductory chapter the electrolyte-membrane interface of the MIS we examined included both blocked and nonblocked interface membranes. In this chapter is presented a summary of our contributions. Also presented are some suggestions for future work that may be done to shed more light to the subjects of this thesis.

5.1 Summary of contributions

Most of our study was done by AC impedance analysis. Characterization of the impedance response of the MIS was made possible through an equivalent circuit model consisting of simple circuit elements, as shown in chapter 2. This model is different from that of Smith and Janata [2] in that it includes the surface states at the insulator-semiconductor interface. However, a circuit element representing the membrane-insulator interface, whose time constant, being very large, does not show up in the impedance response, is not included in our model. Most importantly, in this follow-up work that was begun by Elisabeth Verpoorte [1] we have shown a quantitative comparison between model calculations and experimental results that was not done earlier [1-3].

This study reveals that impedance characteristics of the semiconductor are strongly modified by the membrane resistance. Both model calculations and experimental results show that increasing the impedance of the membrane changes the shape of the CV from sigmoidal as a function of applied potential to a flat, potential independent response. It is even possible to observe cases where the capacitance in the inversion region can be larger than that in the accumulation region. Since the model has been verified experimentally, one can use it to quantitatively determine measurement conditions and the required or desirable impedance parameters of the sensing materials.

In chapter 3 adsorption phenomena are discussed. Surface active agents are known to adsorb onto diverse types of substrates. As a result they are found in a wide range of processes. The adsorption of an

amphiphilic surfactant onto a reversed phase surface evidently can be caused by the tendency of the hydrophobic segment of the surfactant to escape from the aqueous phase. We have used the reactance of the semiconductor space charge for in situ determination of surface potential and adsorbed SDS⁻.

The determination of the amount of SDS⁻ adsorbed on a reversed phase ODS surface discussed in chapter 3 was based on measurement of the shift in potential required to maintain a constant depletion capacitance. That this method can be used for the measurement of double layer potential change can be easily seen from a straight forward extension of the equations in reference 4. We observed that the surface potentials increased at constant activity of SDS⁻ with decreasing ionic strength of the supporting electrolyte. Based on a modified GCSG model in which coordination between SDS⁻ and Na⁺ was also considered this observation was readily accounted for. The adsorbed charge density due to SDS⁻ versus aqueous SDS⁻ concentration was evaluated using this model. The results indicate that the total amount of SDS⁻ adsorbed decreases with increasing ionic strength. While this was consistent throughout our experiments, it is not in agreement with a large number of studies regarding the adsorption of charged species on different kinds of surfaces. However, other studies of adsorption on silanized silicon or polymer surfaces have reported the same trend we observed even when using other measurement techniques. These results will require further clarification.

Our results indicate that at adsorption saturation SDS⁻ does not form a structurally limited monolayer. Similarly, Liu and Cantwell have

shown that the area per molecule of both tetra-n-butyl-ammonium cation and p-nitrobenzenesulfonate anion at maximum adsorption on octadecylsilane silanized silica is larger than their largest cross sectional area at all ionic strengths [5]. On a silver halide surface too, several alkyl sulfates including SDS⁻ occupy areas at maximum adsorption that are about 20 times their respective cross sectional areas [6]. We also observed that while the ionic strength affected the maximum adsorption density, it did not affect the free energy of adsorption.

In chapter 4 we showed that hexadecane thiol forms a self assembled layer on mercury, when adsorbed from solution or the neat thiol. The capacitance of the film agreed with the expected monolayer thickness of a hexadecane film. From cyclic voltammetric studies the film formed was impermeable to all the ions tested except Pb⁺². In general, the film formed was shown to be superior to the often used self assembled thiol films on Au.

5.2 Suggestions for future research

The decrease in the amount of SDS⁻ at surface saturation with increasing ionic strength is unusual in light of the bulk of experimental results in the literature. Note, however, should be made that we know of no other physisorption adsorption isotherm derived from the surface potential of the adsorbate. Still, the results of this study will have to be further evaluated by alternate methods. Several possible approaches are discussed below.

The effect of adsorption of charged species on particles may be determined from zeta potential measurements [7-9]. The zeta potential, ζ , is the potential of the charged surface at the plane of shear between the particle and the surrounding solution as the particle and the solution move with respect to each other. Although ζ may be marginally smaller in magnitude than ψ_d , the errors introduced through the assumption of their equality, especially at hydrophobic surfaces, is usually small [7]. Therefore,

$$\frac{d\zeta}{d[\text{SDS}_{(\text{aq})}^-]} = \left(\frac{d\psi_o}{d[\text{SDS}_{(\text{aq})}^-]} \right) \left(\frac{d\psi_{\text{OHP}}}{d\psi_o} \right) \quad (5.1)$$

Of the different methods used to measure ζ , electrophoresis has the greatest practical applicability. Finely ground, thermally oxidized and finally ODS silanized Si wafer particles can be used to measure ζ as a function of SDS^- activity. The ζ potential can then be used to calculate ψ_o and ultimately the adsorption of SDS^- using double layer models. This is again a measurement of potential, however.

The isotherms obtained through potential measurements are dependent on the double layer model and their associated constants. Moreover, essential constants required in the model like the capacitance at the SiO_2 -electrolyte interface are not directly measurable. This should direct us to seek model independent methods. Gibbs has derived a thermodynamic expression relating the surface excess and the concentration dependence of surface tension with the bulk phase concentrations. The Gibbs adsorption equation holds true for all types of

interfaces. It provides a relation between the surface tension, γ , the surface excess, Γ_i , and the bulk phase activity, a_i , of species i . The Gibbs adsorption equation in its most general form is [9],

$$d\gamma = -\sum_i \Gamma_i d\mu_i \quad (5.2)$$

Where $d\gamma$ is the change in surface or interfacial tension of the solvent and the rest are as defined earlier. At equilibrium, and typical supporting electrolyte concentrations as in our experiments where the activity of only species " i " is changing, equation 5.2 becomes;

$$d\gamma = -RT\Gamma_i d(\ln a_i) \quad (5.3)$$

For surface active solutes the surface excess concentration, Γ_i , can be considered to be equal to the actual surface concentration without any significant error [10]. Applying equation 5.3 to the adsorption of SDS^- onto ODS in NaCl supporting electrolyte gives;

$$\Gamma_{(\text{ODS})} = -\frac{1}{2.303RT} \left(\frac{d\gamma}{d \log [\text{SDS}_{(\text{aq})}^-]} \right) \quad (5.4)$$

Equation 5.4 shows that the total amount of SDS adsorbed at constant temperature can be obtained from the slope of a plot of surface tension versus log bulk activity of SDS^- .

One of the methods employed to obtain surface tension is contact angle measurement [9,11]. We have tried "crude", open air, preliminary

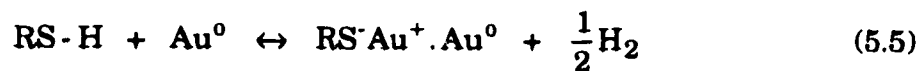
contact angle goniometer measurements on silanized electrodes. These attempts were not rewarding because, although contact angle is a thermodynamic property, the experimental requirements are very stringent [9,11,12]. Another fairly well known reliable method for the measurement of surface tension is the Wilhelmy plate method [9]. The "plate" in this case should be a geometric segment of Si/SiO₂ whose back and front sides are polished. It must also have been treated the same way as the silanized electrodes. An electrobalance may then be used to measure the surface tension changes caused by various concentrations of SDS⁻ in the phase in which the plate is partially dipped. Isotherms may then be calculated from equation 5.4. Such a thermodynamic method contains very few assumptions and therefore could give a reliable check of our impedance based measurements.

In chapter 4 we have shown that hexadecane thiol forms a defect free self assembled film on Hg. Although only one thiol has been tried it is evident that it should work with other types of thiols as well. Thiol self assembled films have been used to tether an electroactive head group at a fixed distance from the surface of the electrode through a carbon chain [13-15]. In the absence of any electroactive group, the carbon chain serves as a molecular precision spacer towards diffusing redox species of the electrolyte. As a result thiol self assembled films are extensively used in the investigation of electron transfer and electron tunneling theory [13,16,17].

The theory for electron tunneling and electron transfer has continuously been developed since the early 1960s [18]. R. Marcus was awarded the 1992 Nobel Prize for chemistry for his contributions in

electron transfer theory. In this area there are discrepancies of parameters such as the tunneling parameter, β , the electron transfer coefficient, α , and the average barrier energy height, E_B , between different groups and between experiment and ab initio calculations. Electrochemical experiments done to obtain these values are undermined by the presence of defects. We believe better experimental conditions for electrochemical studies can be achieved by using thiol-Hg self-assembled films.

The exact reaction that leads to the novel self-assembled structures of thiols on Au is not known with certainty, despite being studied by XPS, FTIR, and STEM [19,20]. It is clear however that the species chemisorbed on the Au surface is a thiolate, probably involving the reaction [20],



Proper understanding of this reaction can lead to the description of the types of molecules that could self-assemble on more widely used metals. Surface spectroscopic studies of the Hg surface should yield more definitive results because of the unusually high thiol-Hg interaction.

5.3. References

1. Verpoorte, E.M.J. Ph.D. Desertation, Univ. of Alberta, 1990.
2. Smith, R.L.; Janata, J. *J. Electrochem. Soc.* 1980, 127, 1599.
3. Li, X.; Verpoorte, E.M.J.; Harrison, D.J. *Anal. Chem.* 1988, 60, 493.
4. Bousse, L. *J. Chem. Phys.* 1982, 76, 5128.
5. Liu, H.J.; Cantwell, F.F. *Anal. Chem.* 1991, 63, 993.
6. Hunter, R.J. *Zeta Potential in Colloid Science*, Academic Press, New York, 1981, pp 312.
7. Shaw, D.J. *Introduction to Colloid and Surface Chemistry*, Butterworths, 3rd ed., Boston, 1980, chapter 7.
8. Hunter, R.J. *Zeta Potential in Colloid Science*, Academic Press, New York, 1981.
9. Adamson, A.W. *Physical Chemistry of Surfaces*, 5th ed.; Wiley, New York, 1990.
10. Rosen, M.J. *Surfactants and Interfacial Phenomena*, 2nd ed.; Wiley, New York, 1989, chapter 2.
11. *Contact Angle, Wettability and Adhesion*: Fowkes, F.M.; Ed.; Advances in Chemistry vol. 43; American Chemical Society, Washington, D.C., 1964.
12. Wyart, F.B.; Redon, C. *Langmuir*, 1992, 9, 2328.
13. Finklea, H.O.; Hanshaw, D.D. *J. Am. Chem. Soc.* 1992, 114, 3173.
14. Chidsey, C.E.D. *Science*, 1991, 251, 919.
15. Creager, S.E.; Hockett, L.A.; Rowe, G.K. *Langmuir* 1992, 8, 854.
16. Becka, A.M.; Miller, C.J. *J. Phys. Chem.* 1992, 96, 2657.
17. Miller, C.J.; Gratzel, M. *J. Phys. Chem.* 1991, 95, 5225.

18. Marcus, R.A.; Sutin, N. *Biochem. Biophys. Acta.* **1985**, *811*, 265.
19. Laibinis, P.E.; Whitesides, G.M. *J. Am. Chem. Soc.* **1992**, *114*, 9022.
20. Sellers, H.; Ulman, A.; Shnidman, Y.; Eilers, J.E. *J. Am. Chem. Soc.* **1993**, *115*, 9390.